LBL-34291
UC-404

Lawrence Berkeley Laboratory
UNIVERSITY OF CALIFORNIA

Materials Sciences Division

The Effect of Composition on the Mechanism of Continuous Recrystallization and Superplastic Response of Aluminum-Scandium Alloys

E.L. Bradley, III
(Ph.D. Thesis)

May 1993

REFERENCE COPY
Does Not
Circulate
Bldg. 50 Library.
LBL-34291
Copy 1

Prepared for the U.S. Department of Energy under Contract Number DE-AC03-76SF00098

DISCLAIMER

This document was prepared as an account of work sponsored by the United States Government. While this document is believed to contain correct information, neither the United States Government nor any agency thereof, nor the Regents of the University of California, nor any of their employees, makes any warranty, express or implied, or assumes any legal responsibility for the accuracy, completeness, or usefulness of any information, apparatus, product, or process disclosed, or represents that its use would not infringe privately owned rights. Reference herein to any specific commercial product, process, or service by its trade name, trademark, manufacturer, or otherwise, does not necessarily constitute or imply its endorsement, recommendation, or favoring by the United States Government or any agency thereof, or the Regents of the University of California. The views and opinions of authors expressed herein do not necessarily state or reflect those of the United States Government or any agency thereof or the Regents of the University of California.

LBL 34291

The Effect of Composition on the Mechanism of Continuous Recrystallization and Superplastic Response of Aluminum-Scandium Alloys

Edwin Luther Bradley, III

Ph.D. Dissertation

Department of Materials Science and Mineral Engineering
University of California

and

Center for Advanced Materials
Materials Sciences Division
Lawrence Berkeley Laboratory
University of California
Berkeley, CA 94720

May 1993

This work was supported by the Director, Office of Energy Research, Office of Basic Energy Science, Materials Science Division of the U.S. Department of Energy under Contract No. DE-AC03-76F00098

The Effect of Composition on the Mechanism of Continuous Recrystallization and Superplastic Response of Aluminum-Scandium Alloys

Edwin Luther Bradley, III

Ph. D. Dissertation

High temperature tensile tests were performed on several Al-Sc alloys containing various amounts of Mg and Li in order to determine the mechanism of continuous recrystallization (CRX), the effect of solutes on the mechanism of CRX in Al, and the effect of solutes on the subsequent deformation of Al-Sc alloys after CRX is complete. In this case CRX is both a thermal and stress assisted process that is not strongly influenced by the presence of solutes in the matrix. All of the Al-Sc alloys tested show an increase in the boundary misorientation of the subgrains with strain to the point they become true grains at strains greater than 0.7. However, solutes indirectly play a role in the observation of superplasticity that often results from CRX. Other studies have inferred that a microstructure capable of superplastic deformation always results from CRX. However, in Al-Sc alloys other factors may prevent the occurrence of extremely high m-values even when CRX happens.

The highest maximum m-values are seen in the alloys with the lowest melting points; and therefore, the alloys with the greatest amount of alloying elements. The Al-Mg-Sc alloys exhibit high m-values over the broadest range of strain rates and at the highest strain rates. This is due to the higher stresses at which of power-law creep is observed in these alloys compared to the alloys without Mg. The Al-Li-Sc and Al-Sc alloys go directly from superplastic creep to power-law breakdown at higher strain rates which results in a rapid drop in m with strain rate. The Al-Mg-Sc alloys exhibit a transition to power-law creep from superplastic creep at higher stresses than those observed for the transition to power-law breakdown in the Al-Sc alloys without Mg. This results in the high m-values exhibited at the higher strain rates. The transition from superplastic creep to regular power-law creep results in a slower decrease in m with strain rate. Overall, the Al-Mg-Sc alloys have the best properties from a superplastic formability perspective.

TABLE OF CONTENTS

ACKNOWLEGDEMENTS iv
1. INTRODUCTION 1
2. BACKGROUND 3
2.1 Softening Processes in Metals 3
2.1.1 Static and dynamic recovery 3
2.1.2 Dynamic and static recrystallization 4
2.1.3 Zener drag 5
2.2 Proposed Theories of Continuous Recrystallization 5
2.3 Creep 6
2.3.1 Creep tests 7
2.3.2 Strain-rate sensitivity (*m*) 9
2.4 Creep Mechanisms 11
2.4.1 Power-law creep 11
2.4.2 Power-law breakdown 12
2.4.3 Viscous glide creep 12
2.4.4 Harper-Dorn creep 12
2.4.5 Nabarro-Herring creep 13
2.4.6 Coble creep 13
2.4.7 Grain boundary sliding creep (Superplasticity) 13
2.5 Interaction of simultaneous deformation mechanisms 14
2.6 Aluminum System 16
2.6.1 Superplasticity of Al alloys 16
2.6.2 Important alloying additives to aluminum 16
3. EXPERIMENTAL PROCEDURE 17
3.1 Material Preparation 17
3.2 Tensile Tests 18
3.2.1 *m*-value calculation 19
3.2.2 *m* vs. strain 20
3.2.3 *m* vs. strain rate 21
3.2.4 Work hardening rate and constant strain rate tests 21
3.3 Microstructural Analysis 22
3.3.1 Optical microscopy 22
3.3.2 Transmission electron microscopy (TEM) 22
3.3.3 Scanning electron microscopy (SEM) 25
4. RESULTS 26
4.1 Microstructure Prior to Creep Deformation 26
4.1.1 Al-0.5Sc (AS) 26
4.1.2 Al-1.2Li-0.5Sc (ALS) 26
4.1.3 Al-2.7Mg-0.5Sc (AMS) 30
4.1.4 Al-2.4Mg-1.8Li-0.5Sc (AMLS) 30
4.1.5 Al-8.3Zn-0.5Sc (AZS) 37
4.1.6 Non-Sc alloys 37
4.2 Microstructures after Creep Deformation 38
4.2.1 Grain morphology 38
4.2.2 Grain boundary misorientation 46

4.3 Tensile Data 52
4.3.1 *m* vs. strain and strain rate 52
4.3.1.1 Alloys with Sc 52
4.3.1.2 Alloys without Sc 56
4.3.2 Effect of strain rate on the evolution of *m* 56
4.3.3 Flow stress vs. strain rate 57
4.3.4 Stress-strain curves 59
4.3.5 Elongation and failure 62
4.4 Activation Energy 63
5. DISCUSSION 65
5.1 Effect of solutes on CRX 65
5.1.1 Evolution of the microstructure in the Al-Sc alloys 65
5.1.2 Evolution of *m* in the Al-Sc alloys. 65
5.1.3 Comparison to previous results on binary alloys 66
5.2 Mechanism of Continuous Recrystallization 69
5.2.1 Subgrain coalescence and additional dislocation generation 69
5.2.2 Stress level in CRX 71
5.2.3 Criticism of currently proposed theories on CRX 72
5.2.3.1 Theories of McNelley *et al.* 73
5.2.3.2 Theory of GBS-induced CRX 74
5.2.3.3 Theory of Qing *et al.* 75
5.2.3.4 Theory of Grimes *et al.* 76
5.3 Role of ν-phase on CRX 76
5.4 Effect of Grain Size on CRX 77
5.5 Role of Solutes on Deformation after CRX 78
5.5.1 High strain rates 78
5.5.2 Low strain rates 79
5.6 Stable deformation and elongation in Al-Sc alloys 80
6. CONCLUSIONS 82
7. FUTURE WORK 83
REFERENCES 84
APPENDIX A 93
APPENDIX B 95

ACKNOWLEDGMENTS

There is a famous saying that I'll paraphrase which really sums up my experience here in the Morris Group: It is the journey itself that is important, not the final destination. Because of that journey I feel I have little in common with that younger man who came to this group some four and one-half years ago. I was newly married and I thought I knew quite a bit about materials science and myself. Now I have a delightful daughter, a thriving marriage and a much broader knowledge of all things scientific and otherwise.

I want to first and foremost thank my loving wife Sheila for her support during all the tough times and making the good times much better. My daughter Meghan gives me the daily reminder that play is as important as work and has a smile that can make me forget the troubles I may have faced earlier in the day. I also want to thank my parents for stressing the importance of education so that I would be able to have the opportunity to reach this milestone.

There have been so many people who have touched me throughout my stay at Berkeley. I must first thank Professor Morris for giving me this unbelievable chance to come to Berkeley and learn from him firsthand. I would also like to thank David Chu for surviving as my officemate for several years and for being an excellent source of information and common sense, Jin Chan for his helpful disposition and the knowledge of all things that make a lab work well, Choongun Kim who came to the group at the same time as me and has shared with me his unique way of looking at all things, and Zequn Mei and Ping Xu for their selflessness and example of what hard work can achieve. I would also like to thank Anne Sunwoo, Judy Glazer, Dana Tribula, Pat Johnson, Shelly Miyasato, and Roger Emigh for their advice and help along the way. To Heidi Linch, Dan Dietderich, Rusty Cinque, Carol Tseng, Pete Skarpelos, Hiro Hayashigatani, Pamela Kramer, and Julia Freer Goldstein: thanks for the good times.

In building 62 I'd like to thank James Wu for all of his help and good humor. I'd also like to thank John Holthuis, Chuck Covey, Chip Flor, Peter Ruegg, Jim Severns, Bob Ybarra, and Gary Tabler for doing a job well done. I'd also like to thank Professors Gareth Thomas and Iain Finnie along with Professor Morris for serving on my thesis committee and Professors Gareth Thomas, Robert Ritchie, Eicke Weber, and Frank Hauser for serving on my qualifying exam committee.

This work was supported by the Director, Office of Energy Research, Office of Basic Energy Science, U. S. Department of Energy, under contract No. DE-AC03-76SF00098. The Al-Sc master alloy used in this study was supplied by ALCOA.

1. INTRODUCTION

Recently there has been interest in identifying the mechanism of continuous recrystallization (CRX) that is observed during the high temperature deformation of a number of Al alloys [Diskin *et al.* 1986; Grimes *et al.*, 1976; Bradley *et al.*, 1991; Gardener and Grimes, 1979; Ash and Hamilton, 1988; Qing *et al.*, 1991] and minerals [Guillope and Poirier, 1979 and Tungatt and Humphreys, 1981]. Previous work has shown that during the high temperature creep of Al alloys containing a fine dispersion of insoluble precipitates, an initially rolled microstructure of pancake-shaped grains gradually evolves into a microstructure of equiaxed grains. There is no discontinuous recrystallization such as is seen in regular dynamic and static recrystallization. The new microstructure that forms is almost always superplastic, which is interesting from both applied and fundamental perspectives. Because superplastic forming (SPF) has advantages in certain cases over conventional forming and fabricating operations, CRX is an important mechanism in Al alloys and possibly other alloy systems. However, there is some disagreement over the exact mechanism of CRX in Al alloys and conflicting results on whether alloying additions are necessary for CRX to be observed in these alloys.

Typically, metals are made superplastic by severely deforming and then statically recrystallizing them to a small grain size. This route has also been taken with certain Al alloys that exhibit CRX [Wadsworth, *et al.*, 1983 and Shin *et al.*, 1992]. A benefit of CRX in Al alloys is that it appears that the CRX grain size is smaller than that achieved by static recrystallization (SRX) [Amichi and Ridley, 1989]. This permits greater strain rates to be used in superplastic forming and decreases the part forming time. The only superplastically-formed Al alloy used in structural applications is 7475, which is processed by SRX. It typically exhibits superplasticity at strain rates one-third of those seen in Al alloys exhibiting CRX. Another advantage is since alloys exhibiting CRX are conventionally worked to a highly textured condition and develop the recrystallized microstructure on creep deformation, processing steps are saved and costs are lowered.

Most Al alloys utilize small amounts of transition elements to form intermetallics that inhibit recrystallization [Hatch, 1984]. In the Al-Li alloys, Zr is often used as it forms the metastable phase β' (Al_3Zr) of very small size that exerts a large Zener drag on the grain boundaries. However, the maximum solubility of Zr in Al is ~ 0.03 at% [Hansen, 1958] which limits the maximum volume fraction of β' to ~ 0.12%. Sc forms a phase (Al_3Sc) of the same structure which is thermodynamically stable [Gschneider and Calderwood, 1989] and has a eutectic composition of ~ 0.3 at% so that a volume fraction of ~ 1.2% can be formed. Sawtell and Jensen [1990] and Drits *et al.* [1985] showed that

the Sc increases the strength of Al-Mg alloys and demonstrated that they have good SPF properties. Emigh cast and fabricated Al-Li alloys with scandium to see if similar gains could be made in these alloys by replacing the Zr with Sc. Good strengths were achieved; however, the Sc forms a ternary phase with Li that is insoluble and limits the possible gain in strength. Tests on an Al-Mg-Li-Sc alloy at high temperatures showed that they also exhibited CRX. As a result, it was decided to use the Al-Sc system to conduct a thorough study of the mechanism of CRX.

The goals of this work are to (1) understand the process of CRX, (2) determine the influence of composition on the CRX mechanism, and (3) determine the influence of composition on the high temperature properties of Al-Sc alloys after CRX. It is important that the composition effect on CRX be identified since commercially viable Al alloys always contain alloying elements such that sufficient strength is achieved. With this understanding it should be possible to improve the high temperature forming properties of Al alloys while maximizing their post-formed mechanical properties.

2. BACKGROUND

2.1 Softening Processes in Metals

Dislocations raise the overall energy of a crystal due to the elastic energy associated with the defect structure [*e.g.* Nabarro, 1987]. As a result, there is a thermodynamic driving force to rid the crystal of this excess energy and this is accomplished by two types of processes: recovery and recrystallization. Both of these processes are kinetically driven by thermal activation and stress.

2.1.1 Static and dynamic recovery

Recovery is a process by which individual dislocations of different signs mutually annihilate one another or align in lower energy configurations such as subgrain boundaries or cell walls [*e.g.* Reed-Hill, 1973]. Static recovery occurs under the action of internal stress and thermal activation while dynamic recovery occurs during warm or hot deformation as a result of an externally applied stress. Dynamic recovery is the more efficient process since the stress is applied at temperature. Both of these processes are expected to play a role in the evolution of the microstructures and final properties of the Al-Sc alloys during processing and testing.

The ease of recovery in a material is determined by the presence of precipitates, solutes, and the degree of dislocation dissociation [Honeycombe, 1984]. Precipitates hinder the movement of dislocations and decrease the opportunities for their interaction and annihilation. Basic dislocation theory states that the line energy of a dislocation is proportional to $|\mathbf{b}|^2$ where **b** is the Burgers vector of the dislocation. Perfect dislocations with $\mathbf{b} = \frac{a}{2}[110]$ (where a is the lattice constant) in FCC lattices can decrease their energy by dissociating into two partials of the type $\frac{a}{6}[112]$ separated by a ribbon of HCP stacking, or stacking fault. The stacking fault energy (SFE) is the energy associated with the HCP stacking in an FCC lattice. Seeger [1957] showed the separation of the partials is related to the SFE by the relation

$$d_o \propto \frac{\Gamma}{Gb} \tag{2.1}$$

where Γ = stacking fault energy. Thus, a lower the SFE results in a greater separation of the partial dislocations. Cross-slip of screw dislocations is hindered by the presence of stacking faults since the Burgers vector and dislocation line are no longer parallel for the partials. Climb is hindered since the separate partials will produce more faulted crystal if

they move perpendicular to the glide plane. Thus recovery is inhibited and a greater density of dislocations are able to be stored in the material. Table 2.1 has the calculated SFE of several FCC alloys and the equilibrium partial separation for edge and screw dislocations. Al and its alloys have very high stacking fault energies (~ 200 mJ/m^2) [Ruff, 1970 and Gallagher, 1970], therefore recovery is very prominent and the subgrain boundaries are very tight and orderly in appearance.

Table 2.1. Best estimates for the stacking fault energies of FCC metals with the calculated equilibrium partial separations for both edge and screw dislocations [after Gallagher, 1970].

Material	Assumed SFE mJ/m	Calculated Dislocation Width, nm Edge	Screw
Al	200	0.5	0.2
Cu	70	2.3	0.6
Au	45	3.1	0.6
Ag	22	6.1	1.5
Ag-8Sn	4	31.0	7.5

2.1.2 Static and dynamic recrystallization

All conventional recrystallization processes are the result of the accumulation of elastic strain energy associated with the storage of dislocations during deformation [Reed-Hill, 1973]. Both static and dynamic recrystallization result from the motion of large-angle grain boundaries initiated at $T_H > 0.5$ which sweep out regions of deformed material and leave behind nearly dislocation free grains. Static recrystallization (SRX) results from the grain boundary motion driven by internal stresses and thermal activation. Dynamic recrystallization (DRX) is a similar process which is initiated during deformation under an external stress. Recrystallization results in larger reductions in the dislocation density than does recovery [Gordon, 1955].

The appearance of recrystallization is a function of a number of variables including precipitate distribution, deformation strain, deformation temperature, strain rate, initial grain size, and stacking fault energy. Precipitates can act to either inhibit or promote recrystallization. If the Zener drag [see below] of the precipitates on the grain boundaries is high enough, DRX and SRX are prevented from occurring by the pinning of the boundaries. However, large precipitates (~ 1 μm) can promote recrystallization by

acting as strain centers during deformation [Mould and Cotterill, 1967]. During bulk forming, the matrix around the large particles is more severely deformed, causing high dislocation densities and large, short range lattice curvature. Normally these large particles are not present in sufficient quantities to prevent grain boundary motion. Thus, recrystallization is promoted.

Dynamic recovery can, under certain conditions, prevent a critical dislocation density for recrystallization from ever developing during hot deformation. DRX is much harder to achieve in Al than SRX, because it must be initiated at high temperatures where recovery is more efficient. It has only been since *ca.* 1980 that papers on the DRX of Al have been found in the literature. The greater ease of DRX in Al-Mg alloys is attributed to the lowering of the SFE and can result in a fine, equiaxed microstructure [Sheppard, *et al.*, 1986].

2.1.3 Zener drag

Zener, in a communication reported by Smith [1948], first proposed that precipitates inhibit recrystallization by preventing the motion of grain boundaries that nucleate new, strain-free grains. This is accomplished by the forces exerted on the boundaries by the precipitates; which is analogous to that which is exerted on a single dislocation. This force may be overcome with sufficient driving force (stored strain energy) and thermal activation. The relationship between a uniform precipitate distribution and the limiting Zener grain size is

$$d \approx \frac{3r}{4f} \tag{2.2}$$

where d = grain size, f = precipitate volume fraction, and r = radius of the precipitates. This equation was derived in a general way, so the constant does not reflect any structural feature of the boundary, precipitate, or matrix. However, if the precipitates are coherent, the constant is higher since the precipitates lose coherency when bypassed by the boundary due of the additional precipitate/matrix surface energy that results [Ryum, Hunderi, and Nes, 1983].

2.2 Proposed Theories of Continuous Recrystallization

Several theories describing the CRX mechanism can be found in the recent literature. Hales and McNelley [1988] proposed that the initially small-angle (subgrain) boundaries (2-7°) that form during rolling slide under the applied creep stress and

progressive grain rotation results. This mechanism has been questioned since there is no evidence that small-angle boundaries are capable of sliding [Weinberg, 1958; Rhines, *et al.*, 1956; and Gleiter and Chalmers, 1972]. They have also claimed to have utilized CRX during rolling [Hales *et al.*, 1991] to recrystallize an Al-10Mg-0.1Zr alloy. However, there are a number of questions concerning the interpretation of their results. More on this will be described in the Discussion section. Sawtell and Jensen [1990] showed that Al-Mg-Sc alloys achieved good elongation and stated that it was accomplished due to the sliding of "moderate" angle boundaries although no GBM data was reported. Grimes [1976] along with Gardner [1979] proposed that the additions of solutes were necessary to achieve CRX and that these either a) lowered the stacking fault energy of the alloy and promoted CRX or b) influenced the as-cast microstructure and thereby made CRX possible. Gudmundsson *et al.* [1991] claimed that the large-angle grain boundaries present from the as-cast structure in the plane of rolling slide under the creep stress and that this causes grain rotation and CRX. Why this should be so is not elaborated. Qing *et al.* [1992] described CRX as a process where dislocations glide into the boundaries under the applied stress, thereby increasing the misorientation of the boundary.

Almost all of the work relating to CRX has been performed on alloys with large amounts of alloying additions, although there are a few cases where this is not the case. Watts *et al.* [1976] reported that the Al-0.5Zr binary alloy had poor high temperature ductility compared with the Al-Cu-Zr alloys studied and did not demonstrate CRX. Sawtell and Jensen [1990] reported at 400°C that $m_{max} = 0.4$ for an Al-4Mg-0.5Sc alloy while an Al-0.5Sc alloy had a $m_{max} = 0.2$ and claimed that Mg was necessary to see high m-values in Al-Sc alloys. Gudmundsson *et al.* [1991] studied a low additive alloy, Al-0.24Zr-0.1Si; their results demonstrated that a refinement of the microstructure occurred at 400°C and $\dot{\varepsilon} = 9.5 \times 10^{-4} s^{-1}$ which appeared to be from CRX, but the ductility remained low (< 100%) and no m-values were reported. Thus, it is both implied and stated in the literature that the process of CRX is tied to alloying additions and that the appearance superplasticity after CRX is only seen in highly alloyed Al.

2.3 Creep

Creep is the name given to time-dependent deformation and is very important in applications where parts see high service temperatures and require tight tolerances, such as for turbine blades. As described by Poirier [1985], the first modern experiments on

creep were performed by Trouton and Rankine in 1904. Andrade [1910] studied the creep of many metals and first reported that the strain rate reaches a steady-state regime if the sample is deformed under constant stress. Other work has been carried out on hot forming processes such as rolling, forging and extrusion that are carried out at much higher strain rates. Many similarities are seen in these processes although they differ in strain rates by orders of magnitude [McQueen and Jonas, 1975].

2.3.1 Creep tests

A traditional creep test is one where the sample is deformed under constant stress or constant load and the strain is measured as a function of time. Constant load tests where the stress changes with time are more commonly used for engineering applications while constant stress tests are used in scientific studies of deformation mechanisms. In constant stress tests the stress is kept constant in one of two ways. A shear sample can be tested under constant load, which is equivalent to constant stress in a shear test. Alternately, a tension sample can be tested under constant stress during uniform deformation using a constant load. Uniform deformation is a constant volume process such that

$$A_o l_o = A_f l_f \tag{2.8}$$

where A_o, l_o = initial area and length and A_f, l_f = area and length at any subsequent time in the test. As the sample elongates, the area decreases at a rate equivalent to the increase in total elongation. The load on the sample can be made to decrease at the identical rate the area of the gage is shrinking with deformation by connecting the dead weight over an eccentric cam. As the sample elongates, the cam rotates and shortens the moment arm to which the load is attached. This decreases the effective load on the sample and allows the stress to remain constant. The disadvantage of the tensile test is that the samples are prone to localized deformation in the gage, unlike shear samples [see Appendix B].

When a specimen is initially loaded at high temperature, there is usually a transient strain where the strain rate either increases or decreases with time to a constant value. That initial portion of creep is referred to as primary creep and the constant portion as steady state creep. Primary creep results from the rearrangement of dislocations such that a steady state configuration is achieved in the material during deformation [Takeuchi and Argon, 1970]. Once the steady state configuration is achieved, the sample is in steady state deformation. After a period of time (strain) at steady state, the creep rate will increase rapidly and failure will occur. This is called

tertiary creep and in constant stress tests is typically due to the development and linkage of voids at the grain boundaries, although there are examples of microstructural instabilities precipitating tertiary creep. Tribula [1990] showed that Pb-Sn solders tested in double shear develop a narrow, recrystallized band in the eutectic microstructure that is softer than the surrounding material. Subsequent deformation occurs entirely in that region, causing early failure. Dynamic recrystallization also causes premature failure in tension samples [Frost, 1985 and Gandhi, 1985].

Since typically the greatest amount of time spent in creep is in the steady-state regime and the deformation is simplest in that regime, this is the aspect of creep that has been studied the most. Out of this work came a phenomenological equation to describe the steady-state deformation by Dorn called, appropriately enough, the Dorn equation. It is semi-empirical and incorporates all the various microstructural and mechanistic parameters found in all the different creep equations associated with the various creep mechanisms. Its form is

$$\dot{\gamma} = \frac{A_s GbD}{kT}\left(\frac{b}{d}\right)^p\left(\frac{\tau}{G}\right)^n \tag{2.3}$$

where $\dot{\gamma}$ = steady-state shear strain rate, A_s = constant associated with geometric terms of grain shape and crystal structure, G = shear modulus, b = Burgers vector magnitude of the significant dislocation type in deformation, D = diffusivity of the controlling process during deformation, k = Boltzmann's constant, T = absolute temperature, d = grain size, p = grain size dependence on the flow stress, τ = steady-state shear stress, and $n = 1/m$ = stress exponent. If the tensile or compressive stress is used then the Dorn Eq. is

$$\dot{\varepsilon} = \frac{A_t EbD}{kT}\left(\frac{b}{d}\right)^p\left(\frac{\sigma}{E}\right)^n \tag{2.4}$$

where $\dot{\varepsilon}$ = steady state uniaxial strain rate, E = Elastic modulus, σ = steady-state uniaxial flow stress, and A_t = constant for uniaxial deformation. The two equations can be related using the equivalent stress and equivalent strain rate criteria. For the equivalent stress criterion, the uniaxial tensile stress and the simple shear stress are related as

$$\sigma = \sqrt{3}\tau. \tag{2.5}$$

The uniaxial tensile and shear strain rates are related by

$$\dot{\varepsilon} = \frac{\dot{\gamma}}{\sqrt{3}}. \tag{2.6}$$

This has been experimentally determined to be valid and is used by Frost and Ashby [1982] to combine data from different sources in the form of deformation mechanism maps. Thus the constants A_s and A_t are related by the corrections shown above along with the correction associated with the shear and Young's moduli taken to the appropriate power.

The diffusivity (D) can be either grain boundary, dislocation pipe, or bulk diffusion depending on the operative creep mechanism. The form of the diffusivity is

$$D = D_o \exp\left(\frac{-Q}{kT}\right) \tag{2.7}$$

where D_o = diffusion constant and Q = activation energy of diffusion. Thus the true activation energy of creep is the activation energy of diffusion. A more detailed explanation of the activation energy of creep can be found in Appendix A.

2.3.2 Strain-rate sensitivity (m)

All materials have a strain-rate sensitivity (m), *i. e.* the flow stress is dependent on the macroscopic strain rate. At low homologous temperatures the relationship is very weak and is usually ignored for the purposes of analyzing the mechanical properties. However, at high temperatures ($T_H > 0.5$), deformation is thermally activated and there is a strong dependence on m as shown in the Dorn eq.. It is well known that particular values of m are associated with the different identified creep mechanisms [Cadek, 1988]. Table 2.2 shows the most common mechanisms and their characteristic of m-values based on shear tests. Most importantly to this work, $m = 0.5$ is associated with grain boundary sliding-controlled creep, commonly called superplastic creep or intergranular creep. There is nothing special about the value of $m = 0.5$, as a continuum of m-values have been experimentally measured and related to GBS-controlled deformation. However, most values fall around 0.5 and this value has also been derived theoretically [Arieli and Mukherjee, 1980 and Gifkins, 1976] As is shown below, good elongations are always the result of high m-values no matter what the precise value of m is; but, the presence of a high m-value is a necessary but not a sufficient condition for good elongations. Ceramics exhibiting $m = 1$ can have low elongations due to premature, intergranular failure [Sherby and Wadsworth, 1989] and elongations in metals are lowered by the development of grain boundary voids called cavitation [Pilling and Ridley, 1987].

Table 2.2. Compilation of the different creep mechanisms with their average m-values.

Mechanism	Average m
Power-law, climb	0.15-0.25
Power-law, glide	0.25-0.35
Grain boundary sliding	0.5-1.0
power-law breakdown	<0.15
Harper-Dorn Nabarro-Herring Coble	1

The reason that high m-values can confer good elongations is shown in Fig. 2.1. If it is assumed that the gage of a tensile sample already contains a neck (a region of decreased cross-sectional area in the gage), then the true streses in the necked and unnecked regions are different by the factor of the decreased area. The values of stress in the two regions are arbitrarily chosen and shown on the $\sigma-\dot{\varepsilon}$ plot. The curve with the small slope has the low m-value and it can be seen that the difference in strain rates when the m-value is low is much greater than that where m is high. Thus further development of the neck is much more rapid in the low m-value material and as a result the total elongation is much less. One point to make is that high values of m generally do not confer resistance to neck formation, but only to the rate of neck development. The exception is when $m = 1$ (Newtonian viscous flow). During a tensile test this results in change of the cross-sectional area in the gage that is independent of area anywhere in the gage, *i.e.* no necking.

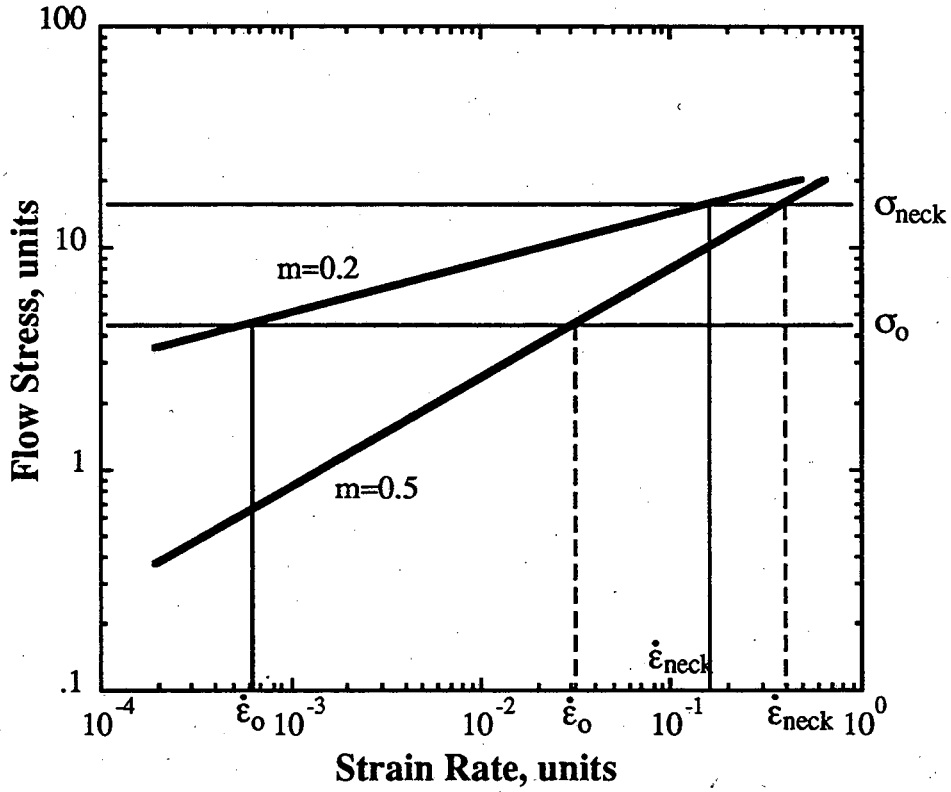

Figure 2.1. Schematic illustration of the effect of m on the variation of strain rates in a tensile gage containing a neck. The low m response results in a much greater disparity in the strain rates between the two regions of the gage resulting in a lower total elongation.

2.4 Creep Mechanisms

2.4.1 Power-law creep

Power-law creep (PLC) or recovery-controlled creep is the most common creep mechanism and occurs when the rate of deformation is controlled by the rate of recovery of dislocations [see General Creep References]. The rate of recovery is controlled by the climb velocity which is controlled by the diffusion of vacancies to the dislocations, so $Q = Q_l$. In addition, m = 0.15-0.25 depending on the type of test used to generate the data (tensile or shear) [Bradley and Morris, 1992] and it is generally reported that $p = 0$.

2.4.2 Power-law breakdown

This occurs at creep stresses above those where PLC is observed. It is believed that the rate-controlling process at these high stresses is the generation of dislocations, not the velocity of the dislocations in the lattice, and thus is similar to low temperature deformation mechanisms [Goodman *et al.*, 1981 and Nix and Gibeling, 1985]. It has $Q < Q_l$, decreasing m with increasing strain rate, and little or no grain size dependence.

2.4.3 Viscous glide creep

This is a less commonly observed mechanism of creep and occurs when the rate of deformation is controlled by the glide velocity of dislocations. Here solutes interact with the dislocations and take up positions around the core that inhibit the movement of the dislocation. If the stress on the dislocations is high enough, they can break away from the solutes and cause normal power-law creep or power-law breakdown occur [Yavari and Langdon, 1982]. Otherwise, both the glide and climb velocities are limited by the rate of diffusion of vacancies to the solutes around the dislocations. For this mechanism $m = 0.25$-0.35 and Q_l = lattice diffusivity of the solute species in the solvent.

One alloy system that readily exhibits viscous glide creep is the Al-Mg system. Mg has a large misfit in Al yet has a high solubility, which makes viscous behavior easy to observe. Mohamed [1983] has pointed out that any solute which interacts in any way with a dislocation has a potential to cause viscous glide behavior. These include the Snoek, Suzuki, Fisher, and anti-phase boundary interactions. Most of the studies on these alloys were performed on large grained materials and no grain size dependence on the flow stress was observed. However, Lee *et al.* [1992] reported that the breakaway stress decreased slightly with smaller grain size.

2.4.4 Harper-Dorn creep

This process is controlled by the diffusion of vacancies through the lattice to edge dislocation segments [Mohamed *et al.*, 1973]. It is usually seen only at very high temperatures ($T_H > 0.9$) and has a $Q = Q_l$, $m = 1$ and a grain size dependence of $p = 2$. Although it sounds very similar to power-law creep, it has been found to have a constant dislocation density with stress and to only occur at very low stresses.

2.4.5 Nabarro-Herring creep

This process involves the diffusion of atoms through the lattice from the sides of grains to the ends of grains [Herring, 1953]. The ends of the grains are under more of a tensile stress that the sides, so there exists a difference in the chemical potentials between the two regions that drives the redistribution of atoms. This mechanism has a $Q = Q_l$ and $m = 1$ and a grain size dependence $p = 2$. Normally, this mechanism is observed at small strain rates that are not a viable for superplastic deformation. In addition, even if the Nabarro-Herring creep strain rate is reasonably fast to begin with it must decrease with increasing strain due to the grain elongation that results from this mechanism. The increased diffusion distance that results lowers the strain rate at a given stress and causes the process to slowly extinguish itself.

2.4.6 Coble creep

This process is identical to Nabarro-Herring except that the movement of atoms is along the grain boundaries [Coble, 1963]. As a result, $Q = Q_b$, $m = 1$ and $p = 3$. It is usually observed at lower temperatures where grain boundary diffusion is dominant and suffers from the same problems mentioned above for Nabarro-Herring creep in being utilized for superplastic forming.

2.4.7 Grain boundary sliding creep (Superplasticity)

This creep mechanism occurs when grain boundary sliding (GBS) is the rate-controlling step of deformation. Because this mechanism is associated with large strains-to-failure it is sometimes referred to as superplastic creep. The definition of superplasticity is not precise, but is usually taken to mean that a material has $m \geq 0.4$ and is capable of large strains to failure (> 500%). A microstructure of equiaxed, fine grains (< 15μm) facilitates GBS [Edington, *et al.*, 1976 and Mukherjee, 1979]. Materials which exhibit superplasticity have low flow stresses and are highly resistant to developing processing defects due to their excellent ductility. GBS is not self-extinguishing like the diffusion mechanisms listed above because the grain morphology is preserved during deformation. In addition, it is observed at strain rates much higher than the other creep mechanisms that have high values of m and is utilized as a forming process, unlike the other creep mechanisms.

The engineering advantage of superplastic materials is that with a low flow stresses they are able to be shaped using inexpensive dies and forming equipment [Edington, 1976]. The excellent ductility allows large strains to be sustained during

forming and this permits parts of great complexity to be fabricated with greatly decreased use of fasteners or welding [Sherby and Wadsworth, 1984 and Hahn, 1991].

2.5 Interaction of simultaneous deformation mechanisms

The different deformation mechanisms described above act either in parallel or in series with each other. The parallel processes sum together to produce the overall creep rate as shown below

$$\dot{\varepsilon}_T = \sum_i \dot{\varepsilon}_i . \tag{2.9}$$

In series one gets

$$\frac{1}{\dot{\varepsilon}_T} = \sum_i \frac{1}{\dot{\varepsilon}_i} \tag{2.10}$$

which rearranged becomes

$$\dot{\varepsilon}_T = \frac{\prod_i \dot{\varepsilon}_i}{\sum_i \dot{\varepsilon}_2} \tag{2.11}$$

If the processes act in parallel, then the fastest one will be rate-controlling. For two serial mechanisms, when $\dot{\varepsilon}_1 >> \dot{\varepsilon}_2$, then $\dot{\varepsilon}_T \approx \dot{\varepsilon}_2$ and the slowest one is rate controlling.

Processes in parallel always result in a high m-value mechanism giving way to a low m-value mechanism at higher stresses. This is shown in Fig. 2.2 where the hypothetical stress-strain rate curve is shown along with the extrapolation of the individual processes and shows that the fastest process is dominant. Contrast that with the change from high m to low m which necessarily implies that the processes are in series since the slowest process is dominant.

The above analysis is taken on a continuum level. At the atomic level, a first approximation is that creep processes that utilize the same defect are always competitive and so must be in series. For example, dislocation creep processes are either climb or glide controlled. They cannot be both since climb and glide are sequential processes of the moving dislocations. However, different grains may deform under climb or glide control so that on the atomic level they are in series while being in parallel on the level of grains. For this pseudo-parallel response to be generally possible, the stress necessary to

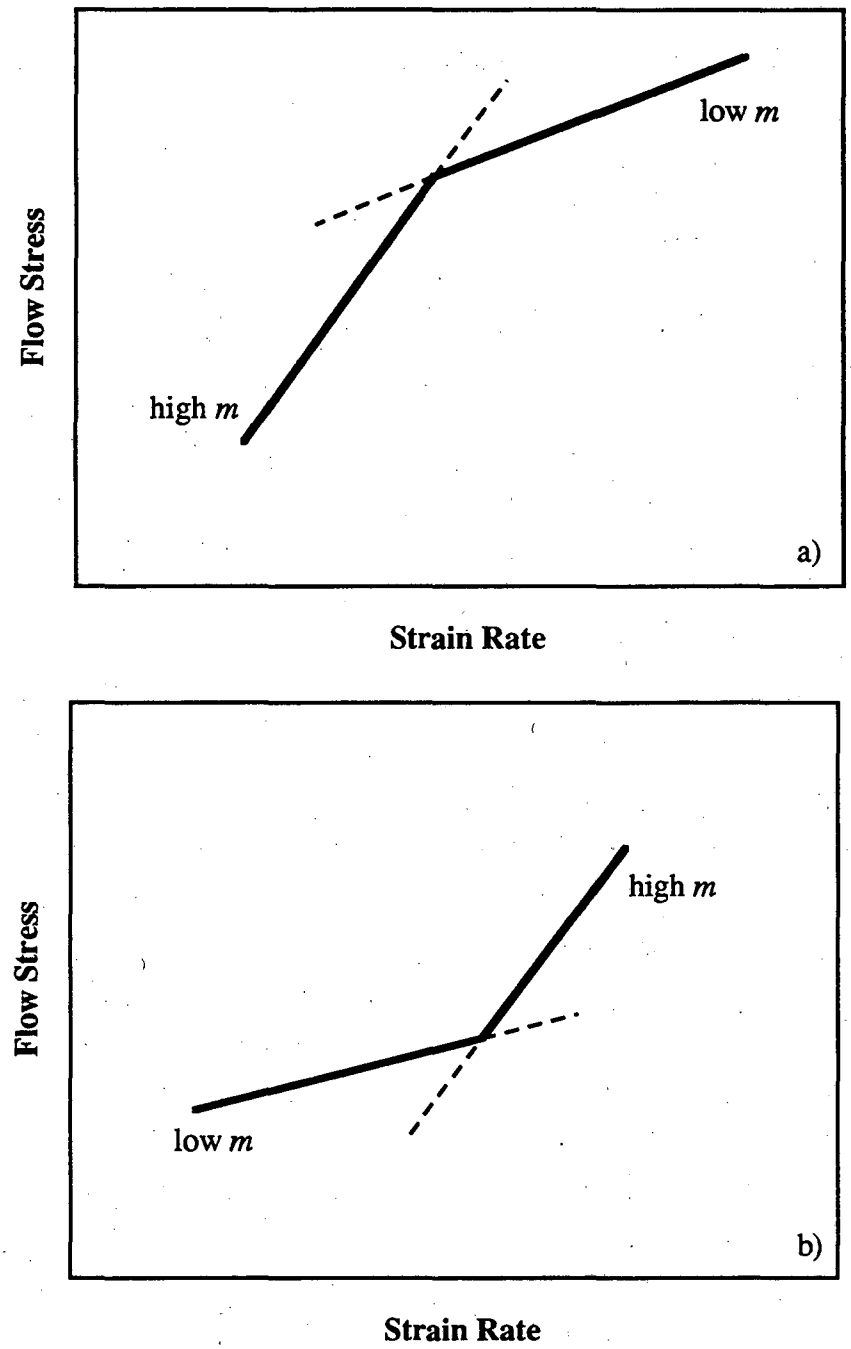

Figure 2.2. Schematics of the stress vs. strain rate response plotted on a logarithmic scale of a microstructure deforming in creep with two processes in a) parallel and b) series.

drive both processes must be comparable. For truly parallel processes, such as GBS creep and PLC, this dual contribution contributes to the overall *m*-value measured for a particular microstructure as shown in the results earlier.

2.6 Aluminum System

2.6.1 Superplasticity of Al alloys

A number of papers have been published on the superplastic properties of Al alloys, especially those with Li [Al-Li Intl. Confs.]. Most of the data cannot strictly be directly compared due to differences in thermomechanical processing (TMP), testing parameters, and choice of data plotted (*e.g.* the strain at which the flow stress is calculated). Even so, there are enough similarities that some generalizations about the properties of these alloys can be established. The optimum strain rate ($\dot{\varepsilon}$ at m_{max}) is around $.001\,s^{-1}$ and the flow stress at this strain rate is around 3 MPa (400 psi). This can vary greatly with forming temperature but is still better than 7475.

2.6.2 Important alloying additives to aluminum

It has been shown that Li is the only known element besides Be (which has not been widely used due to its health risks) that simultaneously raises the elastic modulus and decreases the density of Al [see Al-Li Confs.]. Li has a high solid solubility in Al [Massalski, 1986] and forms the metastable strengthening precipitate δ' (Al_3Li) through a spinodal decomposition on quenching [Khachaturyan *et al.*, 1988].

Magnesium is another element with a high solid solubility in Al [Massalski, 1986]. It is used primarily as a solid solution strengthener and in precipitation hardening in Zn and Cu containing alloys. It slightly depresses both the density and modulus of Al [Hatch, 1984].

Copper is utilized as a potent precipitation strengthener as it forms θ' (Al_2Cu) and ternary phases such as T_1 (Al_2CuLi) and S (Al_2CuMg) [Hardy and Silcock, 1955-56 and Flower and Gregson, 1987].

Zinc is a potent strengthener as it combines with Mg to form G.P. zones in Al [Thomas and Nutting, 1959-60]. It also has a high solubility in Al and depresses the modulus and density [Hatch, 1984].

3. EXPERIMENTAL PROCEDURE

3.1 Material Preparation

Alloys of the composition shown in Table 3.1 were tested. Most of the alloys were cast in a special melting facility constructed at LBL [Emigh, 1990]. This facility allows production of Al-Li alloys by utilizing vacuum induction melting and argon gas flushing for the removal of dissolved gases. A water-cooled chill mold solidified the alloy at approximately 5-10°C/s (9-18°F/s) and kept the scandium partially in a solid solution. Two other alloys (Al-2.7Mg-0.5Sc and Al-8.3Zn-0.5Sc) were fabricated at LBL by tungsten arc casting furnace in an Ar atmosphere.

Table 3.1. Composition (in weight percent) of the alloys used in this study.

Mg	Li	Sc	Zn
-	-	0.5	-
-	1.2	0.5	-
2.7	-	0.5	-
2.4	1.8	0.5	-
-	-	0.5	8.3
-	-	-	-
-	1.3	-	-
2.9	-	-	-
2.4	1.0	-	-

All of the alloys tested were thermomechanically processed (TMP) by rolling at 400°C (752°F) to a thickness of ~ 2.54 mm (0.1 in.) at true strain reduction increments of 0.25/pass. The rolling strain rate ($\dot{\varepsilon}_R$) varied during rolling but typically started at ~ $1s^{-1}$ and finished at ~ $4s^{-1}$ based on the formula found in Schey [1977]

$$\dot{\varepsilon}_R = \frac{v\left[\ln\left(h_o/h_1\right)\right]}{\sqrt{R(h_o - h_1)}} \tag{3.1}$$

where v = velocity of the outer surface of the roll, h_o = starting plate thickness, h_1 = plate thickness after the rolling pass, R = roll radius. Preserving a constant true strain per pass results in an increase in $\dot{\varepsilon}_R$ since the rolling velocity was fixed and the value of h_o–h_1 decreases as the plate becomes thinner.

Between passes the material was heated for 1800s at 400°C (752°F). After rolling, the material was machined into tensile specimens with the longitudinal orientation parallel to the rolling direction. The specimens had an initial gage lengths of 9.5 mm (0.375 in.), gage widths of 3.8 mm (0.15 in.) and a zero radius at the grip section as shown in Fig. 3.1.

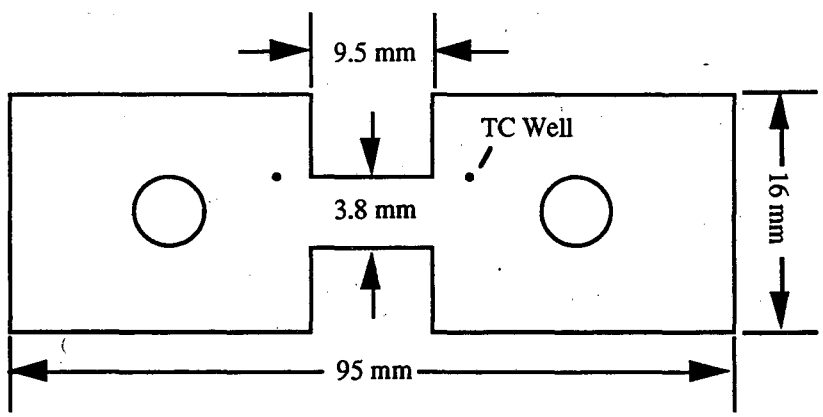

Figure 3.1. Schematic representation of the tensile specimen used in this study.

3.2 Tensile Tests

All tensile specimens were tested in air in a three-zone, Satec clamshell-type resistance furnace after being placed in the furnace for 2700s (45 min.). The temperature at the sample rose to within 20°C (36°F) of the test temperature within 300s (5 min.) and was fully equilibrated at 2700s. The temperature was controlled by three Eurotherm 808 controllers wired in a ΔT configuration with a type-K thermocouple at the center of each zone. This resulted in a constant temperature zone of several inches in the center of the

furnace. The variation in temperature along the gage was less than 2°C (3.6°F) and was measured by thermocouples placed in the specimen at both the grips (Fig. 3.1). The variability of the temperature during the test at any one point was less than 2°C (3.6°F) as also measured by those same thermocouples. The variability in temperature between tests was believed to be less than 2°C (3.6°F) based on the fact that the set point used at any given temperature was always within ±1°C of the value used for all tests and the temperatures measured by the thermocouples correlated with those of the controller. Although the thermocouples were not calibrated to a standard, they all came from the same spool of wire and were calibrated against one another.

The specimens were held by grips that utilized both friction and pin loading and were tested at temperatures from 425-560°C (797-1040°F) depending on the composition of the specimen. Two types of testing apparatus were used depending on the type of data desired. The *m*-value data was generated on a screw-driven Instron machine because of the ease of changing the crosshead rate during deformation. The control panel has push buttons corresponding to crosshead rates from 0.05 to 500 mm/min. This allowed the crosshead rate to be changed instantaneously for accurate *m*-value determination.

3.2.1 *m*-value calculation

The *m*-value was measured using the velocity change technique described by Hedworth and Stowell [1971]. The specimens were deformed at a certain velocity (strain rate) at which time the velocity was increased and the specimen was further deformed until a relatively steady state condition was achieved. Because the tests were conducted in tension, a constant load with displacement indicated work hardening and primary creep deformation since the cross-sectional area decreases with strain. Thus, the relative steady state condition was assumed to occur when the load-displacement curve had a negative slope which remained constant. As shown in Fig. 3.2, the steady-state flow stress is extrapolated back to the strain at which the velocity change was made and the *m*-value is calculated by

$$m = \frac{\ln\left(P_E / P_D\right)}{\ln\left(V_2 / V_1\right)} \tag{3.2}$$

where $P_{E,D}$ = load at steady-state at the same strain for different crosshead velocities $V_{2,1}$. This method is much preferred over testing individual specimens to failure and comparing the flow stresses at a given strain. That method requires large number of tests

and may incorporate slight differences in test conditions, (temperature and material homogeneity) that can increase scatter in the data.

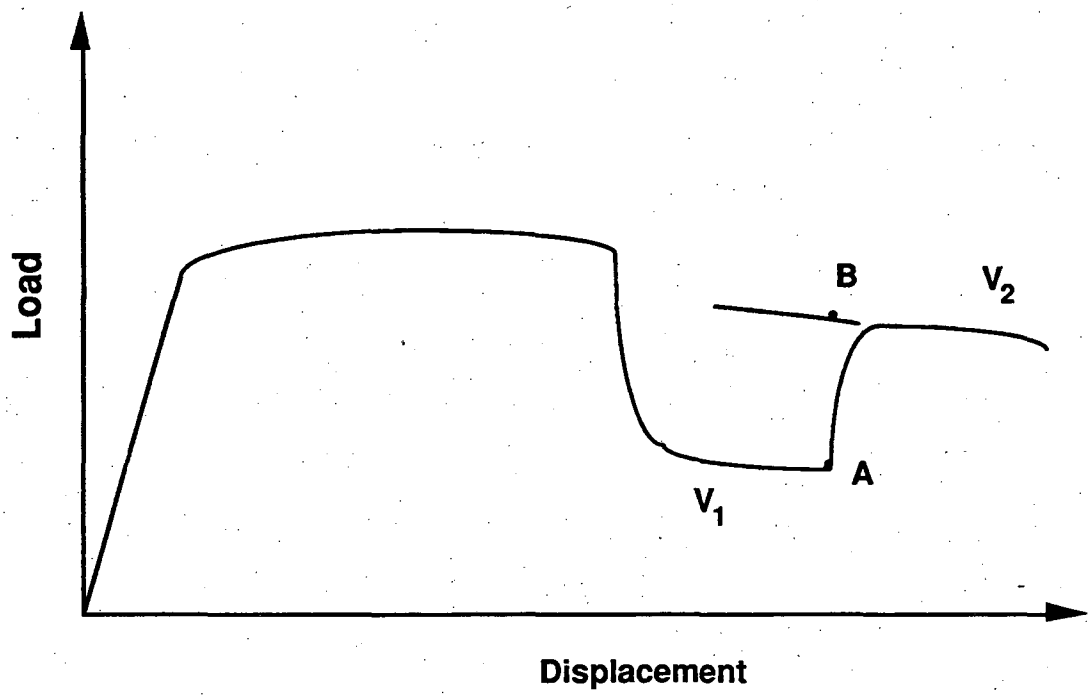

Figure 3.2. Diagram of the velocity change method used to calculate m in this study.

3.2.2 m vs. strain

The m vs. strain tests were carried out by doubling the crosshead velocity (see eq. 3.1) at increments of ~ 0.1 true strain for a period of 0.03 true strain. All specimens were deformed nominally at the strain rate corresponding to the maximum m-value of the material after CRX is completed. For all four Sc alloys this characteristic strain rate was nearly the same and identical crosshead velocities were used on all the specimens ($V = 0.5$ and 1.0 mm/min.). Since the true strain rate drops with strain in constant crosshead velocity tests, Table 3.2 lists the average strain rate at each strain increment for the specimens tested. An ALS specimen was tested at V = 5 and 10 mm/min. to determine the effect of $\dot{\varepsilon}$ on the CRX evolution.

Table 3.2. Average strain rate at each strain increment for the m vs. strain tests.

True Strain	Strain Rate /s
0.1	.00119
0.2	.00107
0.3	.000972
0.4	.000881
0.5	.000797
0.6	.000721
0.7	.000652

3.2.3 m vs. strain rate

The m vs. $\dot{\varepsilon}$ tests were performed on the m vs. strain specimens in order to measure the properties of the fully recrystallized microstructure and to save time and material. Since the evolution of the microstructure occurred over such large strain increments, the specimens were removed from the furnace after a true strain of 0.7 and remachined in order to remove any thinned regions in the gage and to allow for more accurate calculations of m and flow stress at microstructural equilibrium. The specimens were then placed back into the furnace and tested for m vs. $\dot{\varepsilon}$ and flow stress vs. $\dot{\varepsilon}$ data. The data was recorded as load vs. displacement and corrected for change in the gage area and deformation at the grip to get the true stress, true strain and $\dot{\varepsilon}$ during the test. It was assumed the gage deformed uniformly at constant volume.

3.2.4 Work hardening rate and constant strain rate tests

The samples tested for work hardening rate were performed on the Digital Testing Machine (DTM) designed and built at Lawrence Berkeley Laboratory (LBL). The testing program allows different stroke paths to be followed including ramp, square wave, triangle wave, and exponential. The exponential path corresponds to a constant true strain rate test when all of the deformation is restricted to the gage and obeys the following equation

$$y = A\exp(\alpha t) \tag{3.3}$$

where A = starting gage length, α = true strain rate, t = time, and y = relative stroke position at time t. A constant true $\dot{\varepsilon}$ test simulates a creep test where the stress is kept constant. In steady state deformation, both the constant $\dot{\varepsilon}$ and constant stress tests are equal. [Note: Constant engineering strain rate occurs during constant crosshead rate testing where $\dot{e} = \frac{v}{l_o}$ and v (crosshead speed) is constant.]

3.3 Microstructural Analysis

3.3.1 Optical microscopy

The microstructures of the as-cast, TMP, and tensile tested material were mounted in Buehler Transoptic and ground on SiC paper to 600 grit. They were then polished using diamond paste and ethanol on nylon cloth at both 6 and 1 μm sizes. Final polishing was done on Buehler Microcloth with Final Pol, which consists of various types of 0.05 μm size particles suspended in water. The samples were then etched in Keller's reagent (95 ml H_20, 5 ml 70% HNO_3, 2.5 ml 37% HCl, and 1 ml 50% HF) The specimens were then examined on a Nikon metallograph with an inverted stage utilizing either Nomarski interference or polarized light for contrast enhancement. Photomicrographs were taken using Polaroid type 52, 55 and 57 films. The relationship of the metallurgical sections to the rolling plane of the sheet is shown in Fig. 3.3.

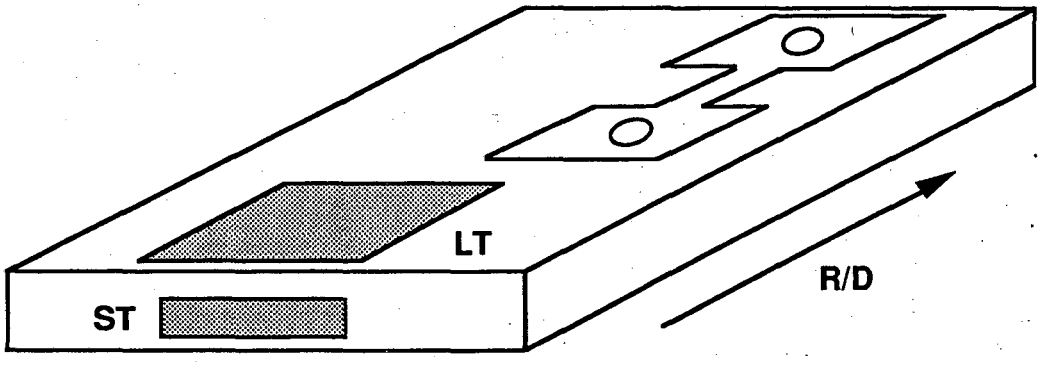

Figure 3.3. Schematic of the as-rolled billet showing the sections examined by optical microscopy relative to the rolling direction and the designation given to each.

3.3.2 Transmission electron microscopy (TEM)

TEM foils were prepared from both the gage and grip sections of Al-0.5Sc, Al-1.2Li-0.5Sc, and Al-2.4Mg-1.8Li-0.5Sc specimens tested at 500°C at a constant true

strain rate of $.0009 s^{-1}$ to true strains of 0.2, 0.4, 0.7 and 1.0. The foil normals were parallel to the sheet normal direction. The sections were ground on SiC paper in water on both sides to produce a blank ~ 250 μm (0.010 in.) thick. The TEM foil blanks were then punched out of the sections and ground down further to ~ 125 μm (0.005 in.). The blanks were then jet electropolished with a Struers Tenupol-2 at a constant voltage of 18V with a solution of 20% nitric acid in methanol at -30°C (-22°F). The foils were examined at 100 kV in a Philips 301 TEM with a double tilt specimen holder.

Measurements of the grain/subgrain size were calculated from TEM negatives taken at 4000X using the mean line intercept method [VanderVoort, 1984]. Fig. 3.4 shows the relative size of the lines and negative. The total line length was 285 mm (11.25 in.) and resulted in ~ 25-35 boundary intercepts for the grip microstructure and ~ 8-25 intercepts for the gage microstructure. No distinction was attempted to distinguish whether the boundaries intercepted were small or large-angle in nature.

Grain boundary misorientations (GBM) were measured by microdiffraction of adjacent grains using the method of Qing [1989]. This method allows a nominal or projected misorientation between grains to be quickly measured. Each grain is tilted to an exact [011] zone axis. By noting the exact angles of the tilt holder at **z**, the misorientation can be calculated using the following equation:

$$\gamma = \cos^{-1}\{\sin(\alpha_2 - \alpha_1)\sin\alpha_1\cos\alpha_1[1-\cos(\beta_2-\beta_1)] + \cos(\alpha_2-\alpha_1)[\sin^2\alpha_1 + \cos^2\alpha_1\cos(\beta_2-\beta_1)]\} \qquad (3.4)$$

where (α_1,β_1) and (α_2,β_2) are the tilt angles for grains 1 and 2, respectively and γ = relative grain boundary misorientation.

Obviously a tilt component in the plane normal to the **z** cannot be measured; however, trends in misorientation can easily be discerned and the speed of the technique is much greater than the graphical method of Goux as described by Edington [1975]. The maximum calculated misorientation using this technique is 35.26° since no effort is made to identify the exact [011] axes observed for each grain in the TEM. For any given [011] type **z**, there are always 4 other [011] **z** only 60° away. Fig. 3.5 is a schematic of a cube showing the ⟨011⟩, ⟨101⟩, ⟨110⟩ vectors. These three vectors form a tetrahedron with the ⟨111⟩ vector as a bisector of the vertex. The ⟨111⟩ vector is equidistant in angular space from all three [011] vectors and lies 35.26° from each of them. Thus this is the maximum misorientation angle that can be measured using this technique.

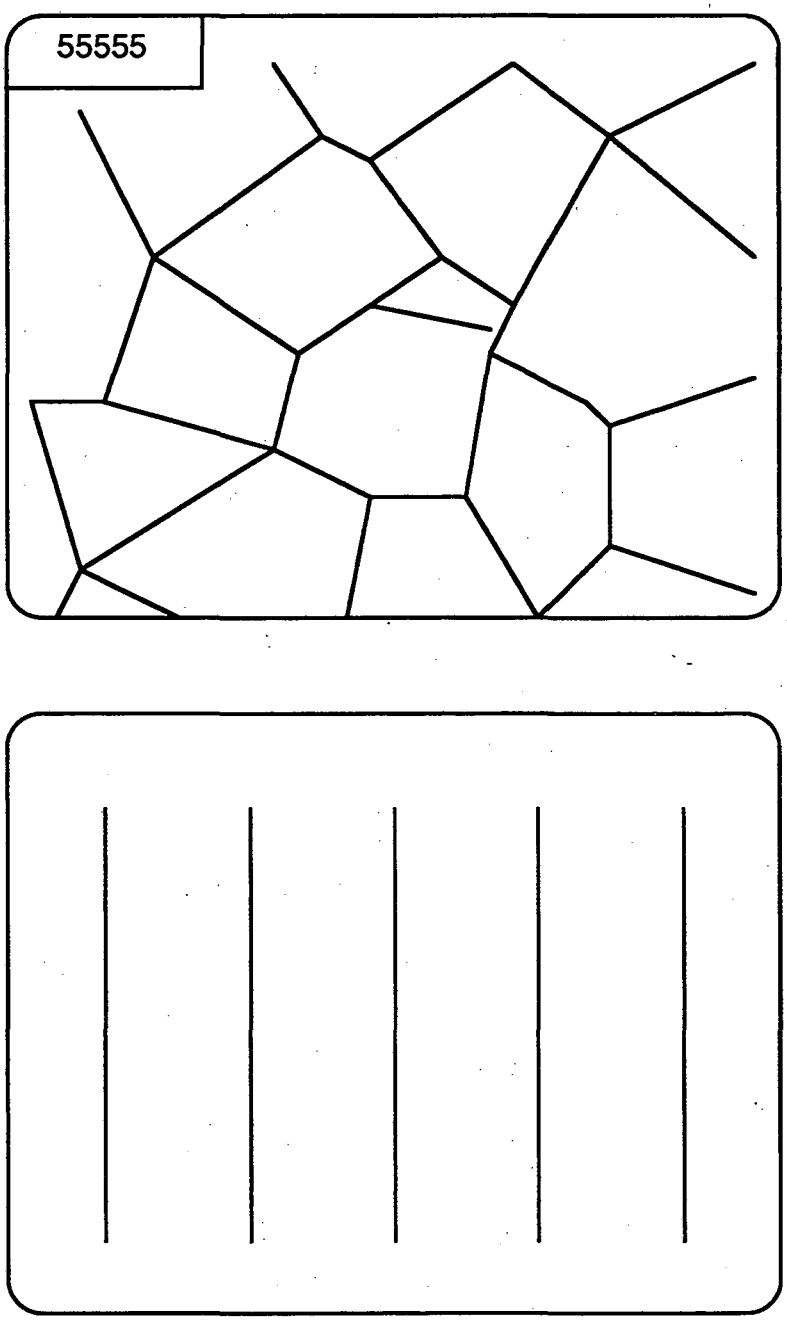

Figure 3.4. Schematic showing the relationship between the intercept lines and the negatives used to calculate the grain size from the TEM foils.

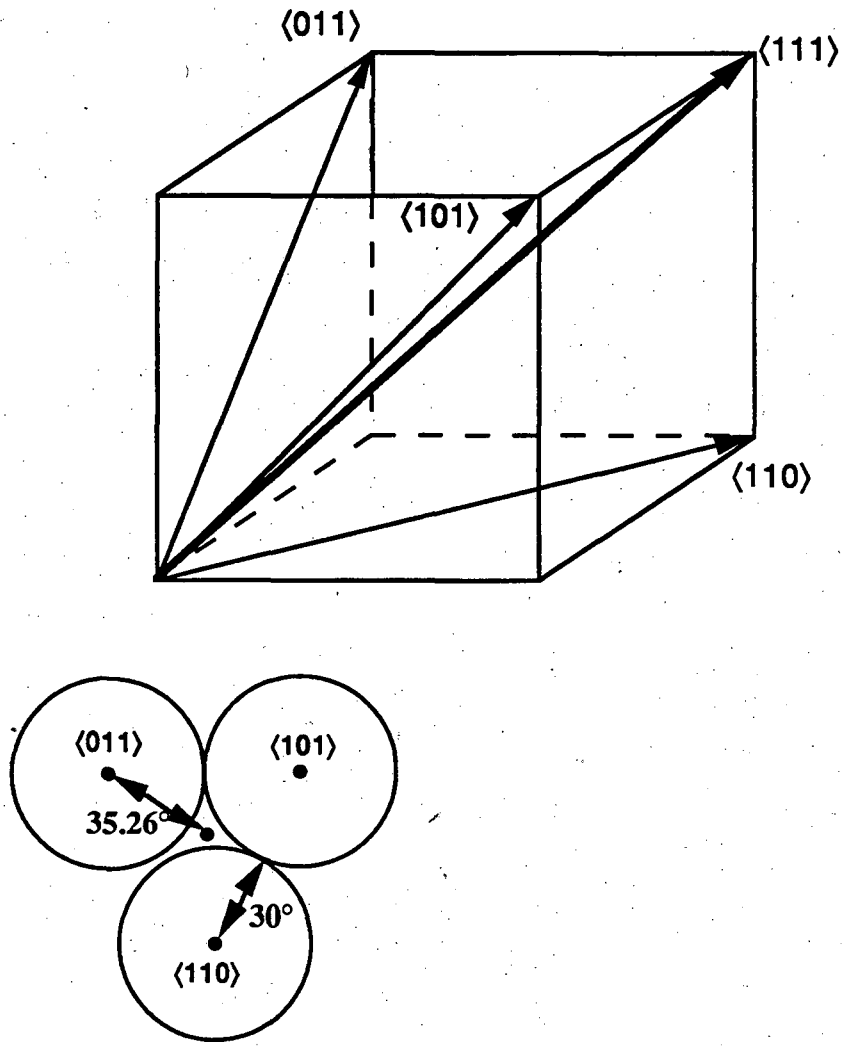

Figure 3.5. Schematic of the maximum angles that can be measured using the technique of Qing for [011] zone axes.

3.3.3 Scanning electron microscopy (SEM)

Scanning electron microscopy was used to study the failure mechanism of the alloys by examination of the fracture surfaces. The microscope was operated at 20 kV with a working distance of 30 mm.

4. RESULTS

4.1 Microstructure Prior to Creep Deformation

4.1.1 Al-0.5Sc (AS)

The AS alloy was TMP from an ingot consisting of a eutectic microstructure very similar to the one shown later for Al-Li-Sc. The microstructures in the LT and ST planes after rolling are shown in Fig. 4.1. Residual eutectic structure is still seen in the LT plane and the overall microstructure is messy and not well defined after etching. The view of the ST plane shows that there is a pancake-type microstructure as the visible grains are thin and wide.

TEM of the as-rolled and annealed microstructure from the grip sections of the tensile specimens show that there is a subgrain structure that is somewhat equiaxed in nature (Fig. 4.2). The grains contain relatively large, incoherent Al_3Sc precipitates (~ 0.1 μm) and very few of the small, coherent Al_3Sc precipitates (Fig. 4.3). These precipitates have the $L1_2$ structure and are coherent when formed from a supersaturated solid solution [Drits *et al.* 1985], but are obviously incoherent when formed during solidification or after coarsening to a large size. No other precipitates were seen and none were detected by Emigh with x-ray diffraction (XRD).

4.1.2 Al-1.2Li-0.5Sc (ALS)

The ALS ingot consisted of a region of eutectic microstructure surrounded by equiaxed grains as depicted in the schematic in Fig. 4.4. The eutectic microstructure is shown in Fig. 4.5. The outer region was removed from the remaining ingot and the completely eutectic microstructure was TMP and tested. After TMP, the rolled eutectic microstructure was very similar to that of the AS alloy. Fig. 4.6 is the LT plane as-polished and shows the lack of intermetallics with the exception of a lone ν-phase particle. The ν-phase is a ternary phase in alloys containing Li and Sc that has been identified as having a composition of $Al_3(Li_{0.5},Sc_{0.5})$. It has the $L1_2$ structure and is insoluble up to the solidus temperature [Emigh *et al.*, 1992] The Al_3Sc precipitates were large and incoherent like those in the AS alloy. The remaining Li was in solution as no δ' (Al_3Li) was observed.

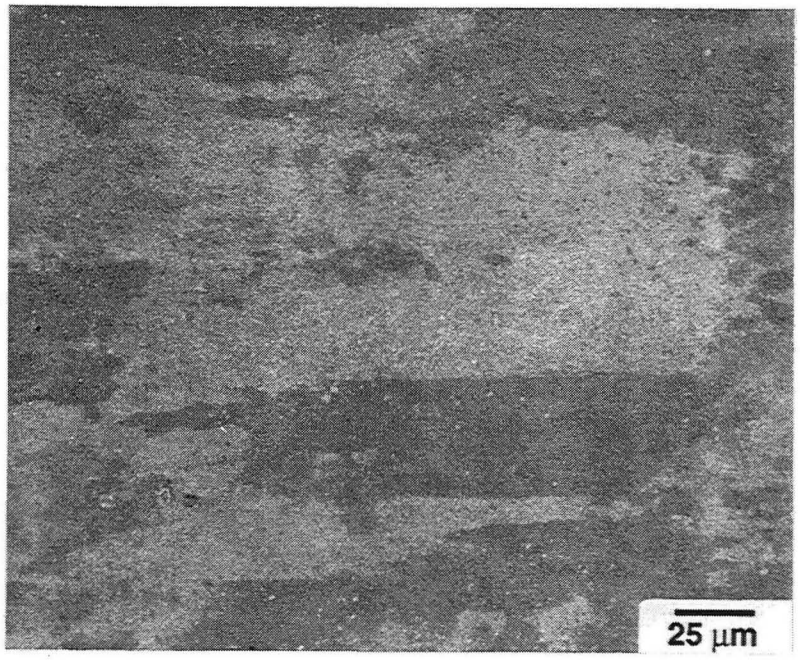

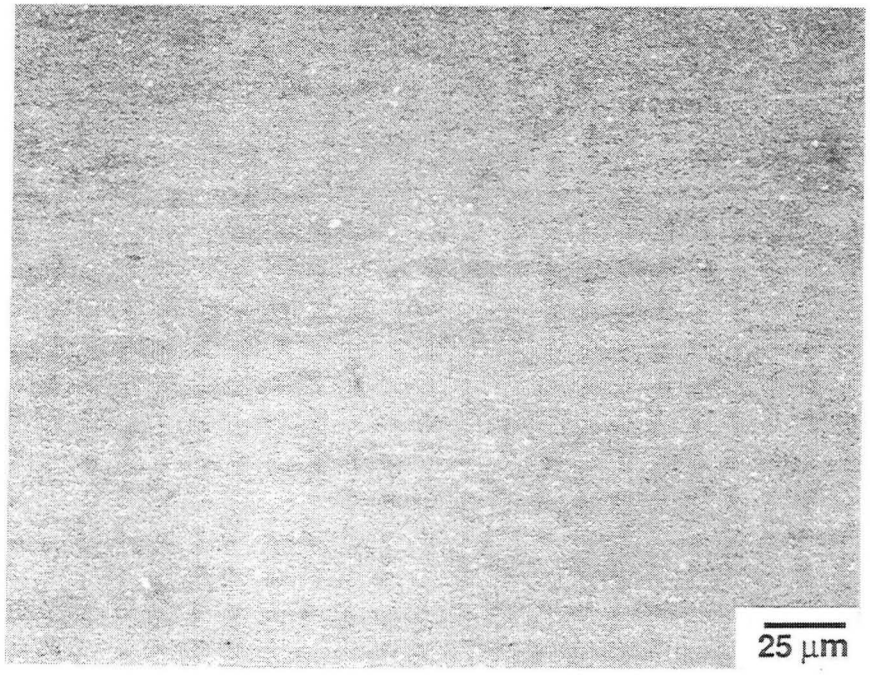

Figure 4.1. Polarized optical micrographs of the as-rolled AS alloy in both the LT and ST planes. Samples were etched for 180 seconds in Keller's reagent. [XBB 931-454 and 933-1715]

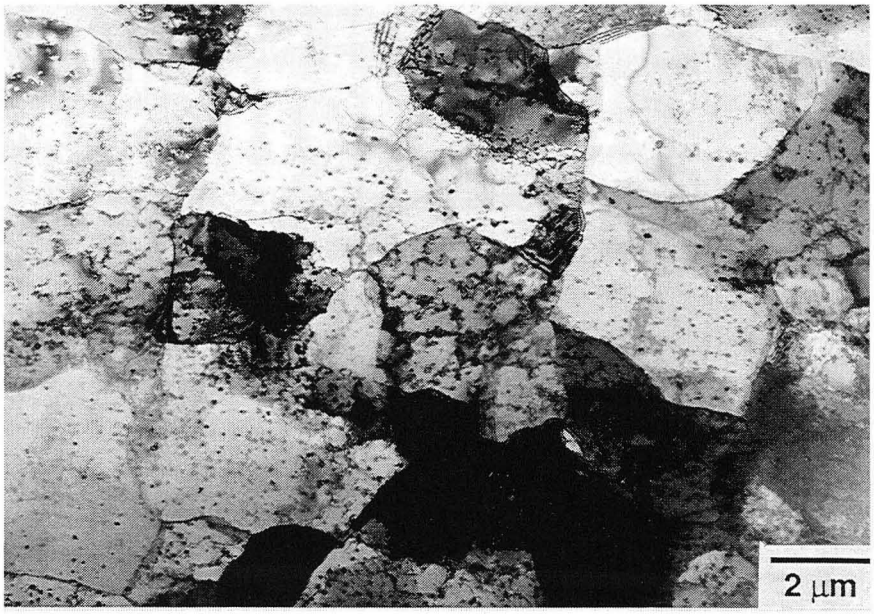

Figure 4.2. Bright field TEM micrograph of the as-rolled AS microstructure in the LT plane showing the more equiaxed nature of the subgrains. [XBB 932-501]

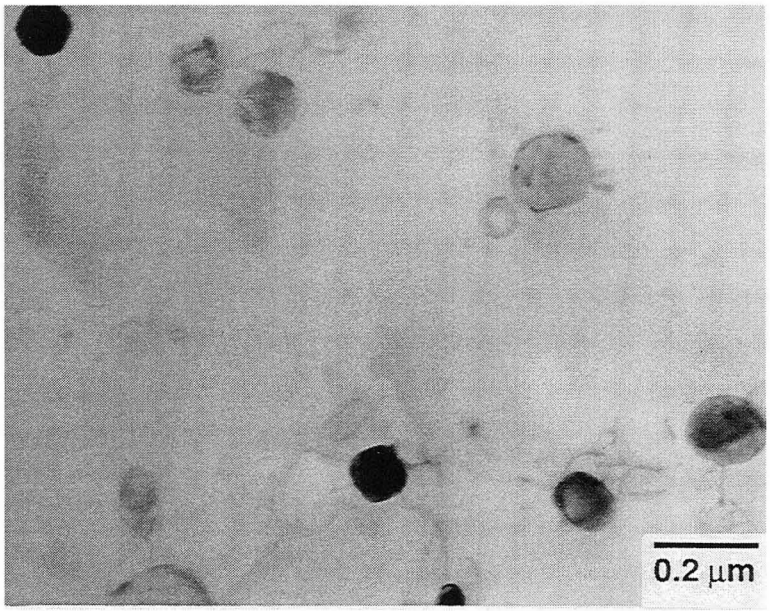

Figure 4.3. TEM micrograph of Al_3Sc precipitates in the AS alloy. [XBB 932-499]

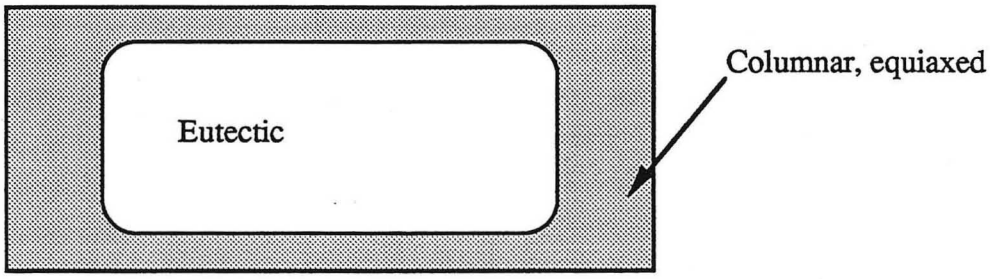

Figure 4.4. Schematic of the distribution of the equiaxed-columnar and eutectic microstructures in the ALS ingot.

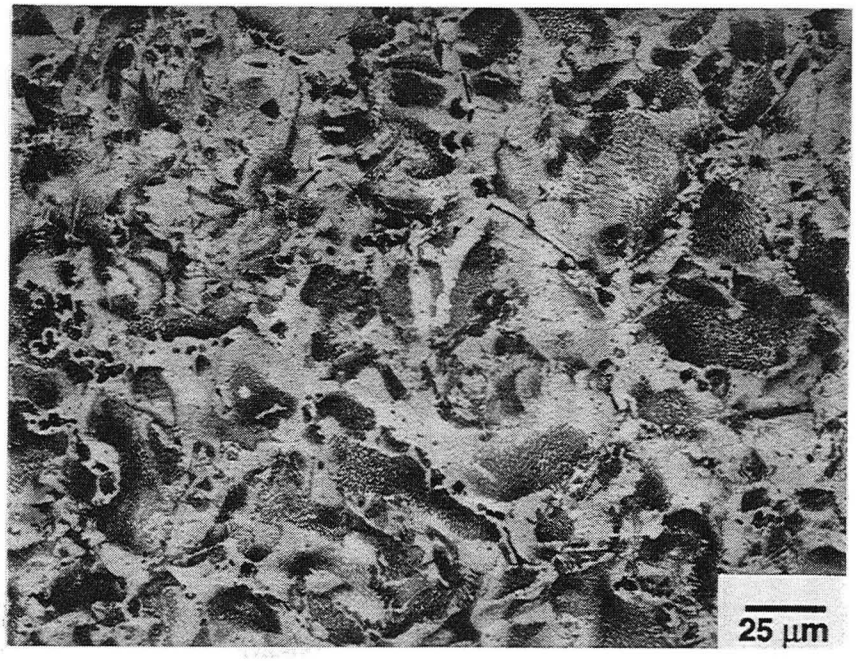

Figure 4.5. Optical micrograph of the eutectic region in the ALS ingot. [XBB 931-457]

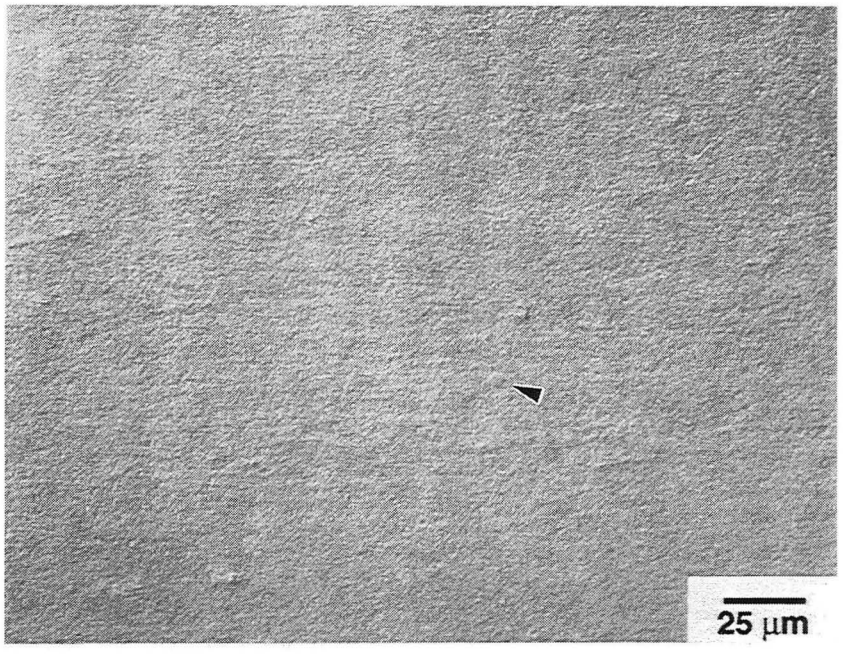

Figure 4.6. Optical micrograph of the as-polished ALS alloy in the LT plane showing a lone ν-phase particle. Image was taken with Nomarski interference contrast. [XBB 931-456]

4.1.3 Al-2.7Mg-0.5Sc (AMS)

The as-cast microstructure, shown in Fig. 4.7, is a mixture of dendrites and equiaxed grains. This material was produced in the tungsten arc casting furnace. After TMP the microstructure resembled that of the AMLS alloy.

4.1.4 Al-2.4Mg-1.8Li-0.5Sc (AMLS)

The AMLS alloy had an equiaxed, as-cast microstructure (Fig. 4.8) although the grain size increased towards the center of the ingot due to the slower solidification rate. There was ν-phase present at the as-cast grain boundaries. After TMP the ν-phase was broken up and distributed in the LT plane as shown in the as-polished microstructure in Fig. 4.9. Quantitative metallography indicates that the ν-phase is present at ~ 1.2 vol% in this alloy and in quantities much greater than in the ALS alloy as can be seen in the comparison of Figs. 4.6 and 4.9. The greater volume fraction of ν is due to the higher Li concentration. The maximum theoretical vol% of ν in the AMLS alloy is ~ 2.4% assuming all of the Sc is utilized in ν and none in the Al_3Sc precipitates. The contrast

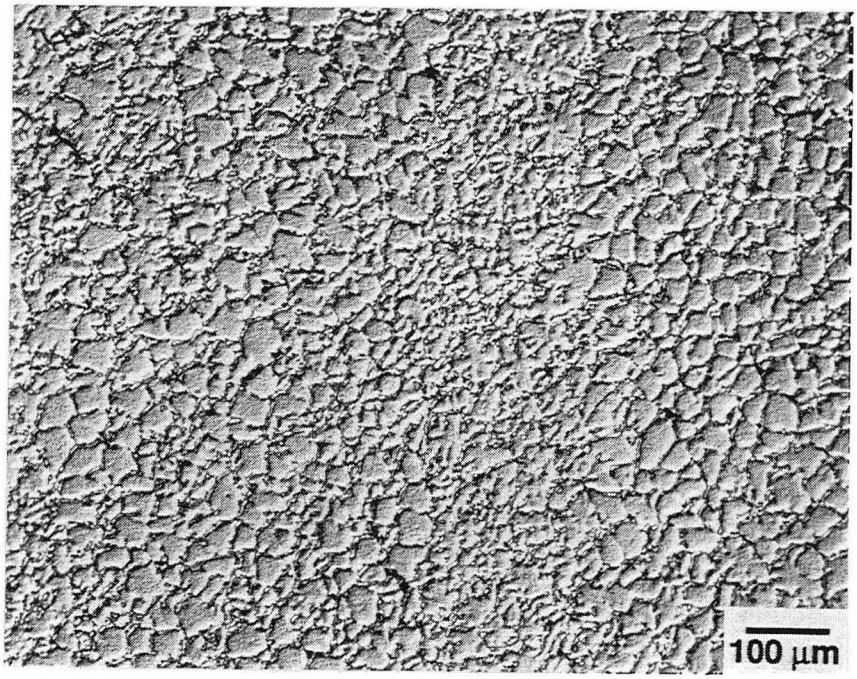

Figure 4.7. Optical micrograph of the as-cast AMS alloy showing the mixed equiaxed and dendritic microstructure. [XBB 932-503]

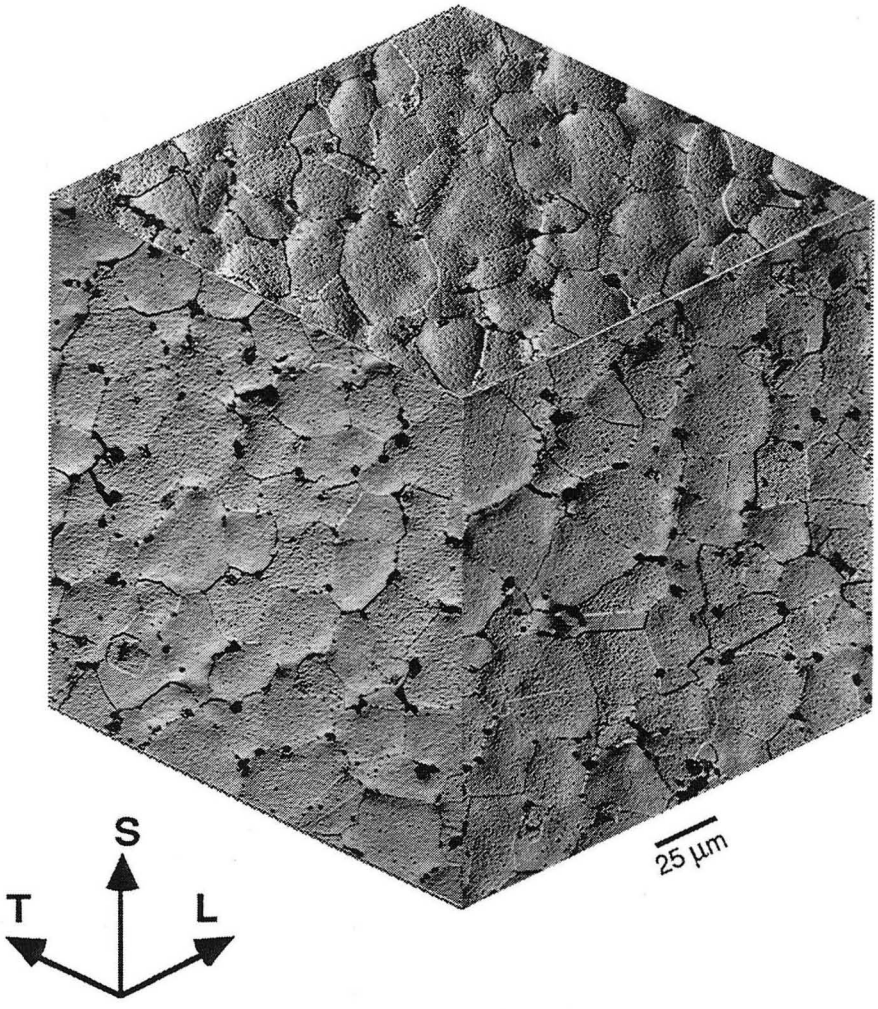

Figure 4.8. Optical micrograph of the as-cast AMLS alloy showing the equiaxed microstructure present throughout the ingot. [XBB 905-3549]

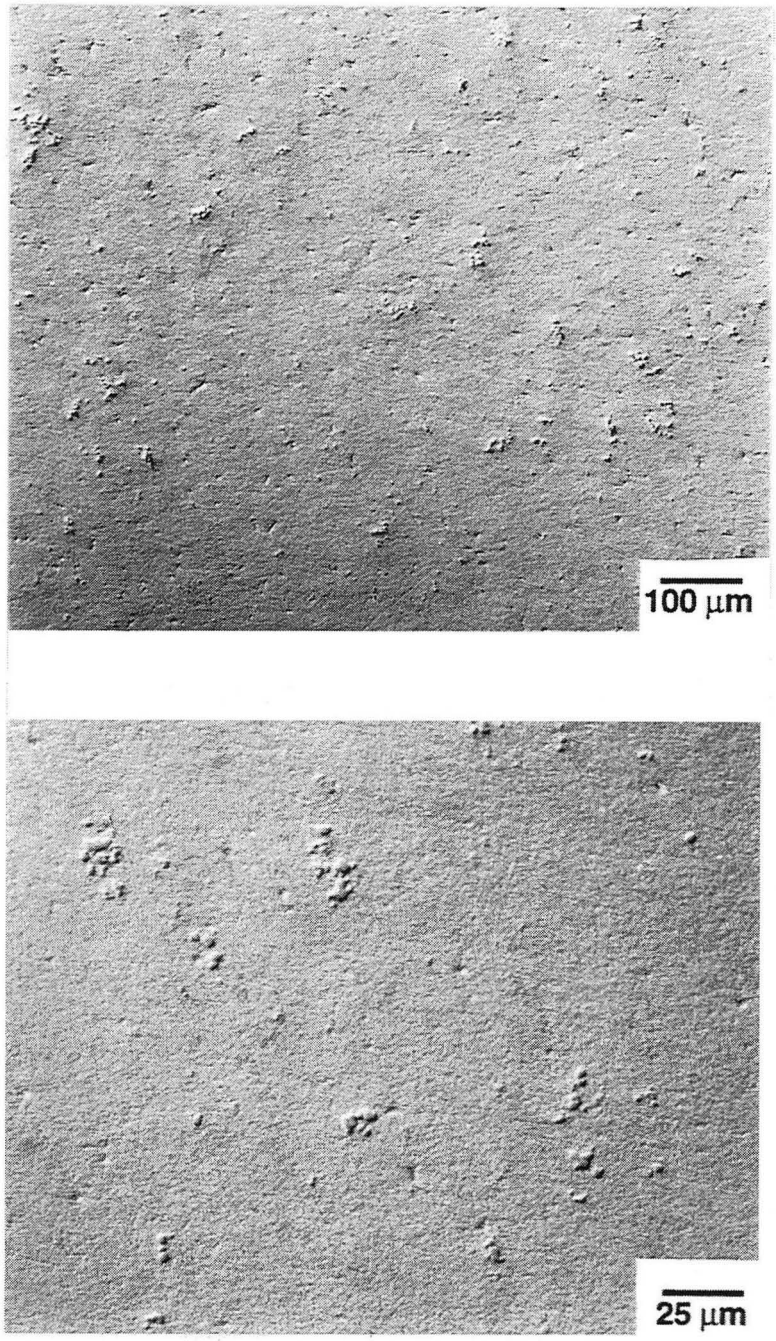

Figure 4.9. Optical micrograph of the as-rolled and as-polished AMLS alloy showing the typical distribution of ν-phase in the LT plane. [XBB 931-450]

fringes in Fig. 4.10 mark the location of the small, coherent Al_3Sc precipitates in the microstructure.

Fig. 4.11 is the etched microstructure of the AMLS alloy after TMP and is the characteristic pancake-type microstructure that results when recrystallization is prevented from occurring during rolling and annealing. Fig. 4.12 is a TEM cube showing the relatively equiaxed subgrains which reside in the pancake grains after rolling and annealing at 500°C for 1800s. It should be noted that the subgrains seen in Fig. 4.12 are not seen in the optical micrographs. The Mg remained in solution from room temperature to 500°C.

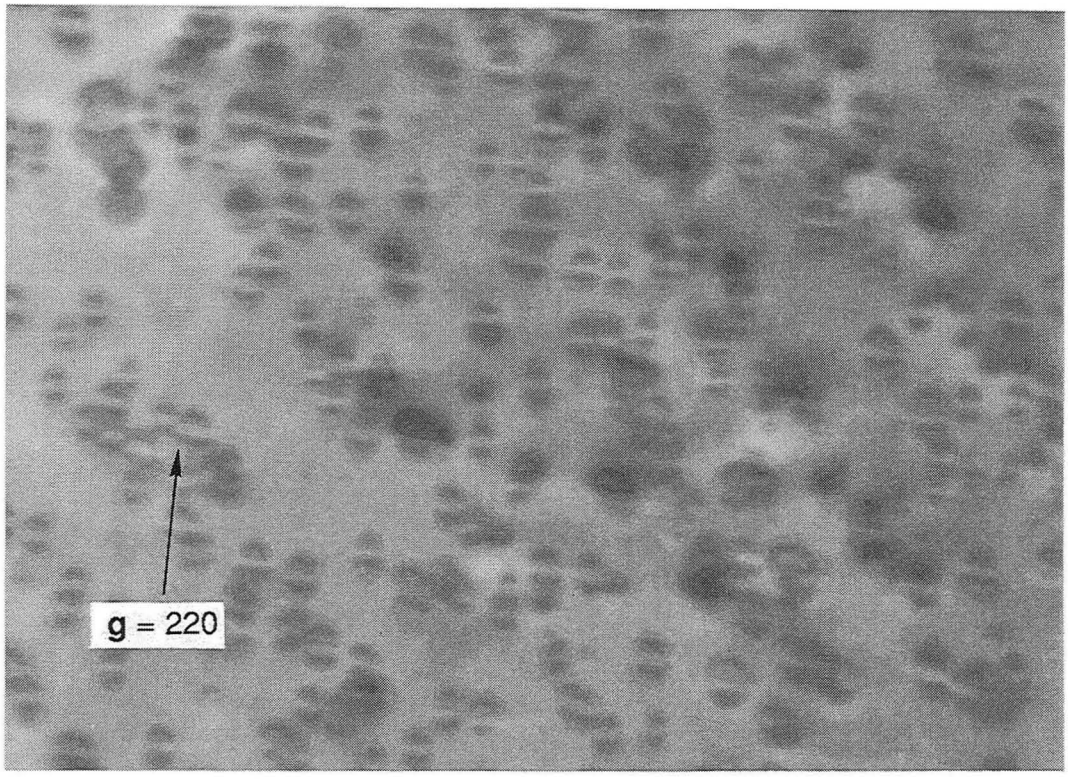

Figure 4.10. TEM micrograph of the Al_3Sc precipitates in the AMLS alloy. The coherency strains give rise to the dark lobes visible in the micrograph. [XBB 932-498]

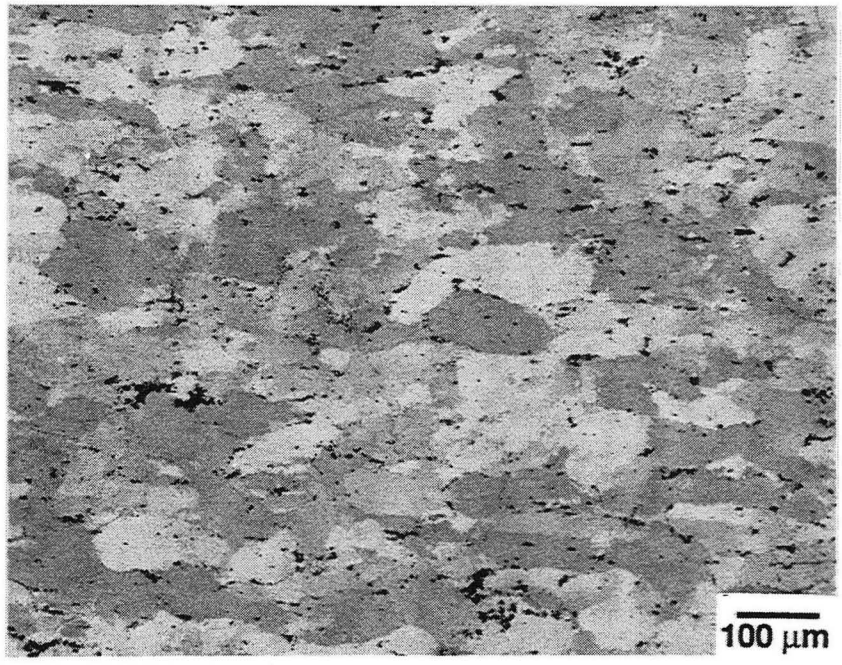

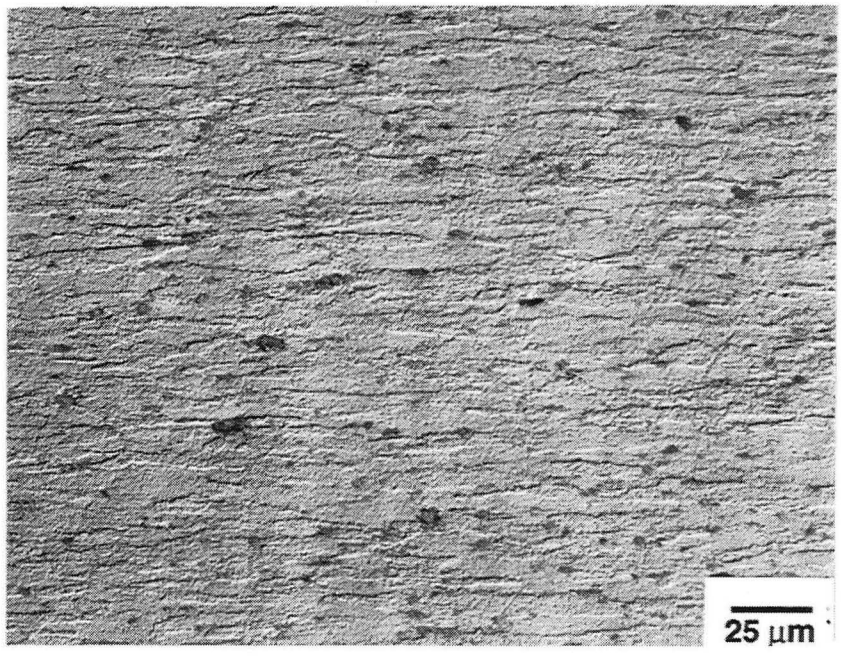

Figure 4.11. Optical micrograph of the as-rolled and etched AMLS alloy showing the pancake-type grains resulting from TMP. [XBB 931-455]

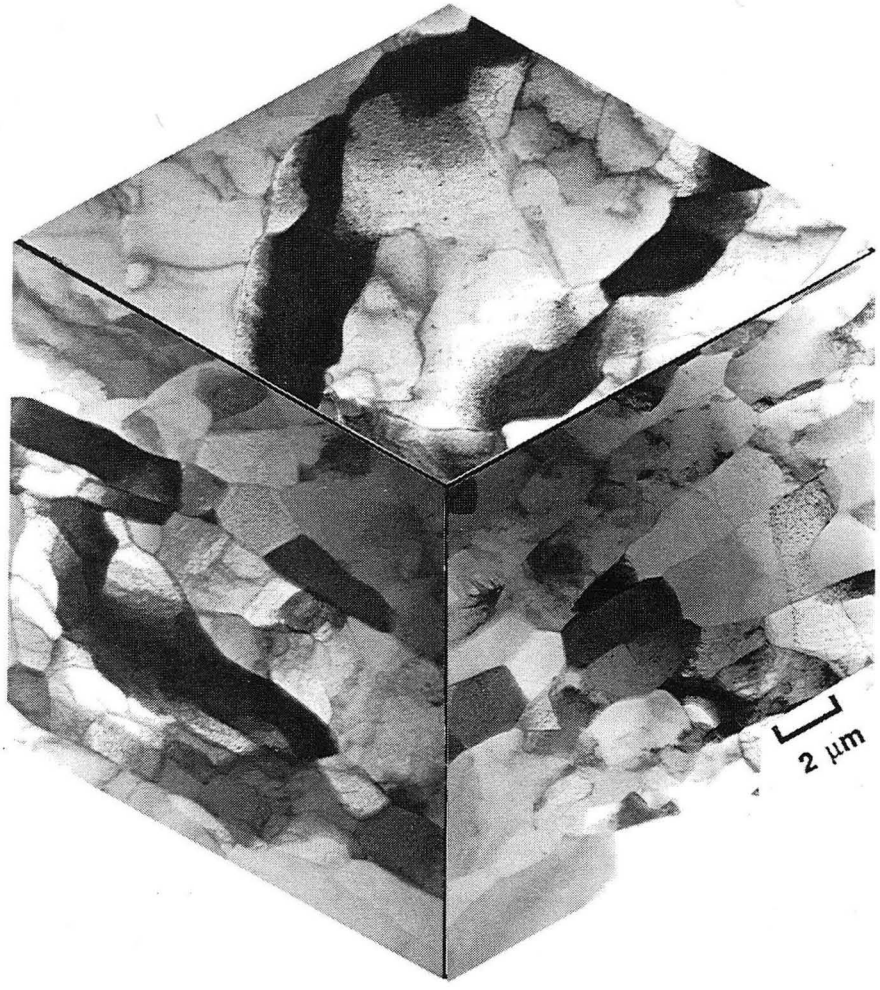

Figure 4.12. TEM cube of the as-rolled and annealed microstructure of the AMLS alloy showing the subgrain structure within the elongated grains. [XBB 912-1127]

4.1.5 Al-8.3Zn-0.5Sc (AZS)

This alloy had a similar as-cast microstructure to that of the Al-Mg-Sc alloy. Very few intermetallics were observed in the as-polished microstructure.

4.1.6 Non-Sc alloys

These four alloys were TMP to a recrystallized condition. Fig. 4.13 shows the microstructure of the Al-2.9Mg alloy and the other non-Sc alloys had similar microstructures. All four alloys were solid solutions at the TMP and testing temperatures.

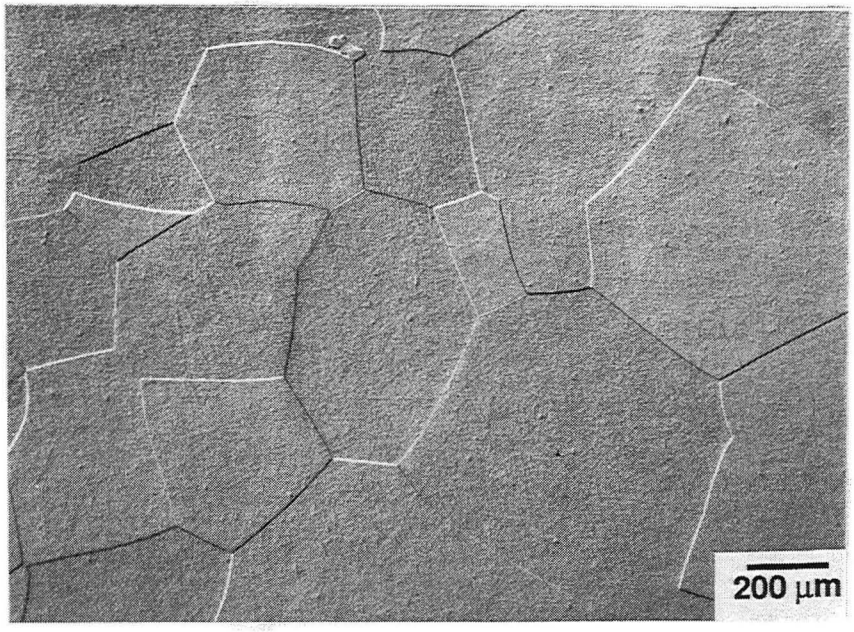

Figure 4.13. Optical micrograph of the Al-2.9Mg alloy after TMP showing the typical recrystallized microstructure characteristic of all of the alloys without Sc. [XBB 931-453]

4.2 Microstructures after Creep Deformation

4.2.1 Grain morphology

Optical micrographs in Figs. 4.14 and 4.15 show that the AS and AMLS alloys do evolve from a rolled microstructure of pancake-shaped grains to one of predominantly equiaxed grains after a true creep strain of 0.7 and a true $\dot{\varepsilon} = 1\text{x}10^{-3}\text{s}^{-1}$ at 500°C. This was also seen in all of the other Sc alloys deformed in creep. The high temperature deformation results in the increase of relative boundary misorientations of the original subgrains in the gage so that they become true grains and are visible upon etching.

The effect of the ν-phase on CRX was observed in the optical micrographs by comparing the regions around ν to those without ν. There was no obvious correlation to the observation of fine grains in the LT plane with the ν-phase. Both large unrecrystallized grains and groups of fine grains were found near ν-phase clumps and in regions away from the clumps.

TEM of the gage and grip sections are shown for the AS (Fig. 4.16 and 4.2), ALS (Fig. 4.17), and AMLS (Fig. 4.18) alloys. The distinct change in morphology of the microstructure with creep strain is evident in all three alloys and agrees with the optical micrographs shown earlier. Quantitative microscopy of the grip and gage sections shows that the grain size evolves to a value over twice as large as the original grip subgrains (5 μm vs. 2 μm) for all three alloys. Grain sizes for the different alloys are shown in Table 4.1 and plotted together in Fig. 4.19. The grip and gage have the same thermal history but different deformation histories, so any difference in the grain morphology is associated with the deformation and not just the thermal activation. The grain size increases rapidly with strain in all of the alloys measured although this begins to level off at around strains around 0.7.

The grain size is stabilized by the presence of the Al_3Sc precipitates. Fig. 4.20 shows the pinning action of the precipitates in both the AS and AMLS alloys. The precipitates are more coarse in the AS alloy but the greater volume faction of precipitate in that alloy over the AMLS alloy results in similar Zener drag coefficients as reflected in the similar grain sizes and misorientations of all three alloys after CRX.

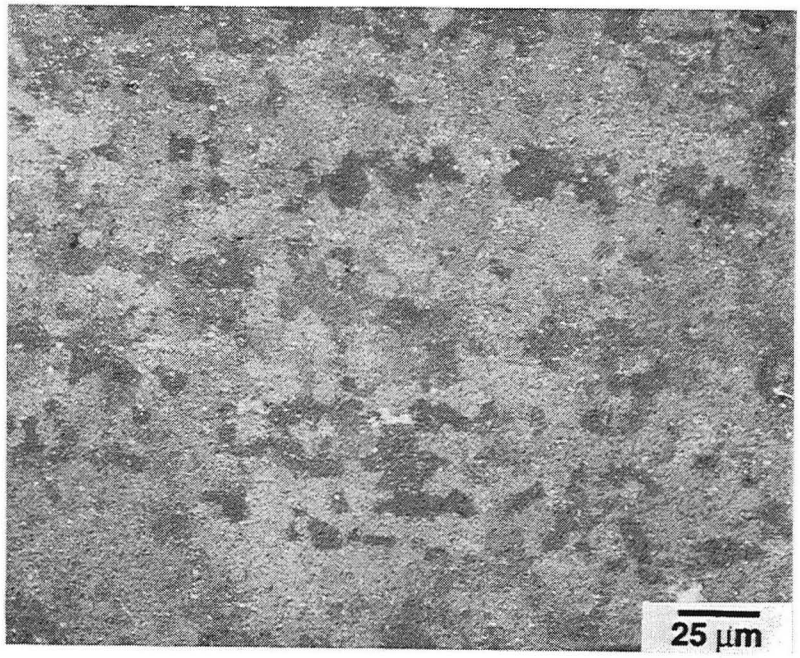

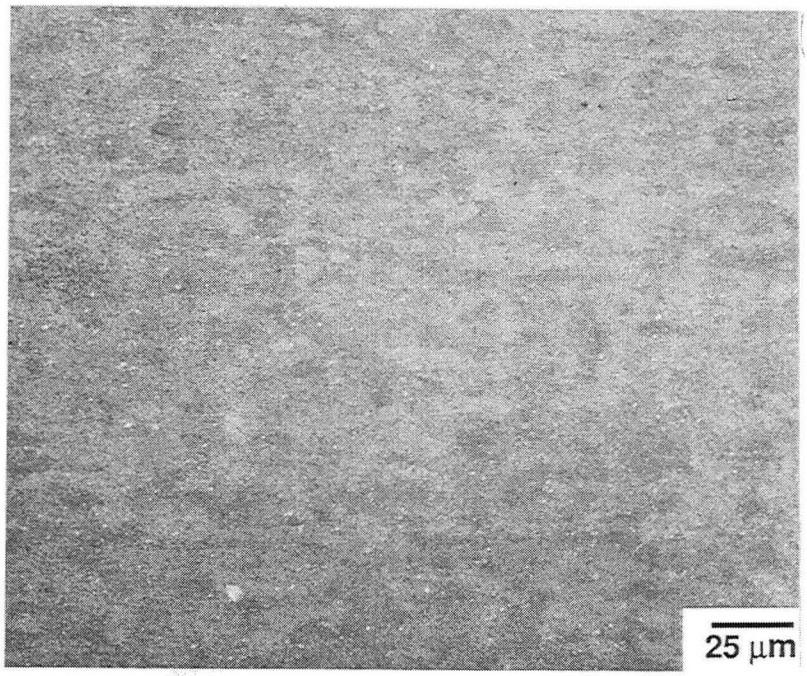

Figure 4.14. Optical micrographs of the AS alloy after deforming to a true strain of 1.2 at 500°C. [XBB 931-454 and 933-1715]

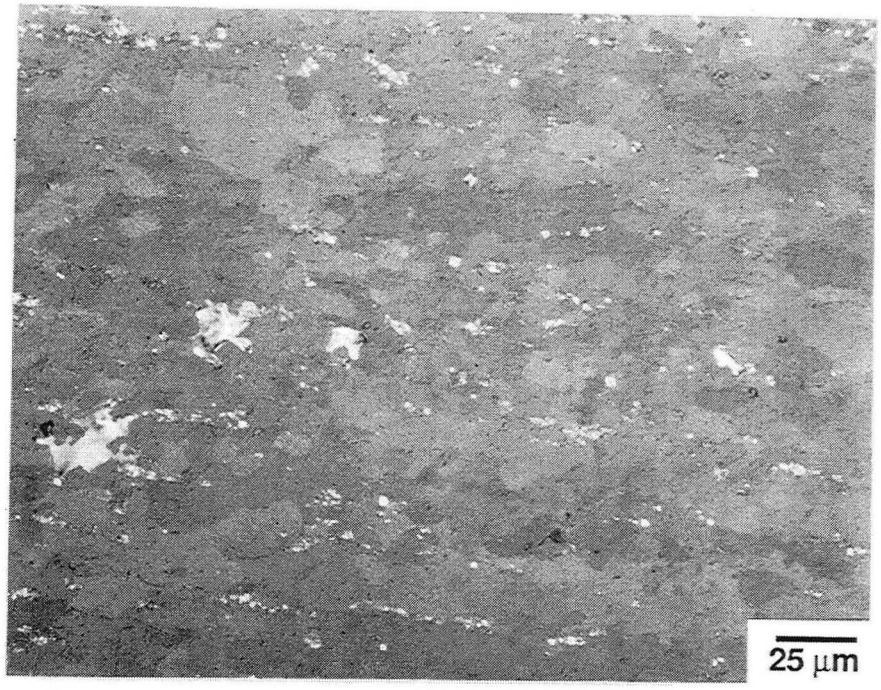

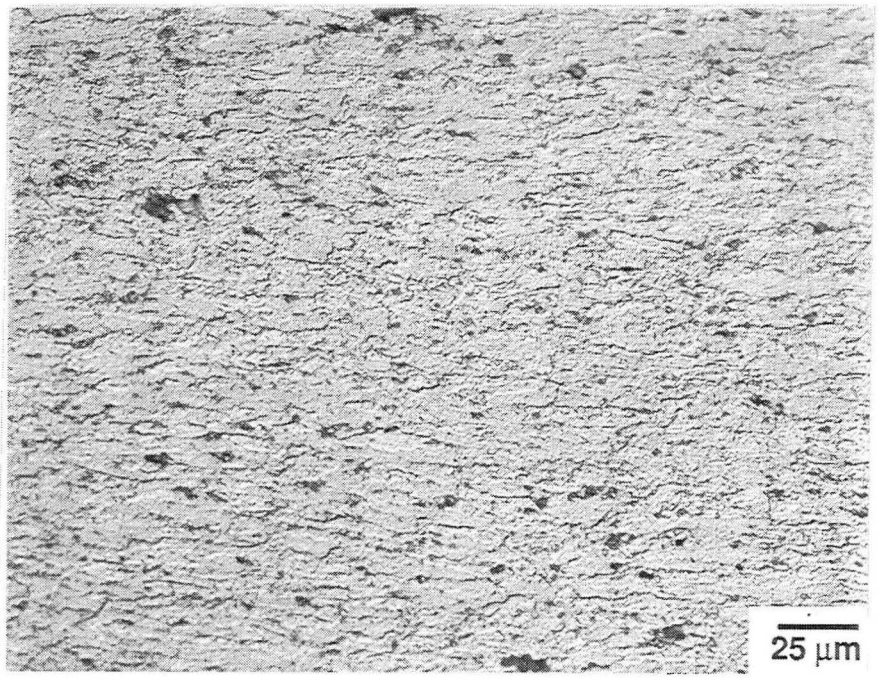

Figure 4.15. Optical micrographs of the AMLS alloy after deforming to a true strain of 1.2 at 500°C. [XBB 933-1717]

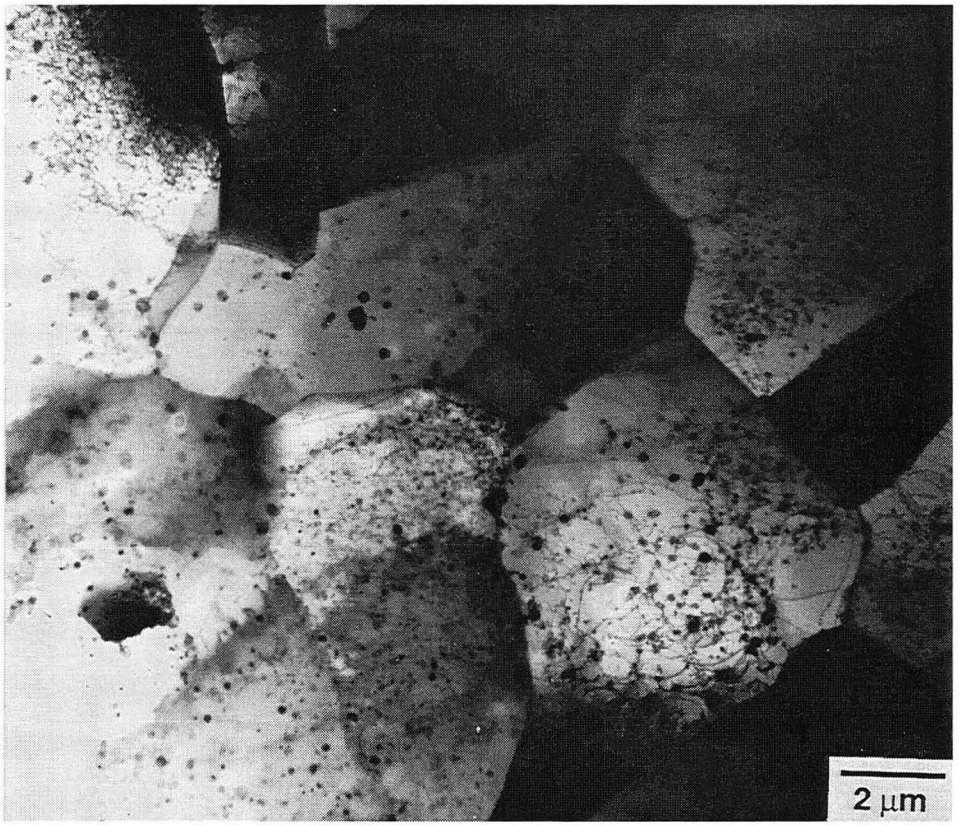

Figure 4.16. TEM micrograph from the gage of the AS alloy deformed at $0.0009 s^{-1}$ at 500°C. [XBB 932-501]

Figure 4.17. TEM micrographs of the a) grip and b) gage microstructures of the ALS alloy deformed at $0.0009\,s^{-1}$ at 500°C. [XBB 932-502]

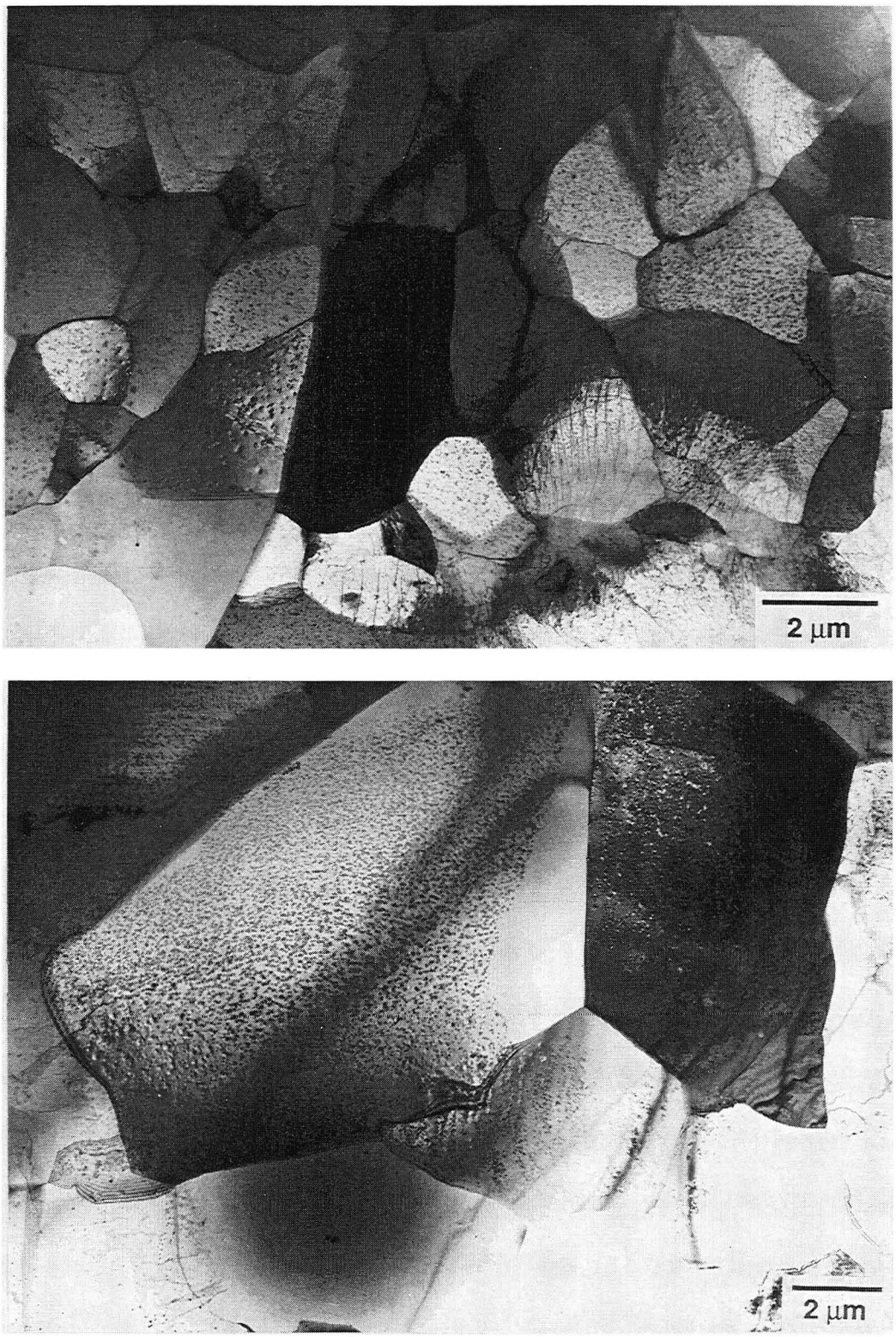

Figure 4.18. TEM micrographs of the grip (top) and gage microstructures of the AMLS alloy deformed at $0.0009 s^{-1}$ at 500°C. [XBB 934-2499]

Table 4.1. Grain/subgrain sizes for the grip and gage sections as a function of strain and composition. Measurements were made in the TEM. Also listed is whether grain boundary misorientation data was also taken.

Alloy	Strain	(sub)grain size µm	GBM
AS	0	2.35	yes
	0.7	5.09	yes
ALS	0	2.38	no
	0.4	4.86	yes
	1.0	5.42	yes
AMLS	0	2.04	yes
	0.2	3.37	no
	0.7	5.29	yes

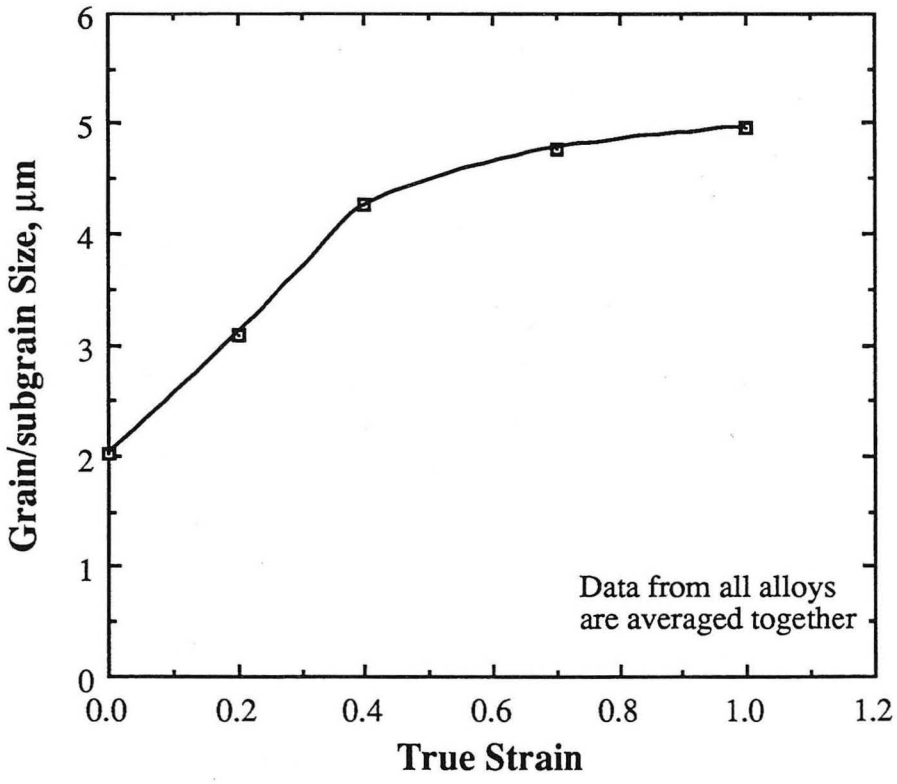

Figure 4.19. Plot of grain/subgrain size vs. strain for all alloys examined in the TEM. Note how the size levels off at large grains.

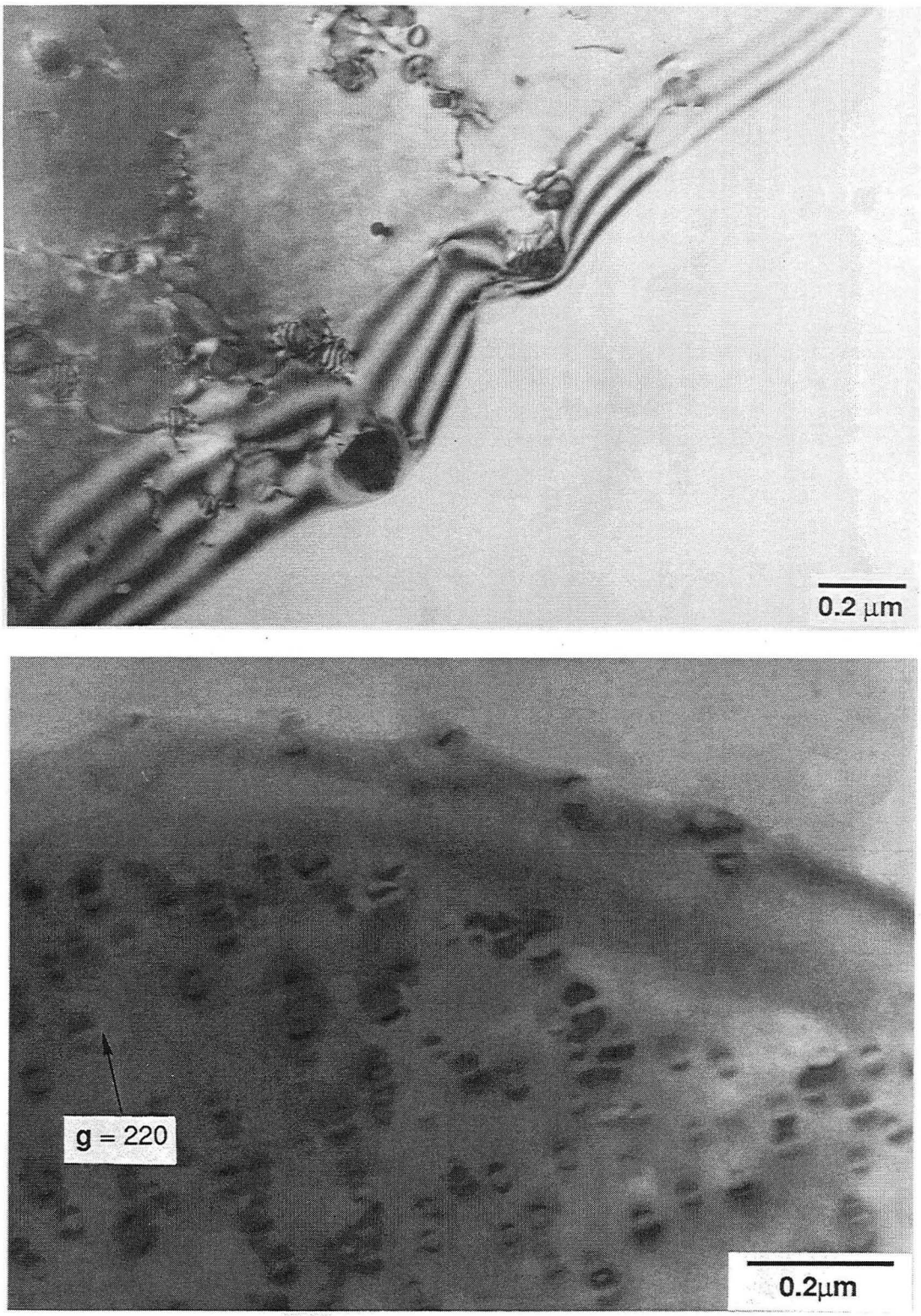

Figure 4.20. TEM micrographs of the grain boundaries from the AS (top) and AMLS alloys after a true strain of 0.7 at 500°C showing the pinning action of the Al_3Sc precipitates. Note the difference in the size of the Al_3Sc precipitates at the boundaries in the two alloys. [XBB 932-497]

The as-cast microstructure of the AMLS alloy was equiaxed, but with a variation in grain size from small grains near the edge of the ingot to larger grains in the interior. This caused the through-thickness grain size to vary as shown in Fig. 4.21. Here, the grain size in the two regions is compared both before and after deformation. Both regions exhibit refinement during deformation, but it appears to be proportional to the original grain size. Fig. 4.22 shows the difference in cavitation between the coarse and fine grained regions in an AMLS specimen pulled to $\varepsilon = 1.1$. The coarse region has much more cavitation and larger voids than the fine-grained region.

4.2.2 Grain boundary misorientation

The measurements of grain boundary misorientation were made on the samples noted in Table 4.1 and compiled into histograms of frequency versus misorientation (Figs. 4.23-25). There is a decided trend towards greater and a more random misorientation with increasing strain in all three alloys. Data for the average misorientation as a function of strain for all the alloys is shown in Fig. 4.26 and it shows the rapid increase in misorientation with tensile deformation.

The measurements made from the grip sections do show that the average misorientation is low; however, these boundaries are all subgrain or low angle and the only relatively large angle boundaries are seen to be between the grains present from casting. In the bright field mode in the TEM, all of the subgrain boundaries can be visible in one grain while none are visible in an adjacent grain. When the specimen is tilted the reverse occurs. The subgrains in the grip are almost entirely $\mathbf{z} = 011$ whereas the gage grains are of different **z**. This matches the change in grain morphology seen in the optical micrographs where the subgrains are not visible until their boundary misorientations increase and they become true grains.

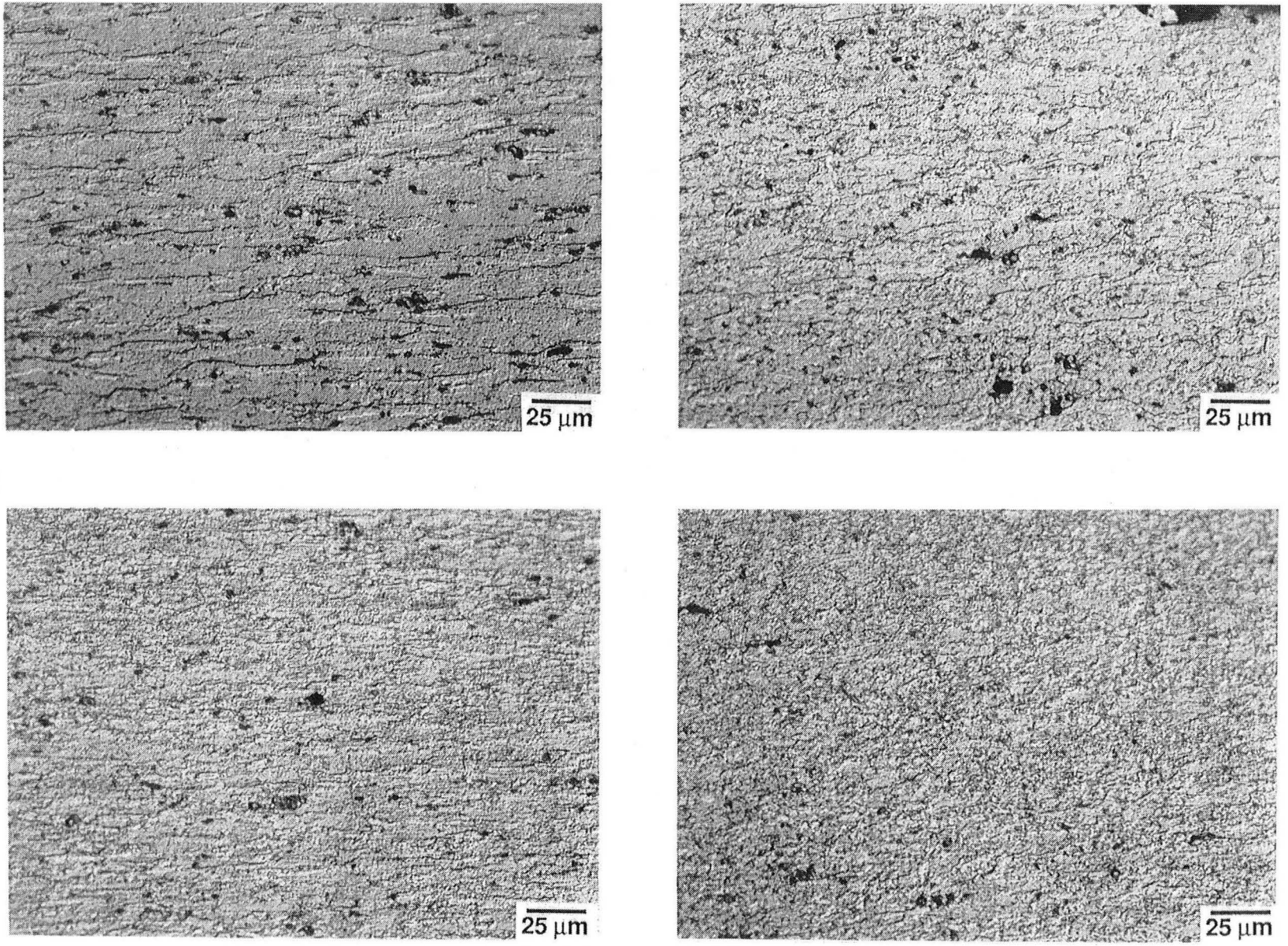

Figure 4.21. Optical micrographs of the coarse and fine-grained microstructures before and after creep deformation at 500°C and .0009/s [XBB 932-690]

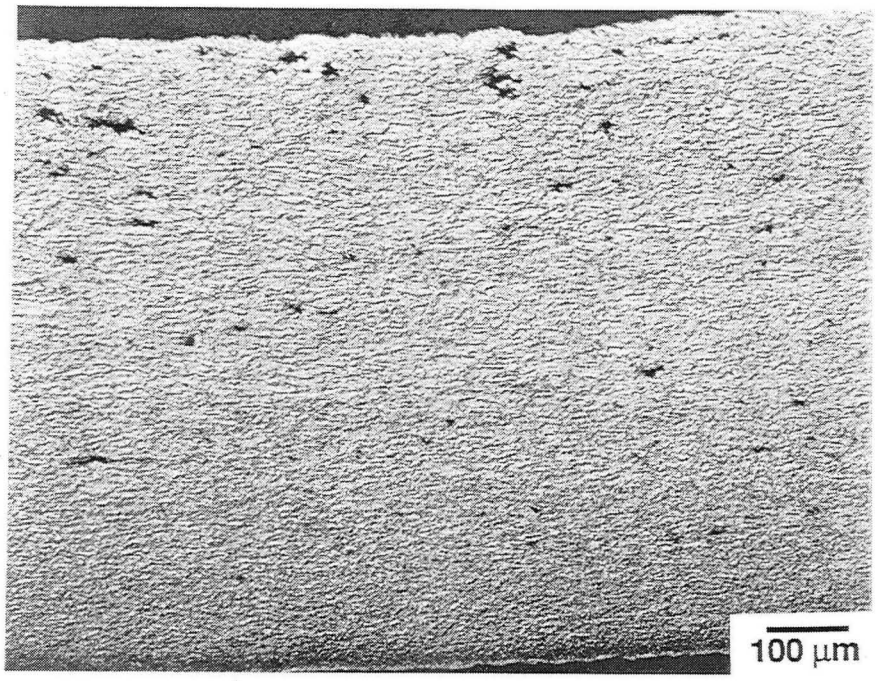

Coarse

Fine

Figure 4.22. Optical micrograph of the AMLS alloy deformed at 475°C to a true strain of 1.1 showing the presence of cavitation in the coarse-grained region and the lack of cavitation in the fine-grained region. [XBB 933-1716]

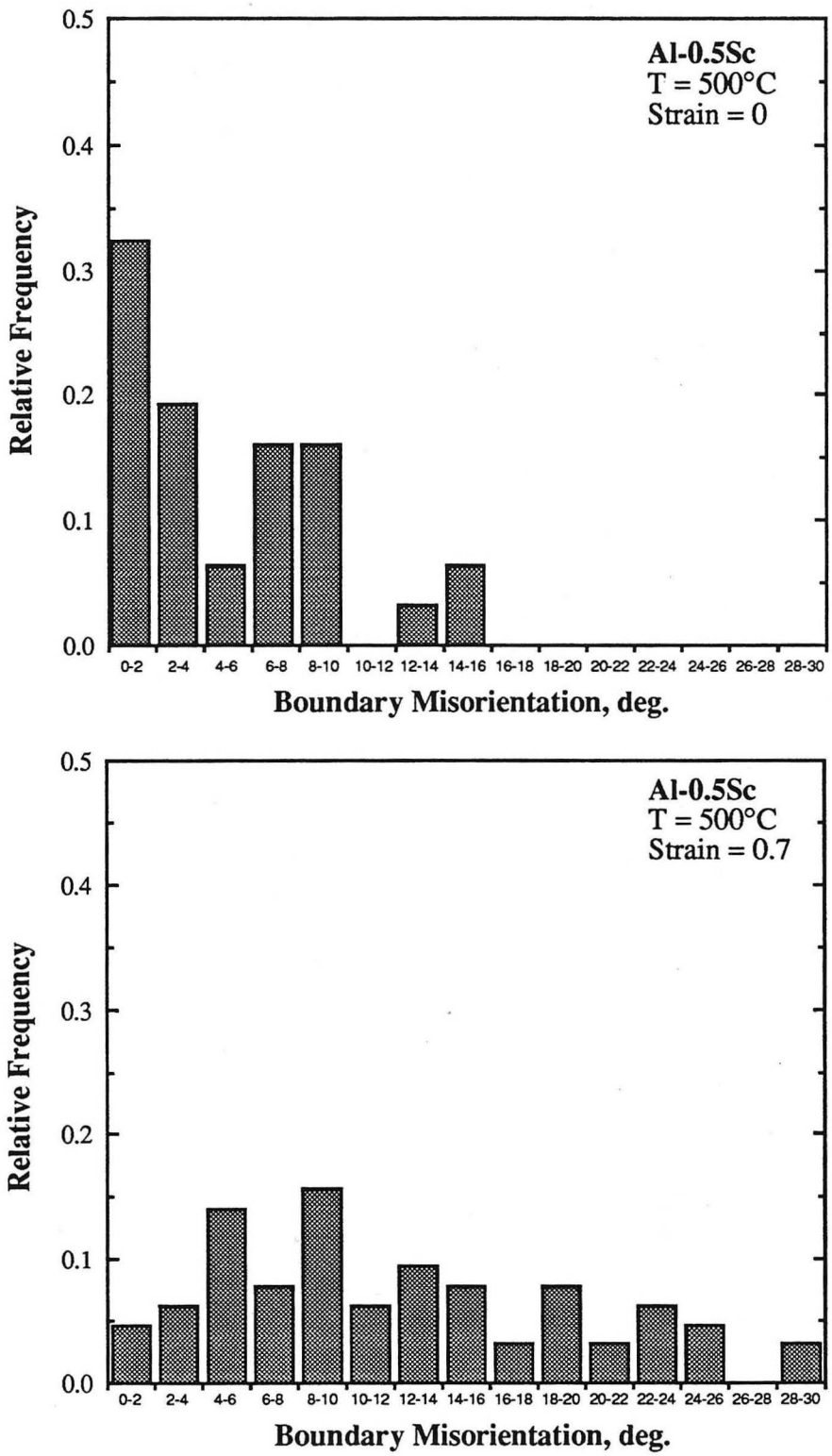

Figure 4.23. Histograms of the relative boundary misorientation for the AS alloy at true strains of a) 0 and b) 0.7. Note how the population of larger angles increases with strain.

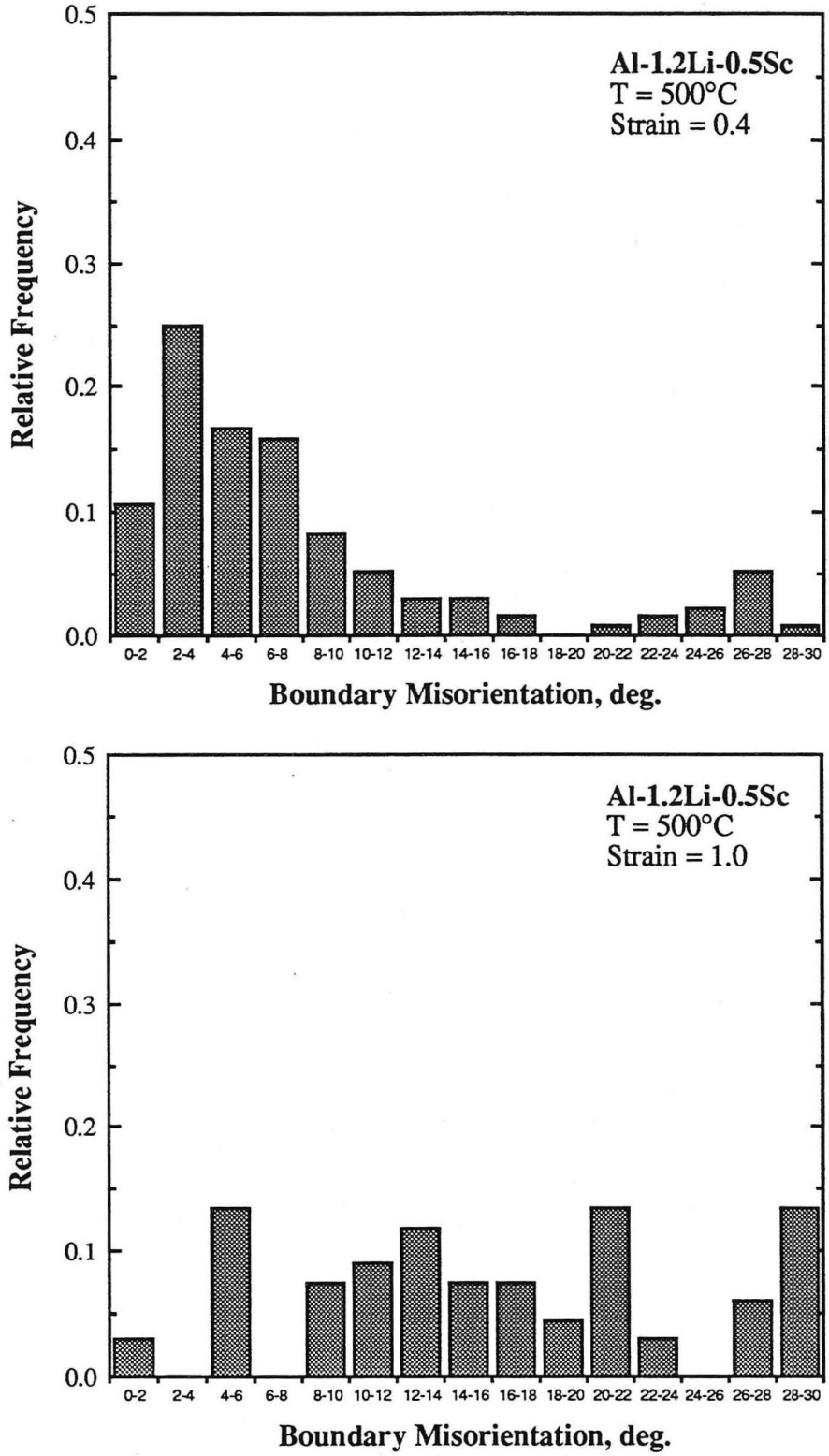

Figure 4.24. Histograms of the relative boundary misorientation for the ALS alloy at true strains of a) 0 and b) 0.7. Again the population of larger angles increases with strain.

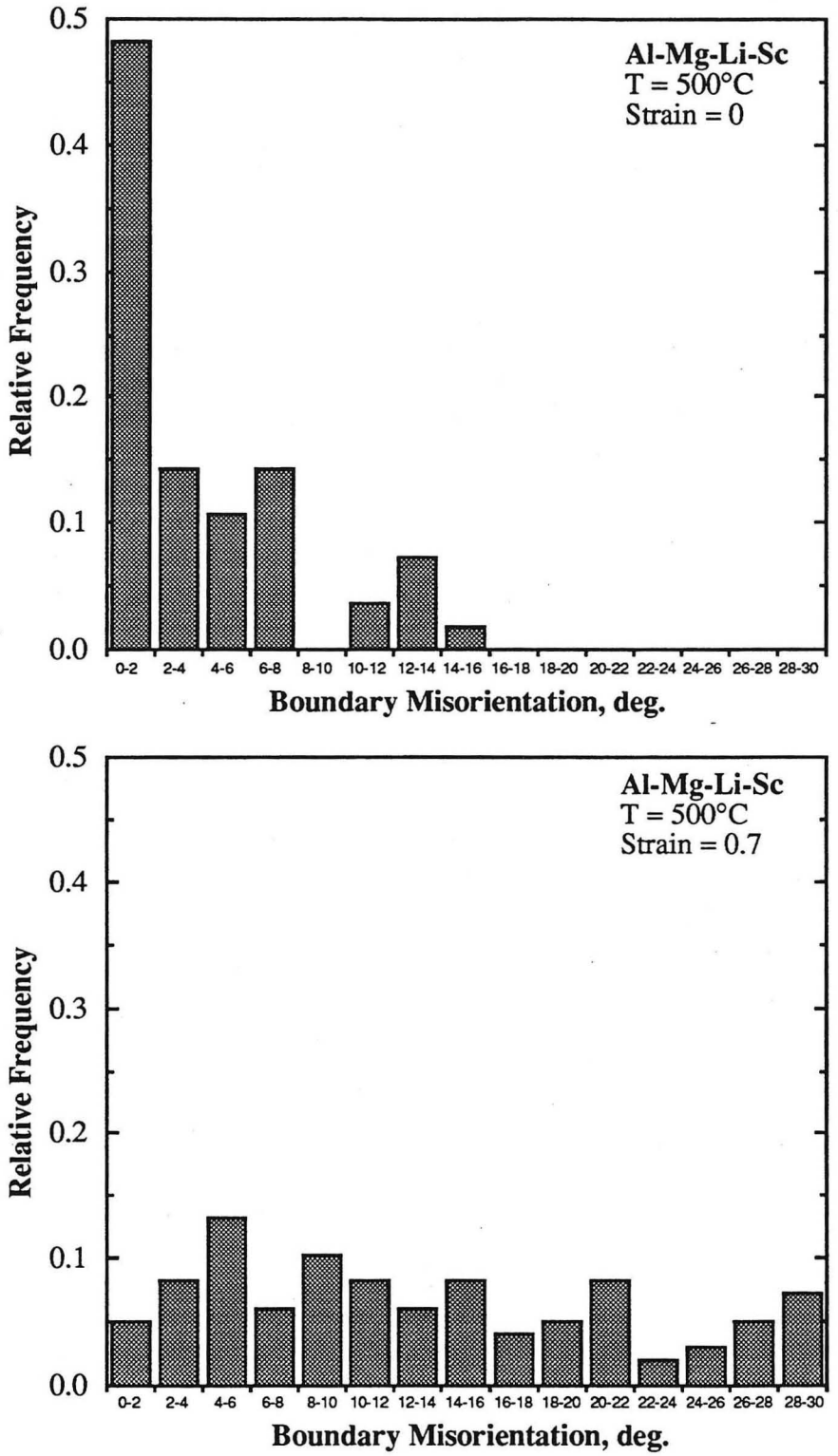

Figure 4.25. Histograms of the relative boundary misorientation for the AMLS alloy at true strains of a) 0 and b) 0.7 shows the population of larger angles increases with strain.

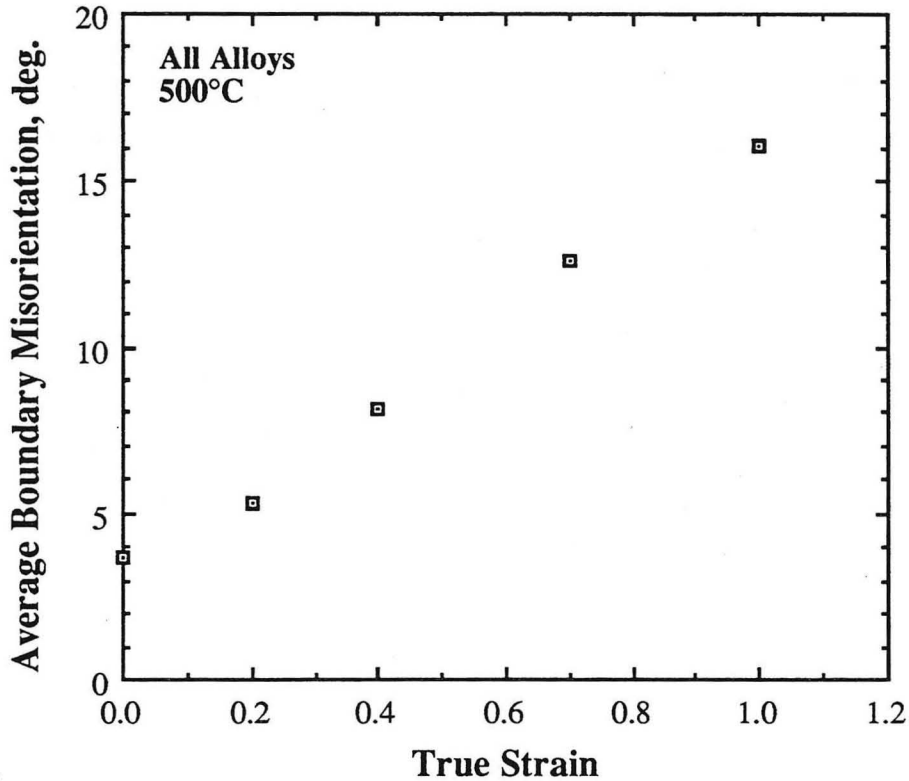

Figure 4.26. Plot of average boundary misorientation vs. strain for all alloys examined in the TEM. Note the rapid increase in misorientation at small strains.

4.3 Tensile Data

4.3.1 *m* vs. strain and strain rate

4.3.1.1 Alloys with Sc

In Fig. 4.27 the results of the *m* vs. strain tests at 500°C (932°F) show that the AMLS alloy has the highest initial *m*-value at $\varepsilon = 0.1$ and it reaches the highest maximum value of the four Sc alloys tested. The value of *m* increases linearly with strain until a steady state value is reached. Fig. 4.28 is a plot of *m* vs. ε for AS at 500°C and 560°C and here the *m*-value at the $\varepsilon = 0.1$ is greater than that seen at 500°C. Because the strain rate decreased with ε during the test, the *m* vs. ε data is plotted with the steady state *m* data associated with the strain rate corresponding to each strain.

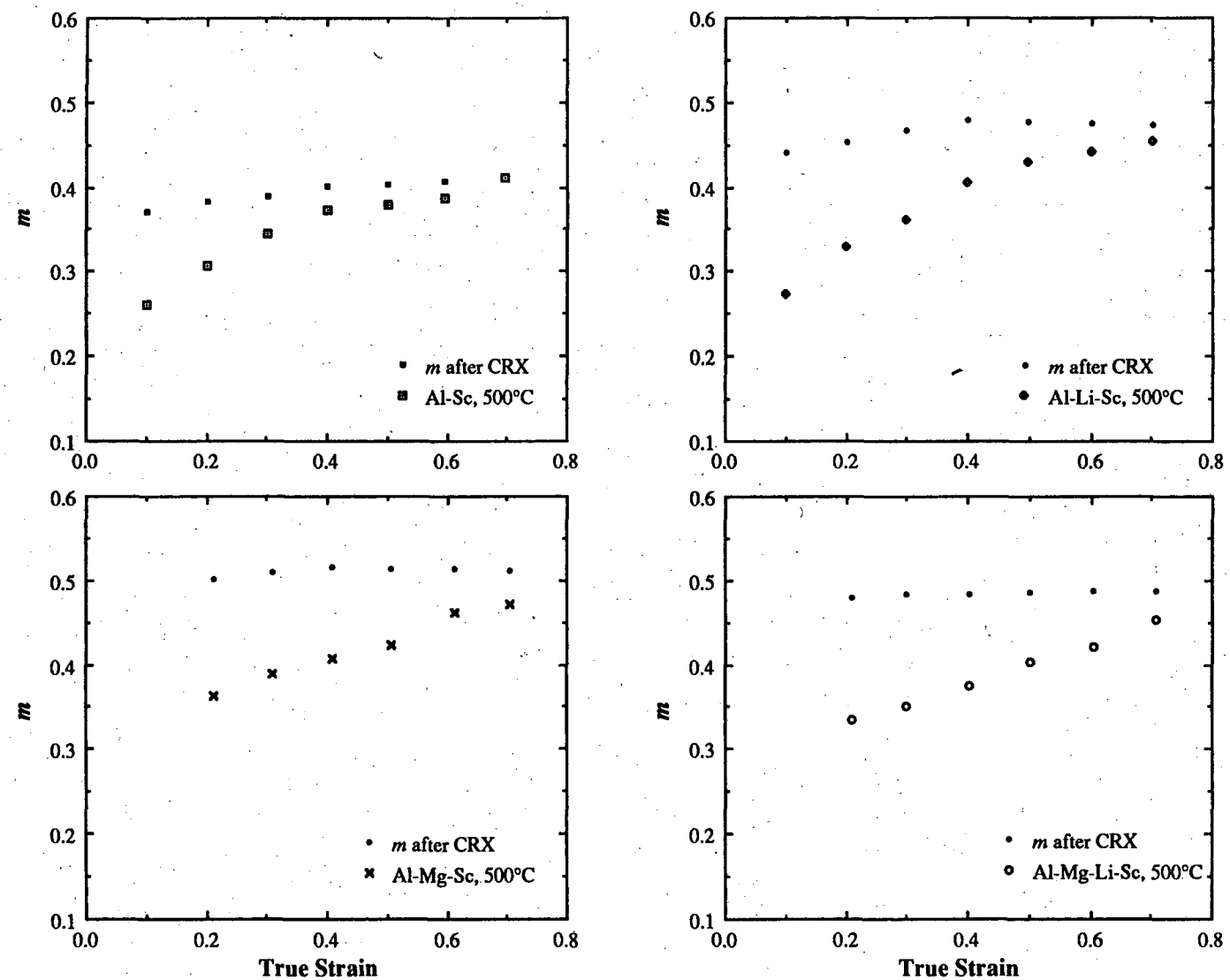

Figure 4.27. Plots showing the *m* vs. strain behavior at 500°C for the a) AS, b) ALS, c) AMS, and d) AMLS alloys. Because the strain rate decreases slightly with strain during the test, the *m*-values for the microstructure at a strain of 1.0 are plotted with the data to emphasize the real increase of *m* with strain.

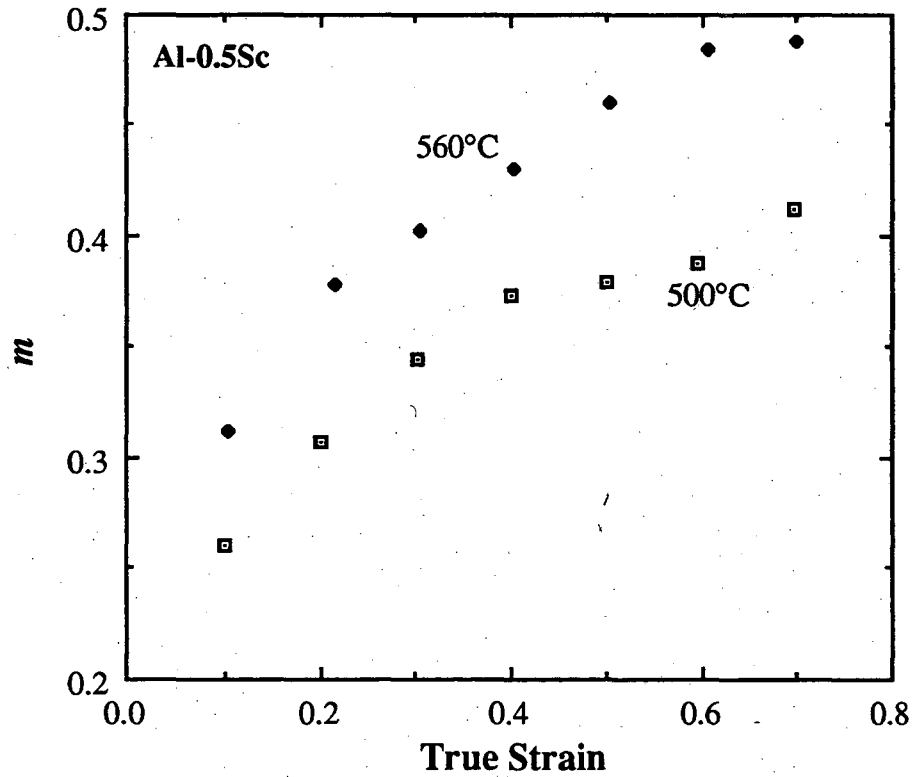

Figure 4.28. Plot of m vs. strain as a function of temperature for the AS alloy. Note that at the higher temperature the m-values are uniformly higher at all strains.

As the m-values appear to flatten out at a true $\varepsilon \approx 0.7$, m vs. strain rate data was taken after a creep strain of ≈ 1.0. This data (Fig. 4.29) shows that the Sc alloys containing Mg exhibit the highest values of m at 500°C (932°F) and that the range of strain rates over which the high m-values persists is much larger than that observed in the Sc alloys without Mg. At 560°C, the Sc alloys without Mg exhibit high m-values over a narrower range of strain rates as compared to the AMLS alloy at 450 and 500°C (Fig. 4.30).

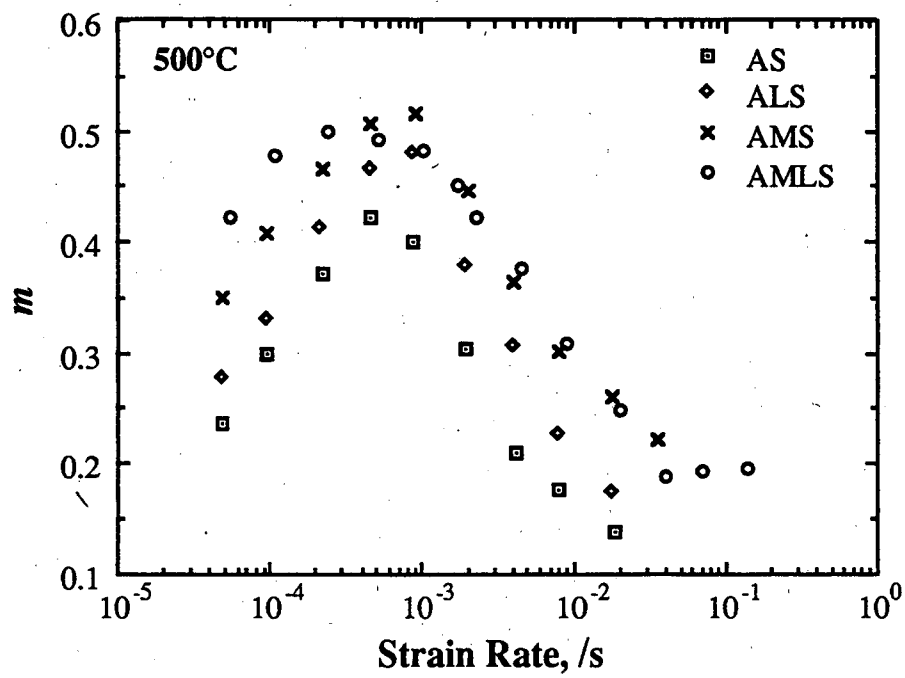

Figure 4.29. Plot of the *m* vs. strain rate for the four Al-Sc alloys after a true strain of 1.0. The alloy with the highest value of *m* has the greatest amount of Mg.

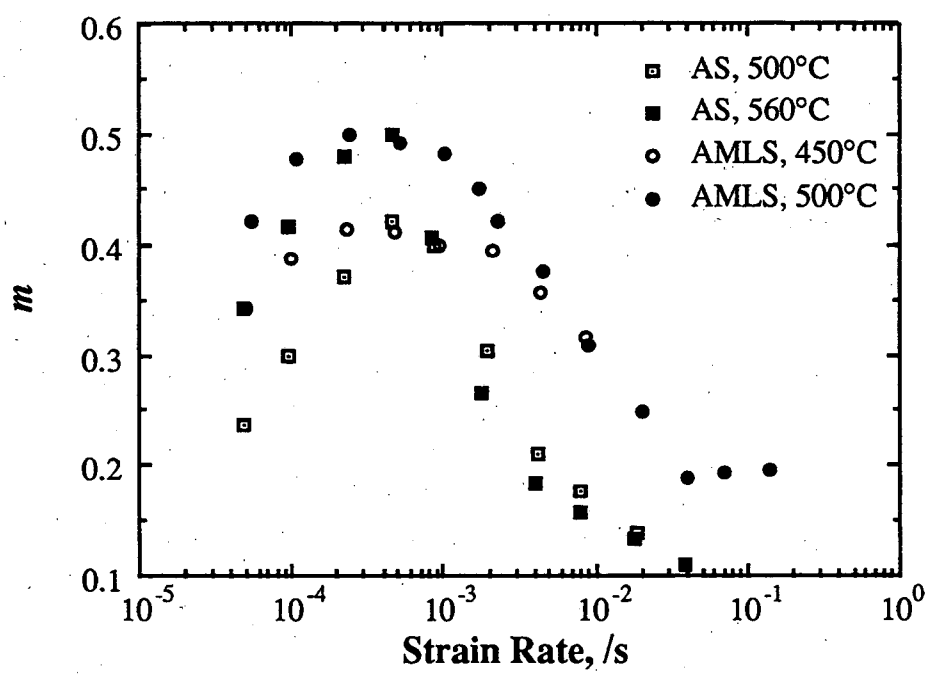

Figure 4.30. Plot of the *m* vs. strain rate for the AMLS and AS alloys as a function of temperature. The AMLS alloy exhibits high values of *m* over a broader range of strain rates than the AS alloy.

4.3.1.2 Alloys without Sc

The non-Sc alloys did not exhibit a strain-dependent m-value. The results for the non-Sc data shows that the m-value is relatively constant over a large range of strain rates and only decreases at high stresses (**Fig. 4.31**). The Li and Mg increase the creep strength of the pure Al. The Al-2.9Mg alloy exhibits the transition from viscous glide ($m \approx 0.3$) to climb-controlled creep ($m \approx 0.15$) at a stress of ~ 30 MPa (~ 4300 psi). The non-Mg alloys exhibit power-law creep (PLC) throughout and do not exhibit power-law breakdown since the flow stresses were too low at all of the strain rates tested. These results agree with that observed in pure Al [Bird *et al.* 1972], Al-Mg [Linga Murty *et al.*, 1972], and Al-Li [Park *et al.*, 1990] alloys tested in shear.

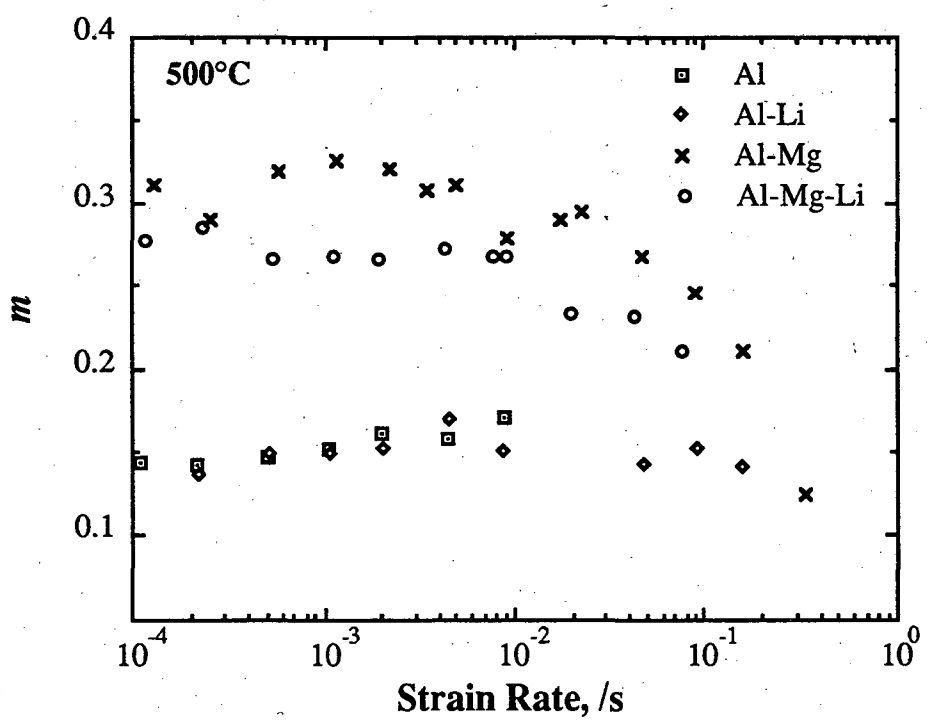

Figure 4.31. Plot of m vs. strain rate for the alloys without Sc. The alloys containing Mg exhibit much higher m-values characteristic of viscous glide-controlled deformation.

4.3.2 Effect of strain rate on the evolution of m

The effect of strain rate on the evolution of m with strain is shown in Fig. 4.32 for the ALS alloy. One sample was cycled between 5 and 10 mm/min. and compared to the data generated at the regular rate of 0.5 and 1.0 mm/min. The m-value at steady state is

lower at the higher strain rate (Fig. 4.29), so the evolution of m with strain appears to be different for the two types of samples. However, when the sample deformed at the higher strain rate is then tested at the lower strain rate, the m-value is similar to that shown for the sample tested entirely at the slower strain rate. This indicates that microstructural evolution is occurring at strain rates associated with power-law creep in recrystallized specimens.

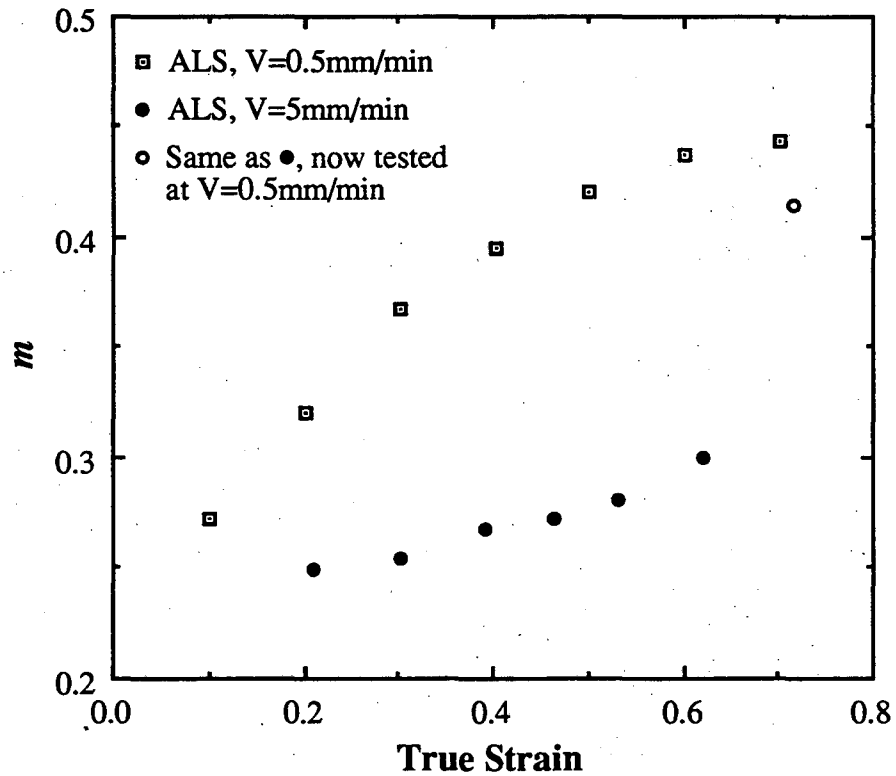

Figure 4.32. Plot of the effect of strain rate on the evolution of m with strain in the ALS alloy. Although the sample was deformed at a strain rate that is in the power-law regime, CRX continued to operate as is shown with the huge increase in m after the strain rate was reduced.

4.3.3 Flow stress vs. strain rate

Flow stress vs. strain rate data was calculated from the tests used to generate the m vs. strain rate data and is shown in Fig. 4.33. The data shows that the Mg alloys have higher flow stresses at high strain rates than do the non-Mg alloys with or without Sc. Li only slightly raises the flow stress of pure Al and does not seem to greatly affect the Al-Sc alloy. Fig. 4.34 compares the $\sigma - \dot{\varepsilon}$ response of both the Sc alloys and their non-Sc counterparts. At the high strain rates the flow stresses are the same in the AMS and Al-

2.9Mg alloys and the AMLS and AML alloys. However, the Sc strengthens Al as is shown with the AS and pure Al alloys.

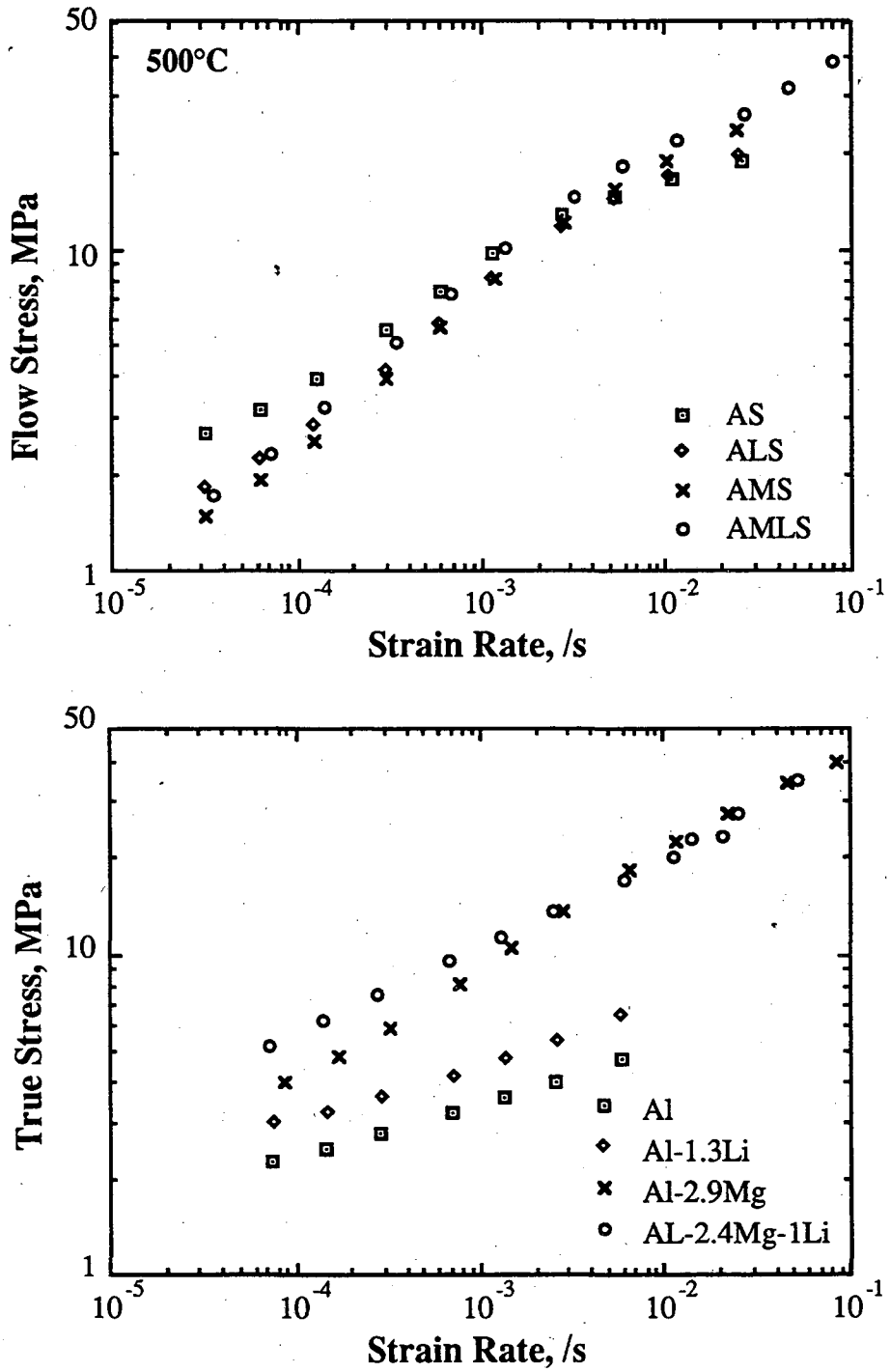

Figure 4.33. Plot of the flow stress vs. strain rate at 500°C for the alloys containing Sc (top) and the alloys without (bottom).

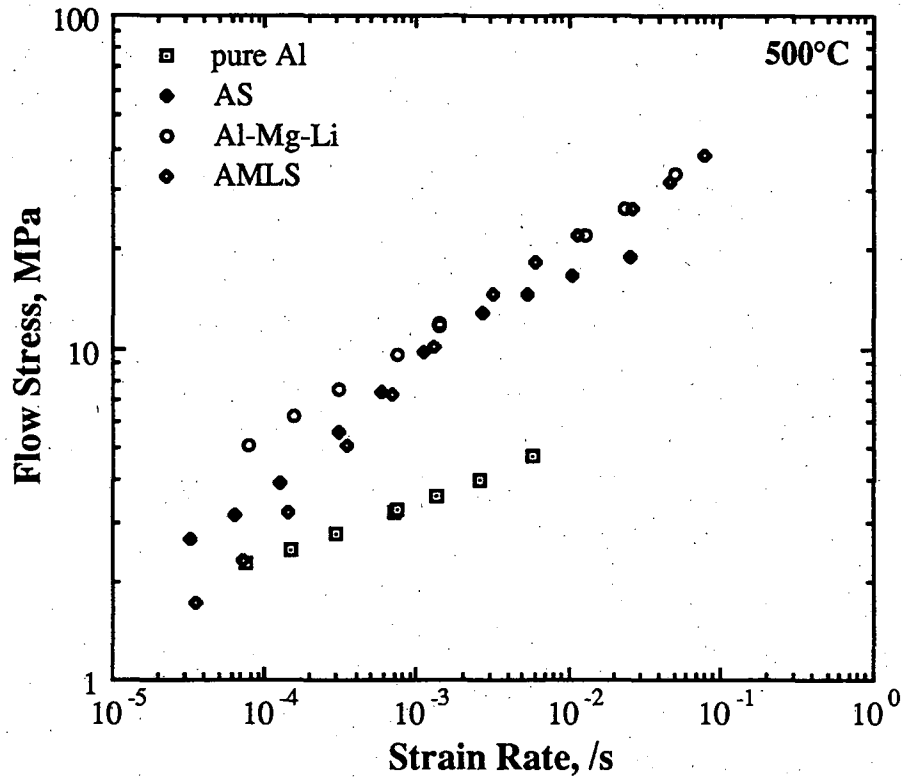

Figure 4.34. Plot of the flow stress vs. strain rate at 500°C as a function of Sc content.

At low strain rates, the alloys exhibiting the highest m_{max} also have the lowest flow stresses. There is no way to determine if these alloys exhibit a threshold stress (σ_o) due to the limitation of the testing machines to deform at such low strain rates.

4.3.4 Stress-strain curves

All of the Sc alloys exhibited similar stress-strain curves as shown in Fig. 4.35. There was a gradual decrease in the work hardening rate with increasing ε associated with (1) general recovery phenomena and (2) the weakening of the overall microstructure due to the increase in grain boundary misorientation that results in greater amounts of GBS. Since the tests were run at constant true strain rate, there was no decrease in the flow stress due to the decrease in $\dot{\varepsilon}$ as is seen in tests run at constant crosshead speed. Fig. 4.36 is a plot showing the satisfaction of the Hart criterion with strain. The AMLS alloy reaches the criterion at a greater strain due to (1) greater work hardening rate and (2) greater m-values at low strains relative to the AS alloy.

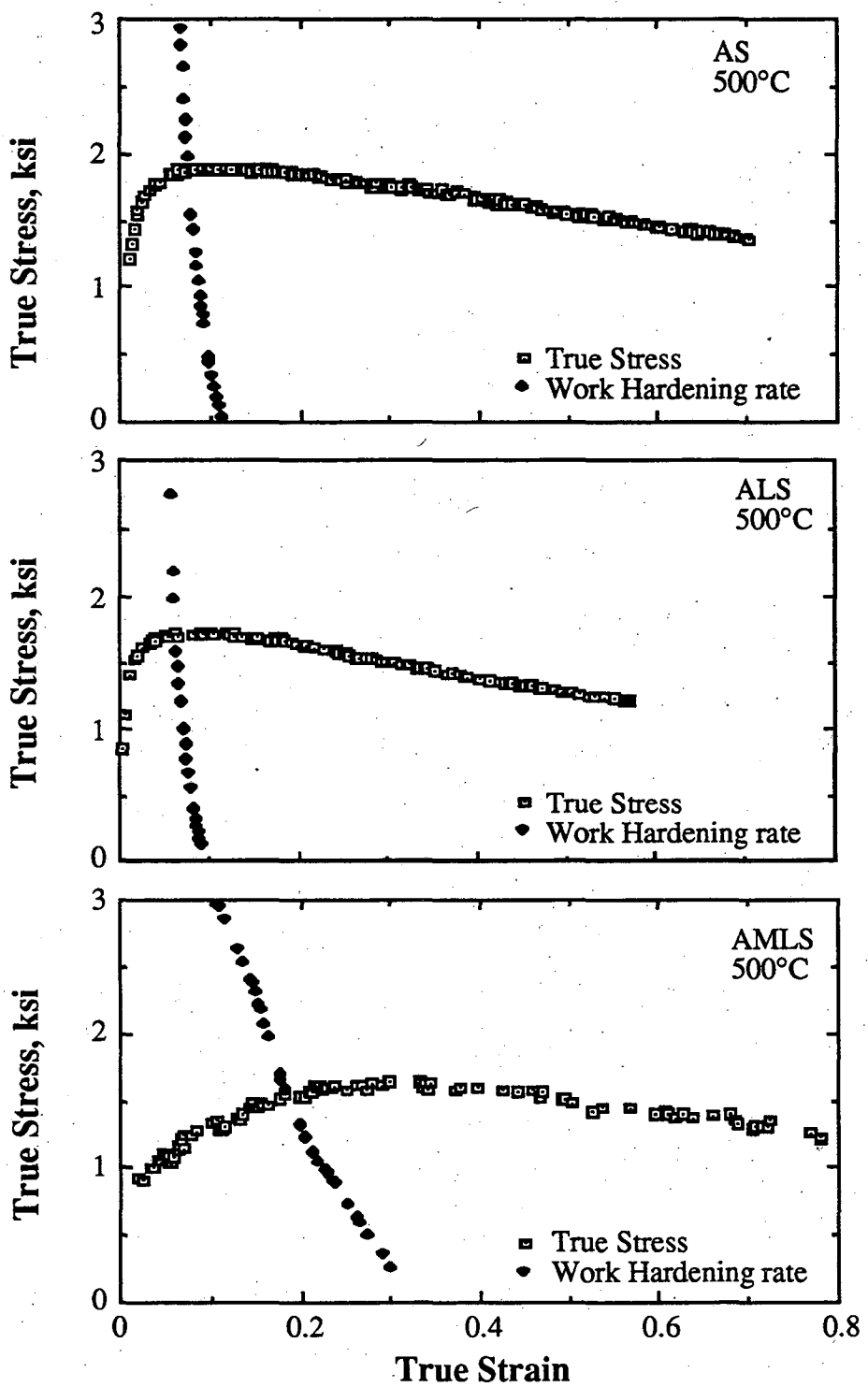

Figure 4.35. Stress-strain curves for the a) AS, b) ALS, and c) AMLS alloys at .001/s and 500°C showing the effect of microstructural evolution on the flow stress with strain. These tests were run at constant true strain rate.

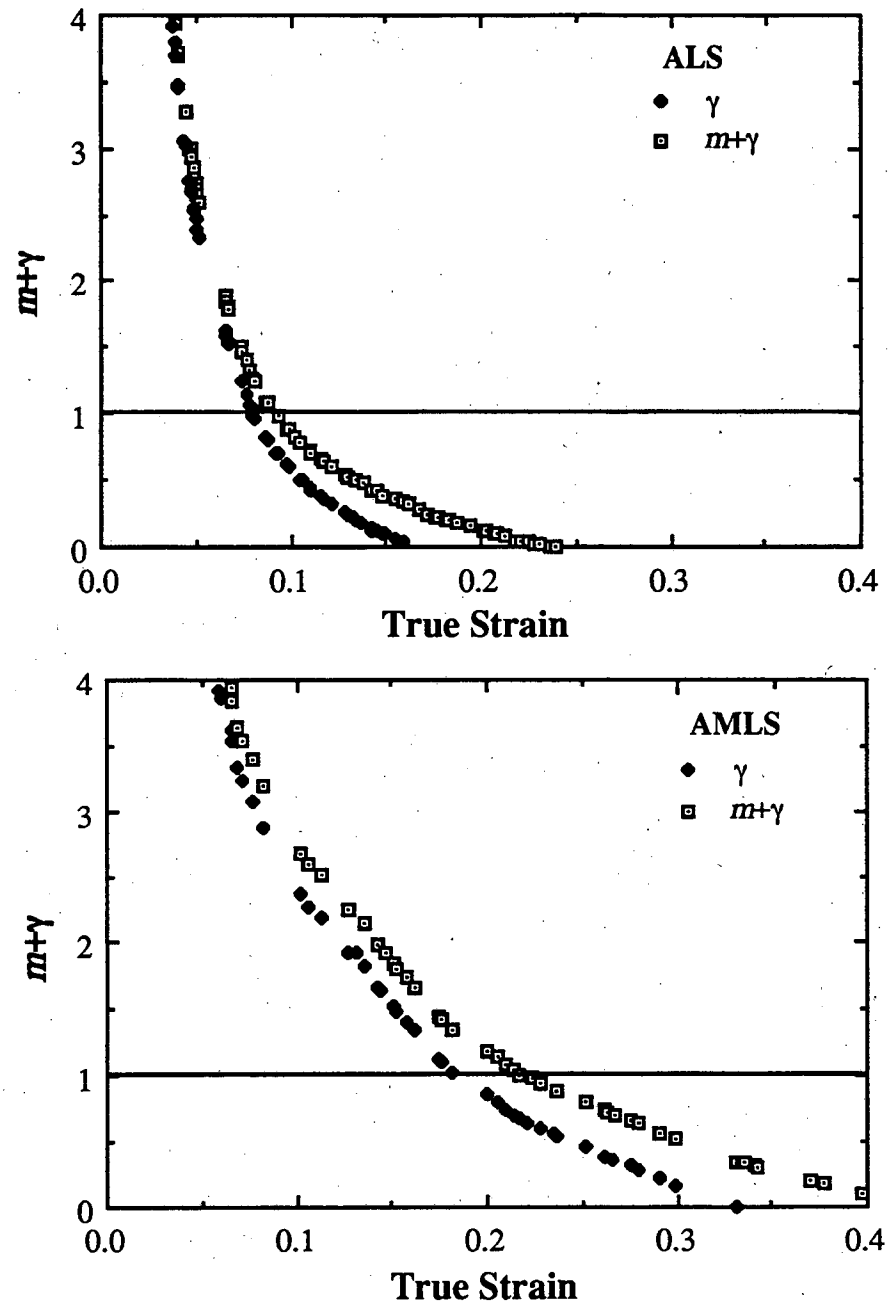

Figure 4.36. Plots of $m+\gamma$ vs. strain and γ vs. strain for the a) ALS and b) AMLS alloys at 500°C showing the early satisfaction of the Hart and Considére criteria.

4.3.5 Elongation and failure

The elongation data in Fig. 4.37 show that the AMLS alloy does exhibit the high elongations characteristic of the measured m-values. However, failure was premature due to cavitation (Fig. 4.22) that was most likely aided by the presence of the ν-phase at the grain boundaries. Fig. 4.38 shows a scanning electron micrograph of the fracture surface which reveals a fully intergranular fracture characteristic of SPF deformation.

Elongation data were only generated for the AMLS alloy. This is because once superplasticity was demonstrated and the m-data correlated with elongation, it was assumed to be unnecessary to perform tests on all of the alloys due to the small supply of material. Since these tests were run at a constant-crosshead rate the elongation data reflect the range of m-values associated with the range of strain rates the sample experienced during deformation.

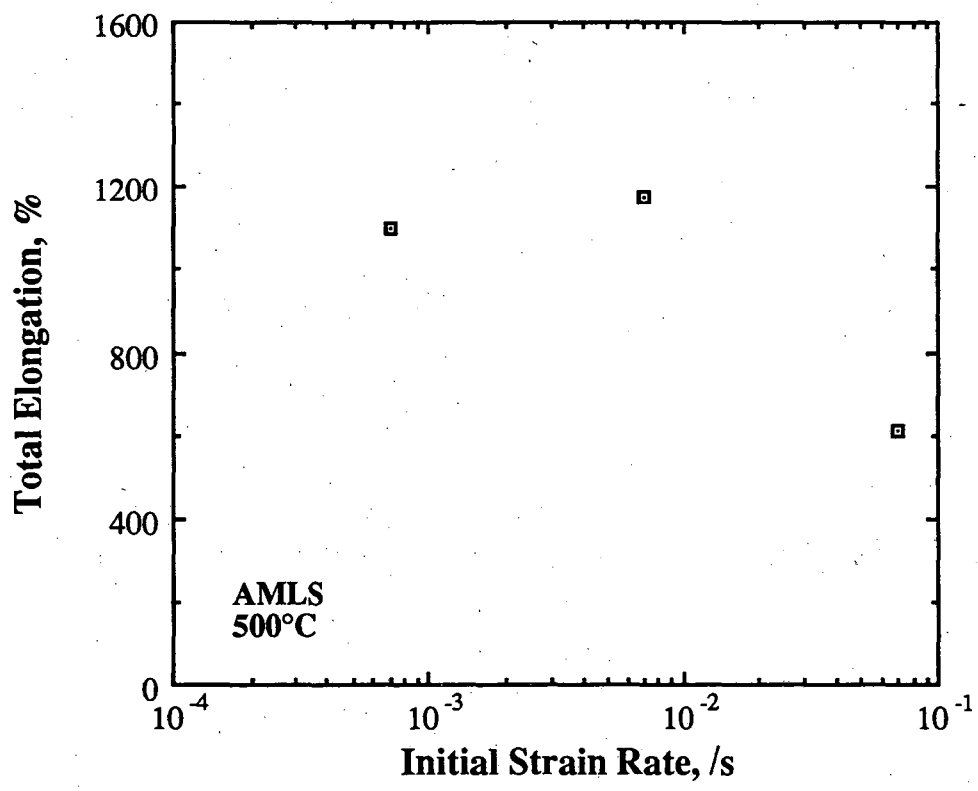

Figure 4.37. Plot of elongation vs. initial strain rate for the AMLS alloy at 500°C. The elongation curve has the same shape as the m vs. strain rate curve indicating the importance of m with respect to the total elongation.

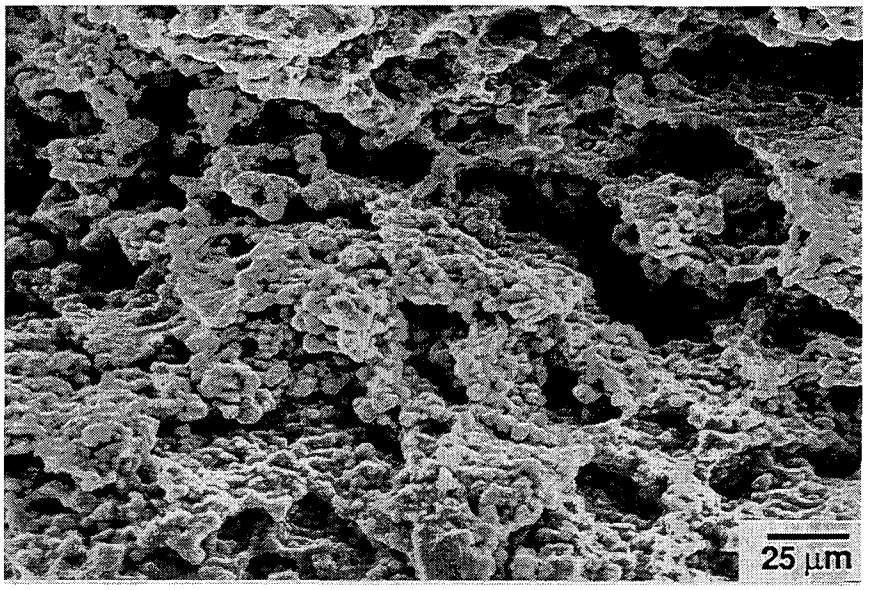

Figure 4.38. Scanning electron micrograph of the fracture surface from an AMLS specimen deformed at 500°C and an initial strain rate of .0067/s.

4.4 Activation Energy

The activation energies (Q) for the Sc alloys were difficult to calculate accurately due to the large variation in the m values at different temperatures and the lack of a regime of constant m with $\dot{\varepsilon}$ in any one sample. However, these values are summarized in Table 4.2 for all the alloys tested at different temperatures. It does appear that for the Sc alloys that the O in the region of high m (GBS) is demonstrably lower than the Q calculated for the PLC regime. This is not surprising since many studies have shown that GBS-controlled creep has an activation energy close to one-half that of bulk creep and is considered to be correlated to grain boundary diffusion. The grain boundary diffusion activation energy is typically found to be about one-half that for lattice diffusion [Smithells, 1983].

The values for Q in the non-Sc alloys were calculated from the specimens pulled at a constant $\dot{\varepsilon}$ on the DTM and the Al and Al-1.3Li alloys also deviate from the accepted values of Q measured for Al and Al-Li alloys in other investigations for creep. These alloys have no microstructural evolution to speak of to influence the results. In any case, the values are equal to or higher than those reported for lattice diffusion in Al. It is expected that lattice diffusion is dominant in these alloys.

Table 4.2. Activation energies for deformation of the alloys tested at more than one temperature.

Alloy	Activation Energy eV/atom
Al	2.12
Al-1.3Li	2.34
Al-2.9Mg	1.35
AS, PLC	2.04
AS, GBS	0.80
AMLS, GBS	0.95

5. DISCUSSION

5.1 Effect of solutes on CRX

5.1.1 Evolution of the microstructure in the Al-Sc alloys

There is no doubt that the Al-Sc alloys studied are exhibiting CRX. The optical micrographs show that during creep the equiaxed grains replace the original pancake-shaped grains in the Sc alloys, which is characteristic of CRX (Fig. 4.14 and 4.15). Further, the histograms of GBM with strain (Fig. 4.23-4.25) from the TEM study in the AS, ALS, and AMLS alloys conclusively demonstrate that microstructural evolution with strain is occurring in the Sc alloys irrespective of composition. The subgrains present after TMP are converted into true grains of large-angle in all of the alloys examined by TEM. As their boundary misorientations increase, the boundaries etch more easily and clearly. With the (sub)grain coarsening observed, the original large-angle boundaries are distorted and are not distinguishable from the newly formed large-angle boundaries. Thus these alloys are exhibiting CRX. From this data it appears that CRX is occurring in all of the Sc alloys irrespective of the composition.

5.1.2 Evolution of *m* in the Al-Sc alloys

It has been shown in tests on Al bi- and tri-crystals [Weinberg, 1957, Gleiter and Chalmers, 1972, and Rhines, *et al.*, 1956] that the misorientation of a boundary greatly affects the ability of the boundary to slide. Fig. 4.27 shows the *m*-value increases with strain for all the Sc alloys tested and Fig. 4.23-4.25 shows the increase in boundary misorientation with strain. Thus, in the Sc alloys, the fraction of boundaries able to support sliding should increase with strain as their misorientation increases. Since the power-law creep and superplastic creep mechanisms must act in parallel (Fig. 2.2), both deformation mechanisms can occur simultaneously throughout the microstructure and form a hybrid *m*-value according to the relative amounts of deformation attributable to each. In the Al-Sc alloys, the CRX process causes grain refinement which allows a greater fraction of the microstructure to exhibit GBS-controlled deformation. The initial microstructure consisting of large, pancake grains exhibit PLC and when the microstructure is predominantly large grains the overall *m*-value is low (Fig. 4.27). As the CRX progresses with strain, the microstructure is refined and a greater fraction can exhibit GBS-controlled deformation if the strain rate is in the appropriate range. Since GBS-controlled deformation results in *m*-values around 0.5, it is expected that in the Al-Sc alloys that the *m*-value will increase from the initially low value of 0.2-0.3 corresponding to primarily power-law creep to ideally one approaching 0.5 corresponding

to GBS creep with increasing strain when tested at appropriate strain rates. This is indeed observed for all of the Al-Sc alloys (Fig. 4.27) In practice, the boundaries reach a random state of misorientation and the microstructure is completely recrystallized, causing the m-value to reach its upper limit and steady-state value for any given strain rate.

The plots of m vs. strain in Fig. 4.27 are linear in nature and the evolution of the microstructure that accompanies this m-variation. Yang and Mukherjee [1992] published data on the deformation of an Mg-1.5Mn-0.3Ce alloy with a bimodal microstructure consisting of 100μm and 10μm size grains. The alloy was processed to various rolling strains to produce mixed microstructures consisting of a fine-grain volume fraction (f_{fg}) that varied from 0 to 1. They deformed the alloy at a strain rate where $\sigma_{plc} / \sigma_{gbs} \approx 1.8$ and observed a linear dependence of m on f_{fg}. The tests on the Al-Sc alloys were performed at strain rates that corresponded to a $\sigma_{plc} / \sigma_{gbs}$ of ≈ 1.5 if the power-law curve in Fig. 4.33 is extrapolated to lower strain rates. Thus the corroboration of Yang and Mukerjee's results to ours is further evidence of the microstructural evolution occurring with strain.

5.1.3 Comparison to previous results on binary alloys

The results reported for the binary Al-0.5Sc alloy by Sawtell and Jensen [1990] and for Al-0.5Zr alloy by Watts *et al.* [1976] appear to contradict the results in this thesis on the Al-Sc binary alloy. Sawtell and Jensen reported that the lack of alloying elements were the primary reason that lower m-values were observed and that this correlated with no CRX although no results were presented for the microstructure of the Al-Sc alloy and very little for the Al-4Mg-0.5Sc alloy. Watts *et al.* measured a $m = 0.33$ for the Al-0.5Zr binary but also measured elongations around 100% and concluded that no CRX was occurring in that alloy. It appears that two things influenced the interpretation of those results: (1) the variation in the microstructures between the alloys before creep testing and (2) the variation in the melting points of the alloys.

As shown in the m vs. strain data (Fig. 4.27), the initial m values of the AS and ALS alloys are low compared to those of the AMS and AMLS alloys. Thus the strain at which the data is taken is very important in interpreting the response of these alloys. Sawtell and Jensen do not say at what strain the m data is taken while Grimes reported both m and m_{max} data for the alloys and this was taken at strains > 0.2. Unless the alloys are compared at a steady state microstructure, microstructural differences will obscure the fundamental variations in m between the alloys.

The most important variable to consider when comparing the different alloys is the homologous temperature. As shown in Fig. 4.30, a variation in test temperature can cause the m to vary greatly. Because Mg greatly depresses both the solidus and liquidus temperatures as compared to pure Al, that should be taken into account when comparing the results for different alloy compositions. Fig. 5.1 is a plot of m_{max} vs. homologous temperature (T_H) for the AS and AMLS alloys and the similarity in m_{max} is striking. Thus, the large difference in m_{max} at 500°C between the two alloys is practically eliminated when the effect of melting point is taken into account. This ties in nicely with the CRX data and further indicates the universality of CRX in Al alloys.

Sawtell and Jensen tested the Al-4Mg-0.5Sc alloy at several temperatures but only tested the binary at 400°C. This is a very low homologous temperature for the binary as compared with the Al-4Mg-0.5Sc alloy. In that case the discrepancy between m_{max} for the two alloys is greater than that reported in this study. The Al-4Mg-0.5Sc alloy had an $m_{max} \approx 0.4$ while the Al-0.5Sc alloy measured only 0.2. They do not say at what strain these m_{max} values were taken, which adds even more uncertainty to the comparison of the values. The 400°C test temperature results in $T_H = 0.73$ for the binary alloy which is probably too low for GBS controlled deformation to occur.

Grimes *et al.* [1976] reported no success in developing superplastic properties in the Al-0.5Zr binary alloy. Watts *et al.* [1976] tested the Al-0.5Zr binary at 375°C and 423°C and measured m-values similar to those for the Al-Cu-Zr alloys. Values of m are shown in Table 5.1 along with the elongations and corresponding test temperatures of the alloys. Generally the better elongations and m_{max} values are seen in the higher Cu alloys. This is to be expected since the test temperatures were very low with respect to the melting point for the binary alloy, high m and elongations are not to be expected. Cu greatly depresses the melting point of Al and this greatly affects the comparison of the alloys at the same temperature. However, it is interesting to note that generally the m_{max} values do not correlate with the elongations, indicating microstructural inhomogeneities were present in a number of test samples, including those with Cu. Indeed, many of the alloys containing Cu have no better properties than those of the binary.

Tests were performed on an Al-4Mg-0.5Sc alloy produced elsewhere with an inhomogeneous microstructure in the rolling direction that exhibited relatively high m-values but also had poor elongations. This was attributed to the differences in flow stress between the coarser and finer microstructures such that the strain localized in the weaker, fine grained regions. The coarser regions did not refine with CRX as fast with strain as the initially finer regions and this caused the flow stresses to vary along the gage length

[Bradley and Morris, 1992]. Thus, the differences between the binary and Cu alloys appear to be more a function of the inhomogeneities of the rolled microstructures than fundamental differences imparted by the addition of the Cu, in agreement with these results on the Al-Sc alloys.

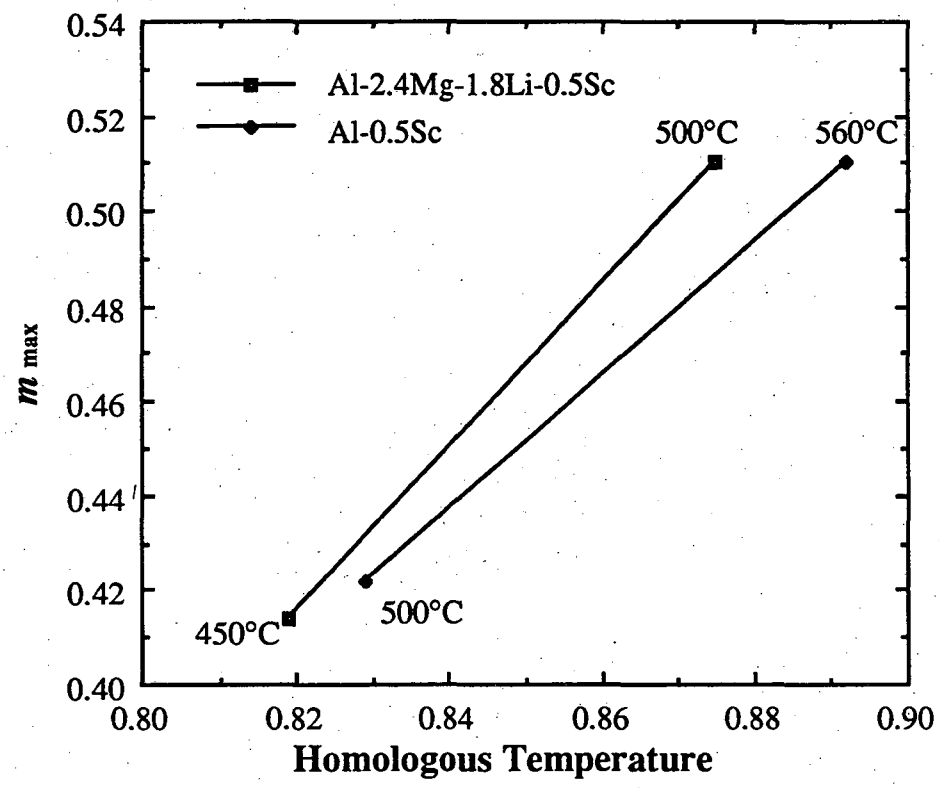

Figure 5.1. Plot of m vs. homologous temperature for the AS and AMLS data. The melting point normalization brings the data together.

Gudmundsson *et al.* [1991] showed that the misorientation of the subgrains did increase during uniaxial deformation at 400°C of a warm rolled Al-0.24Zr-0.1Si alloy. This is essentially a binary alloy due to the low solubility of Si in Al. The fact that some degree of CRX was observed is further evidence that the composition is of secondary importance to the mechanism of CRX. The very poor ductility at of this alloy at 400°C can be attributed to 1) the inhomogeneity of the Al-Zr precipitation which lead to a large, recrystallized grains and 2) the low test temperature ($T_H \approx 0.72$).

Table 5.1. Summary of data by Watts *et al.*, [1976] on Al-Zr alloys

Alloy	m_{max}	Elongation %	Test Temperature °C
	0.36	60	375
Al-0.5Zr	0.33	104	423
	-	-	455
	0.36	150	375
Al-4Cu-0.5Zr	0.43	317	423
	0.30	84	455
	-	-	375
Al-6Cu-0.5Zr	0.39	258	423
	0.38	612	455

5.2 Mechanism of Continuous Recrystallization

A number of theories have been proposed to explain the mechanism of CRX and some are more successful than others. However, the data generated in this study will be used to formulate a theory utilizing thermodynamic and kinetic principles. To review, the process of microstructural evolution occurs at high temperature such that the subgrains present after TMP are converted to true large angle grains with straining irrespective of composition. The strain-rate sensitivity of these alloys increases with strain concurrently with the microstructural evolution. Below is a discussion of the important processes related to CRX.

5.2.1 Subgrain coalescence and additional dislocation generation

The increase in misorientation of the subgrains is accompanied by the coarsening of the subgrains, implying that subgrain coalescence is an important component of CRX. The thermodynamic basis for dislocations incorporating themselves into the boundaries is that dislocation segments of the same sign experience a mutually repulsive force except in certain configurations such as found in boundaries [Cottrell, 1957], which lowers the energy of the dislocations. Thus they tend to spontaneously form boundaries as is very often seen in Al alloys. This is inhibited for alloys with highly dissociated dislocations (low SFE) since they are harder to align and have less mobility than those dislocations

with a low degree of dissociation. Metals of low SFE such as Cu exhibit little recovery and disorganized subgrain boundaries after annealing and are more easily recrystallized.

For grains, the amount of boundary area is inversely proportional to the grain size. This means that a doubling of the grain size will result in a halving of grain boundary area. For tilt boundaries, the relationship between the spacing of the edge dislocations (h) and boundary angle (θ) is [Hirth and Lothe, 1982]

$$\theta = \frac{b}{h}. \tag{5.1}$$

Obviously the dislocation density along a length of such a boundary is proportional to $\frac{1}{h}$. If the grain size doubles by coarsening and all the dislocations remain in the boundaries, then the density in the boundary doubles and θ doubles as well. Obviously this relationship will not hold exactly as the angle becomes large as the individual nature of the dislocation cores disappears as they move close together. Fig. 5.2 shows that the increase in misorientation is not linear with grain size, which implies that there is a change in mechanism associated with the misorientation increase.

The source of these extra dislocations must be from the matrix during deformation. As these dislocations move through the subgrains, a certain fraction will incorporate themselves into the boundaries as do the dislocations from the disintegrating subgrain boundaries. In both cases, these dislocations are both thermally and stress-activated into the boundaries as must be necessary since thermal or stress activation alone do not result in CRX.

The reason large-angle boundaries do not typically form during the creep of relatively pure Al alloys during creep is as follows. Studies of the steady-state microstructure in pure Al show that the average misorientation of the boundaries is of the order of 1° [Caillard and Martin, 1982 and Orlova *et al.*, 1972] and the subgrain size is essentially constant [Servi and Grant, 1951]. McLean [1951] showed that there is an increase in long range misorientation with creep strain, but the local misorientations have been found to be low and constant with creep strain. Exell and Warrington [1972] did an exhaustive study of the creep of pure Al and studied the change of the microstructure with strain by following the evolution of the subgrain boundaries and dislocations. They found that the time-average microstructure is the result of very dynamic processes. It was shown that the subgrain boundaries move in response to the applied stress and mutually

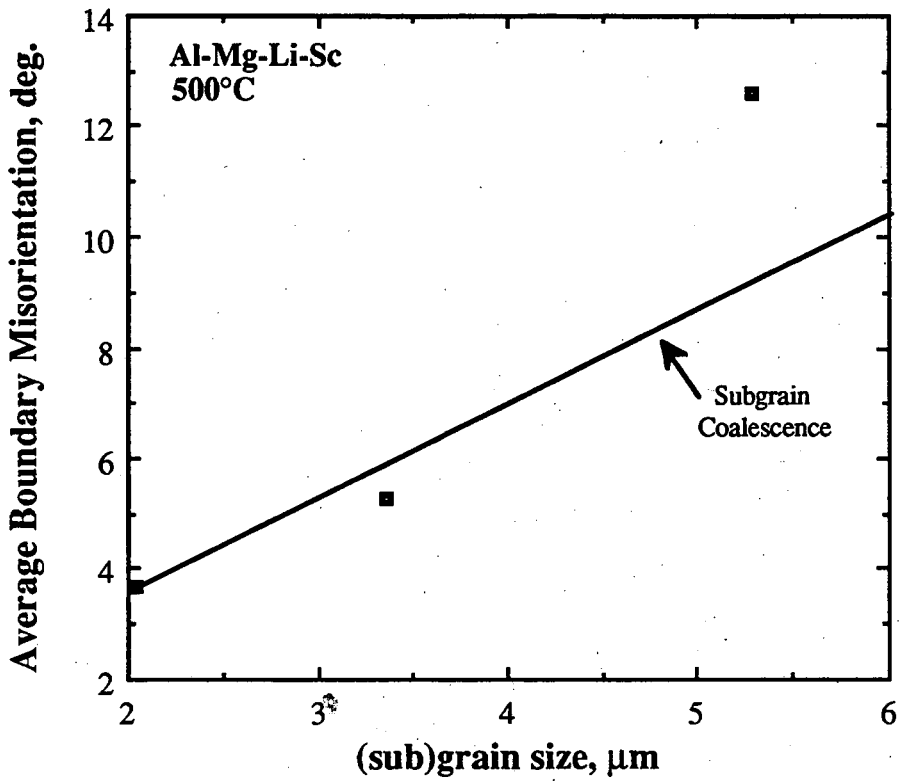

Figure 5.2. Plot of average boundary misorientation vs. grain size for the AMLS alloy. The line indicates the expected relationship if subgrain coalescence is the only mechanism for increasing the misorientation.

annihilate one another, keeping the overall subgrain boundary misorientation low, while new boundaries are formed to take the place of the annihilated boundaries. This movement of boundaries accounts for 5-10% of the total strain in the sample and keeps the average misorientation low during deformation. However, in the Al-Sc alloys the Al_3Sc precipitates pin the subgrain boundaries and keep them from migrating any appreciable distance and this allows the misorientation to grow with strain.

5.2.2. Stress level in CRX

The stress level during creep is relevant to the CRX mechanism since the incorporation of dislocations into the boundaries is a stress-activated process. No stress and the dislocations stay where they are; extremely high values of stress and the velocity of the mobile dislocations in the subgrains is very fast. A higher velocity means the dislocation spends less time near the boundary and its ability to climb or cross-slip into

the boundary is decreased accordingly. This jibes with the data in this study and that of Qing *et al.* in that CRX was found to progress to a greater degree at a much smaller values of strain at low strain rates (stresses). At very high stresses, such as those applied during rolling, there is little if any CRX as reflected in the average misorientations after large rolling strains (Fig. 4.23-4.25).

There is also support for this in the data of Rösler, Joos and Artz [1992] that shows very low m-values and very high flow stresses for a number of dispersion-strengthened Al alloys irrespective of the grain size. One alloy, which was primarily strengthened by ~ 2 vol% Al_2O_3 particles, was processed to both fine-grained and coarse-grained microstructures. Both microstructures had similar creep properties and there was no reported softening such as would be expected if CRX were occurring. In these alloys, the second-phase structure is the rate-controlling feature of the microstructure. Rösler *et al.* [1992] found that the carbide and oxide dispersions in Al control deformation at high temperatures by pinning the dislocations after the particle has been bypassed. The dispersion phases used in commercial Al alloys to inhibit recrystallization do not have this effect as all creep tests on these alloys have produced values of m typical of regular creep mechanisms.

Thus, this theory of CRX states that i) misorientation is increased by the thermal and stress-assisted recovery of dislocations into the boundaries, ii) dislocations are generated during deformation and are incorporated into the boundaries along with those present from rolling in the subgrain boundaries, iii) the level of stress during deformation must be low enough so that the dislocations have a slow enough velocity to enter the boundaries, iv) alloying elements play a secondary role in CRX.

5.2.3 Criticism of currently proposed theories on CRX

Although the experimental data published to date has not permitted the complete understanding of the precise mechanism of CRX, it has only been observed in Al alloys deformed at $T_H > 0.7$ that contain a fine dispersion of precipitates[1-8]. A number of papers published on commercial Al-Li alloys report a decrease in the texture during hot tensile deformation [Al-Li Confs.]. What has not been published in these papers is the relationship of the grain size with misorientation (with the exception of Qing) and the relationship of m to misorientation. Nes [1985] concluded that the increase in misorientation is the result of subgrain coalescence under stress and temperature caused by the dissolution of the β' (Al_3Zr) Qing *et al.* [1992] showed that the coarsening of the

subgrains was not sufficient to explain the increase in misorientation and suggested that dislocations generated in the grains are incorporated into the boundary under stress.

5.2.3.1 Theories of McNelley *et al.*

McNelley and his co-workers have put forth two theories of CRX over the last several years. In 1988, Hales and McNelley published results that claim to show a microstructure consisting of subgrains and small-angle boundaries sustain grain boundary sliding and results in a $m \approx 0.45$. However, this theory has been attacked as there is no evidence such small-angle boundaries can slide [Gleiter and Chalmers, 1972 and Weinberg, 1958] based on tests performed on bi-and tri-crystal Al samples. In addition, those small-angle boundaries increase in misorientation even as the overall texture increases during deformation, indicating GBS and rotation is not occurring on a large scale and bringing into question the m-data reported in the paper. The data on the Al-Sc alloys in this study show that small misorientations (Fig. 4.23-4.25) on the scale of the subgrain dimensions result in low m-values (Fig. 4.27).

The second theory, by Hales, McNelley, and McQueen [1991], states that the dislocations generated during deformation, whether by rolling or creep deformation are incorporated into the boundaries. They developed using a series of warm roll/anneal cycles that sustained large amounts of tensile deformation. Their theory suggests that the subgrain misorientation is gradually increased after every pass and is supported by the fact that increased rolling strain results in higher m-values and elongations. Recently, McNelley *et al.* [1993] stated that the formation of this highly deformable microstructure is due particle-stimulated nucleation of grains. In other words, SRX is responsible for the recrystallized microstructure. This is much more likely to be true and the following discussion shows that CRX is most likely not responsible for the microstructural changes observed.

I. The m values drop from ~ 0.45 at a $\varepsilon = 0.02$ to ~ 0.33 for $\varepsilon > 0.5$. They claim that $m = 0.45$ implies that GBS-controlled deformation is occurring and that it continues throughout the test even though the value of m drops with strain. This means that the bulk of the deformation in the alloy is occurring under much lower values of m than the ones used to justify GBS-controlled deformation. Ghosh and Ayers [1976] have shown that if m varies during deformation, the expected response should mirror the changes in m and that the initial m only correlates to the elongation if m does not change during deformation. Hales *et al.* claim that the decrease in m with strain is due to grain

coarsening. This appears unlikely given the testing temperature of 300°C and since the measured grain size increased only from 2.0 to 2.4 μm during deformation.

II. The alloy was rolled at a constant thickness per pass which results in an increasing strain and strain rate per pass. No matter what starting thickness is chosen, the minimum engineering strain at the final pass is 50% and can be as high as 65%. By Hales *et al.* own description of the rolling process, the rolling $\dot{\varepsilon}$ increased from ~ $1s^{-1}$ for the first pass to ~ $10s^{-1}$ at the final pass. Such a large strain and high strain rate can result in dynamic recrystallization as was shown for an Al-10Mg alloy [Sheppard *et al.*, 1986]. In addition, the Al-10Mg-0.1Zr alloy contains β (Al_8Mg_5) with a size $\geq 1\mu m$. Precipitates of this size are known to accentuate dynamic recrystallization [Sheppard *et al.*, 1986].

III. According to their theory, the misorientation of the grains before the final pass must be substantial since CRX is occurring throughout the rolling. Yet a rolling pass of 50% reduction or greater should result in the elongation of the grains. The microstructures shown are equiaxed, indicating they are either dynamically or statically recrystallized.

IV. The properties of the alloy reported to deform by the sliding of small-angle boundaries [Hales, 1988] are very similar to the alloy reported as having a starting microstructure consisting of large-angle boundaries [Hales, 1991]. Also the data reported in 1988 is presented in the 1991 paper without any mention of the previous interpretation.

V. Sawtell and Jensen report elongation data for Al-4Mg-0.5Sc at 325°C which is similar to that in Hales [1990]. No *m*-values were reported by Sawtell for 325°C, but at 400°C, $m_{max} = 0.4$. Based on the data in this thesis and the bulk of superplasticity data, m_{max} would be expected to be lower at 325°C in agreement with the *m* reported by Hales at a creep strain > 0.5.

5.2.3.2 Theory of GBS-induced CRX

Gudmundsson *et al.* [1991] stated that CRX in the very dilute Al-0.24Zr-0.1Si alloy is caused by the GBS of the large-angle grain boundaries left from the as-cast microstructure which induces grain rotation in the subgrains. The microstructure in this alloy after rolling was very similar to that seen in the Al-Sc alloys. Subgrain misorientations inside the pancake grains increased with strain at 400°C, although the sample had little ductility.

It is not easy to see how GBS of the large pancake-shaped grains induces grain rotation in the subgrains or even why it is necessary to invoke such an explanation. Although it is to be expected that a small amount GBS would occur along those large-angle boundaries to preserve continuity in response to the deformation of the large grains, in no way does that explain why that should automatically induce increases in misorientation of low angle boundaries within those grains. It may be true that if the large, elongated grains do in fact rotate substantially during the tensile deformation, then different slip planes would become activated during deformation, thereby causing a more varied dislocation population to develop with strain and maybe make the misorientation of the subgrains increase more rapidly with strain. However, the elongated grains cannot be expected to rotate very far out of their original positions given their shape without totally destroying the grain continuity. This is especially true when the rolling direction is parallel with stress axis. In this case, the creep deformation would be expected to increase the aspect ratio of the grains as it does in regular PLC to alloys without second-phase particles.

5.2.3.3 Theory of Qing *et al.*

Qing *et al.* [1992] studied the high temperature deformation of an alloy of 8090-type composition. The tests were carried out at 515°C at $\dot{\varepsilon} = .003$ and $.0003 s^{-1}$ on material hot rolled at 400°C, overaged, and then warm rolled 85% at 150°C. They did not report any m-value data although an earlier paper reports values of $m = 0.3$ for a single strain rate test without reporting at what value of strain it was calculated [Qing *et al.*, 1991]. They showed that the boundary misorientation during creep increased at a greater rate than that observed by thermal coarsening alone which is not surprising given the stress activation. Qing also observed that the misorientation at small strains was proportional to the (sub)grain size. This is expected since the amount of boundary area is inversely proportional to the (sub)grain size which means that a doubling of the grain size will result in a halving of grain boundary area. This causes the density of dislocations in the boundary to double and the misorientation angle to double as well. Obviously this relationship will deviate from the model as the angle becomes large, but the data reported by Qing obeys this rule at the start of deformation when the (sub)grain size is small. As the grains coarsen and the average misorientation increases, there is a sharp increase in the misorientation with little additional coarsening which is attributed to GBS.

5.2.3.4 Theories of solute-induced CRX

The theories of CRX related to alloy composition proposed by Watts *et al.* [1976] and Gardner and Grimes [1979] state that a) the stacking-fault energy is lower in Al with solutes and this increases dynamic recrystallization and b) the as-cast microstructure may be affected by the solutes influencing the solidification process. They reported excellent elongations for Al-6Cu-0.5Zr and Al-10Zn-0.5Zr alloys but poor elongations in the Al-0.5Zr alloy. They hypothesized that the microstructural evolution observed might be accentuated in Al if the stacking fault energy was lower so that DRX would be encouraged at the expense of recovery. However, CRX is a different process from DRX so any process promoting DRX would necessarily interfere with CRX. Additionally, solutes which appreciably lower the SFE of Al will result in increased widths between the partial dislocations. This makes it harder to insert dislocations into the (sub)grain boundaries and would inhibit the CRX mechanism since only perfect dislocation segments (ones without stacking faults) can climb into the boundaries. Another theory was that the presence of solutes causes a fine as-cast structure to form which influences the microstructural evolution. The as-cast microstructure of the AMLS alloy was one of equiaxed grains while the AS alloy has a hypereutectic microstructure, yet both behaved very similarly at the same homologous temperature (Fig. 5.1). Thus the theories of Watts *et al.* do not appear to explain the development of CRX in Al-Sc alloys. However, the idea may explain the results of Hales *et al.* in that the large amount of Mg in their alloy should promote DRX.

5.3 Role of ν-phase on CRX

It has been claimed that the presence of large precipitates during cold rolling accentuate CRX [Hales, 1991 and Qing *et al.*, 1992]. This claim is supported by the increase in elongation in material that is rolled in this condition. The Al-10Mg-0.1Zr alloy studied by Hales *et al.* has ~ 10 vol% β (Al_8Mg_5) at the rolling temperature and Qing *et al.* [1992] also overaged their alloy before final rolling. Yoshida *et al.* [1989] demonstrated that the elongations at 500°C are maximized when the extrusion temperature was equal to the temperature for maximum second-phase precipitation in 2090 and 8090. They did not say whether DRX or CRX was the mechanism of microstructural refinement. In this study, only the AMLS alloy had any appreciable amount of large second-phase particles present during rolling, in this case ~ 1.2 vol% ν-

phase. The ALS had very little ν and the AMS had the Mg in solid solution at the rolling temperature. The AS had no large intermetallics.

The m vs. $\dot{\varepsilon}$ curves (Fig. 4.29) show little difference in m_{max} and the strain rate at m_{max} between the AMS and AMLS alloys and comparisons of m vs. strain (Fig. 4.27) show the rate of m evolution with strain is identical. This indicates that small amounts of large second-phase particles are not influencing CRX in these alloys. The location of the ν-phase clusters in the as-polished specimens were correlated to the pits left after etching. The grain morphology around the ν-phase clusters was random; both fine recrystallized regions and coarse unrecrystallized regions were seen in the immediate vicinity of the clusters and away from the same clusters.

5.4 Effect of Grain Size on CRX

The pre-tensile deformation grain size is a function of the as-cast grain size. Since the microstructure is not able to conventionally recrystallize, hot deformation adds texture to the as-cast microstructure. In the AMLS alloy, where the equiaxed grain size increased from the faces of the ingot to the center, the through-thickness grain size varied in the tensile specimens after rolling. Fig. 4.21 shows the microstructure from two regions in the ST plane from a single sample both before and after tensile deformation. The fine region comprises only a small fraction of the total gage area. After tensile deformation the grain size is reduced in both regions, but a difference remains in the respective grain sizes. There is also a reduction in the creep strength at all strain rates in the finer microstructure which is discussed in a later section on post-CRX properties.

The finer grain size is beneficial to CRX in that there is a greater amount of large-angle boundary area present in the microstructure before creep testing. This means that less new boundary area must be produced in the CRX process and this should hasten the completion of CRX over that of a larger grained microstructure. Another way this is beneficial to CRX is that it limits the degree of incompatibility generated between regions of recrystallized grains and those that have not yet recrystallized. Fig. 4.22 shows the difference in the degree of cavitation visible in the ST plane between the large grained and fine grained regions in an AMLS sample. It is harder to preserve continuity in the large grained material due to the overall size of the grains and the increased probability that voids will nucleate at the interface between the two regions. This will lower the elongation in the alloys and result in poorer post-formed properties.

5.5 Role of Solutes on Deformation after CRX

At first glance it appears that the Al-Mg-Sc alloys have much better properties from a SPF perspective. They exhibit a wider range of strain rates with high m-values than the Al-Sc and Al-Li-Sc alloys (Fig. 4.29), which is good from a processing point-of-view, and higher m_{max} values overall after CRX at 500°C. In the Al-0.5Sc alloy at 500°C, m_{max} never reaches the 0.5 threshold and that the peak m-values are sustained only for a narrow range of strain rates. However, all of the alloys exhibit m_{max} at intermediate $\dot{\varepsilon}$ and lower m-values at low and high $\dot{\varepsilon}$. This behavior is due to the interaction between the dislocations and the Mg atoms in solution.

5.5.1 High strain rates

The strengthening effect of the Al_3Sc precipitates is shown in Fig. 4.34 where flow stress of the AS alloy is higher than the pure Al at all strain rates. This is repeated in the ALS alloy when compared with the Al-Li binary. At the higher strain rates the decrease in m arises from the imposition of power-law creep in the AMS and AMLS alloys and power-law breakdown in the ALS and AS alloys. As described in section 2.4.2, power-law breakdown has no particular value of m, but it is less than that for power-law creep and decreases with increasing strain rate. Luthy, *et al.* [1980] have tabulated creep data for Al and found that for that the power-law breakdown occurs around $\left(\frac{E}{\sigma}\right) = 5000$ where E = Young's Modulus at the test temperature and σ = steady state creep stress. At 500°C this works out to 9.7 MPa (1.4 ksi) for pure Al. From this data it appears the Al_3Sc precipitates are only be slightly influencing the stress, if at all, at which the power-law breakdown is observed in the Al-Sc alloys as compared to pure Al. Because the regime of high m is superseded by the power-law breakdown, the decrease in m with increasing strain rate is very severe due to the low values of m in the breakdown regime.

At high strain rates both the AMLS and Al-Mg-Li alloys have similar flow stresses and their $\sigma - \dot{\varepsilon}$ curves overlap (Fig. 4.34). Thus the Mg strengthens the Al more than the Sc precipitates. This also indicates that the same creep mechanism is operative in both alloys. When a stress comparable to that for power-law creep is reached during high temperature deformation, the transition occurs and the mechanism of deformation changes from GBS-controlled creep to power-law creep. At no point in any of the tests on the Al-Mg-Sc alloys does it appear that power-law breakdown is occurring as the Al-Mg-Li-Sc alloy exhibits constant m-values of ~ 0.18 at $\dot{\varepsilon} > .04 s^{-1}$. Thus, the imposition

of power-law creep and not power-law breakdown ends the regime of superplastic behavior. This causes m to decrease but more gradually than seen in the Al-Sc alloys without Mg due to the influence of the Mg atoms on the movement of the dislocations. This allows $m > 0.4$ to be seen at strain rates five times of those in the non-Mg alloys at 500°C.

The effect of Mg on high temperature deformation can be gleaned from the data for alloys without Sc. In Fig. 4.31 the Mg binary and the Mg-Li ternary alloys exhibit m-values close to those reported for viscous glide-controlled power-law creep as expected [Yavari and Langdon, 1982]. In climb-controlled power-law creep, the rate-controlling process of the movement of dislocations is climb-controlled ($m \approx 0.15$ as observed in the tensile tests) and the glide velocity is much faster than the climb velocity. Since climb and glide are sequential processes, the slowest one (climb) controls the rate of deformation. In viscous glide-controlled power-law creep, the two velocities are about equal and the glide velocity is much slower now than it is in climb-controlled creep. Thus a much higher stress is needed to generate the same dislocation velocity necessary to impose a macroscopic strain rate on the specimen. As can be seen in Fig. 4.34, the Mg alloys are much stronger than the non-Mg counterparts and there is a greater range of stress for GBS creep to be observed. Even though true viscous glide behavior is not observed in the AMLS and AMS alloys, the interaction between the Mg atoms and the dislocations that raises the stress for power-law creep and breakdown in the Al-Mg solid solution alloys also holds for the AMS and AMLS alloys.

The validity of the solute-dislocation interaction theory was tested by fabricating an Al-8.3Zn-0.5Sc (AZS) alloy and testing it at 500°C. Zn was chosen because Al-Zn alloys deform by regular power-law creep and large amounts can be added in solid solution. Thus, even with a large amount of solute it is expected that the power-law breakdown will intercede at high stresses in the AZS alloy and cause a rapid drop in m with strain rate like that observed in the AS and ALS alloys. The plot of m vs. $\dot{\varepsilon}$ in Fig. 5.3 shows that the response of the AZS alloy is nearly identical to that of the AS alloy.

5.5.2 Low strain rates

There have been two types of behaviors observed at low strain rates in alloys exhibiting GBS-controlled deformation at intermediate strain rates. Some alloys, including a 7075 Al alloy [Murty and Koczak, 1987] exhibit a threshold stress (σ_o) where m approaches zero which has been associated with a stress necessary for grain boundary sliding [Edington *et al.*, 1976]. Other researchers have observed a power-law

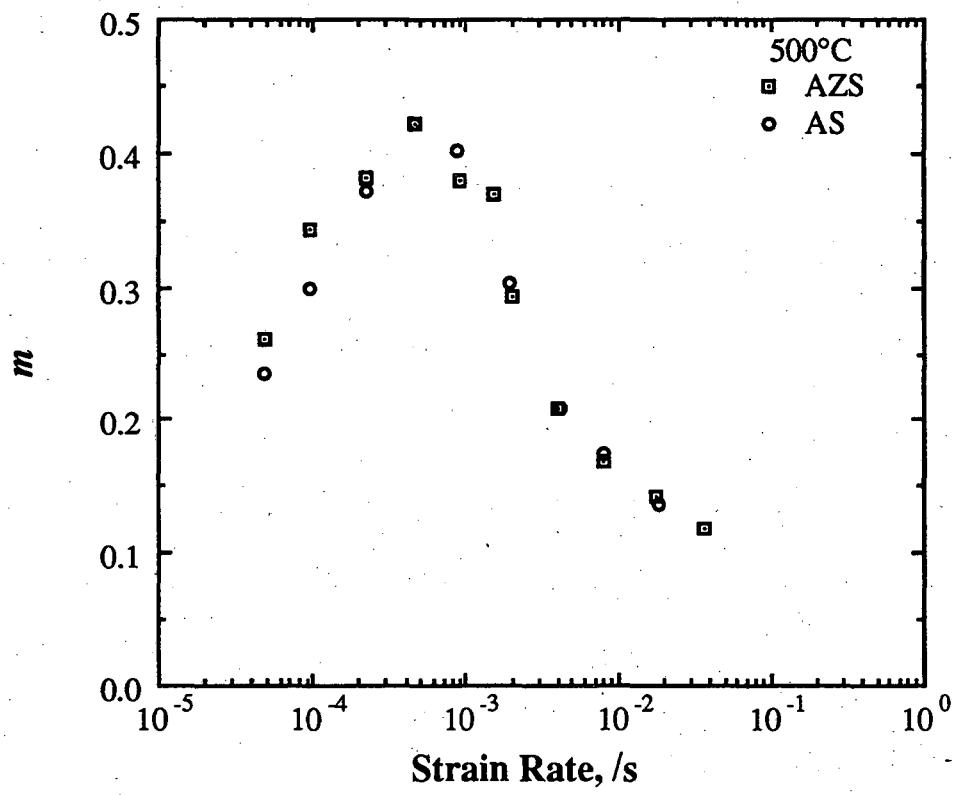

Figure 5.3. Plot of m vs. strain rate for the AS and AZS alloys showing the similar rapid drop-off in m at high strain rates.

response with a $m \approx 0.3$ and no threshold behavior [Grivas, 1978]. In all the Al-Sc alloys, m does decrease at lower strain rates. However, due to the limitation of the Instron testing apparatus it is impossible to determine if m stabilizes at some finite value or goes to zero. At this time there is no experimental evidence in the literature on the effect of solutes on σ_o.

5.6 Stable deformation and elongation in Al-Sc alloys

Table 5.1 shows the strains at which the Hart and Considére criteria are satisfied for the AS, ALS, and AMLS alloys tested at 500°C to $\varepsilon = 0.7$ and the m-values at that point. The early satisfaction of the Hart and Considére criteria means that m must be high or more rapid thinning will occur during deformation. Also listed in Table 5.2 is a summary of the average ratio of the thinnest and thickest regions of the gage for the three alloys . The alloys without Mg have smaller ratios indicating a greater degree of necking

at the point the test was stopped. This is a result of the higher m-value in the AMLS alloy at the satisfaction of the Hart criterion.

Table 5.2. Strains at which the Hart and Considére criteria are satisfied in the Al-Sc alloys tested to strains of 0.7 at 500°C and the ratios of the area of the thinnest and thickest regions of the gages for those alloys.

Alloy	Hart True strain	Considere True strain	m	Ratios of gage areas
AS	0.081	0.072	0.25	0.79
ALS	0.081	0.072	0.26	0.68
AMLS	0.187	0.153	0.33	0.86

6. CONCLUSIONS

The continuous recrystallization mechanism appears to be a fundamental mechanism in Al-Sc alloys since it is observed irrespective of the solute composition of the alloys. It appears the CRX mechanism in Al-Sc alloys is due to a combination of subgrain coalescence at low strains and the incorporation of the additional dislocations generated during grain boundary sliding at higher strains when the misorientation has increased sufficiently. Alloying additives such as Mg and Li are more important with respect to the deformation properties of the alloys after CRX is completed. Mg, and to a lesser extent Li, do affect the maximum *m*-values observed in Al-Sc alloys by changing the melting points and thus the homologous temperatures of the various alloys when tested at identical temperatures. Maximum *m*-values are observed to correlate inversely with melting temperature such that the alloy with the greatest amount of Mg had the highest *m*-values and lowest melting point. A much larger solute effect is seen with Mg since it raises the stress at which power-law creep and breakdown is observed relative to alloys without Mg and effectively broadens the range of strain rates that high *m*-values can be observed. The imposition of the power-law breakdown at much lower stresses in the Al-0.5Sc and Al-1.2Li-0.5Sc alloys causes the *m*-value to decrease much more rapidly with strain rate. Al alloys for commercial superplastic applications which are to be deformed at the highest strain rates should contain element(s) that raise the power-law strength so that the *m*-values are maximized as long as the post-formed mechanical properties are preserved.

7. FUTURE WORK

There are several unanswered questions that were raised as a result of this project.

I. What is the exact mechanism of the incorporation of dislocations in the grain boundaries during deformation and what is the effect of stress on this process.

II. Are there any other alloy systems other than Al-based alloys that exhibit CRX? How general is this mechanism in metals.

III. Does CRX continue after the misorientation reaches a steady-state value.

IV. How does m vary at low strain rates (threshold region) and what general deformation mechanism is occurring at those low strain rates.

REFERENCES

R. Amichi and N. Ridley, "Superplastic Behavior and Microstructural Evolution in Al-Li Alloy 8090 (Lital A)," in Fifth Intl. Al-Li Conf., eds. T. H. Sanders, Jr. and E. A. Starke, Jr., Materials and Component Engr. Publ. Ltd., Birmingham, U.K., 1989, 159-167.

E. N. da C. Andrade, "On the Viscous Flow in Metals and Alloys," Proc. Roy. Soc. London, A84, 1910, 1-12.

A. Arieli and A. K. Mukherjee, "A Model for the Rate-Controlling Mechanism in Superplasticity," Mater. Sci. Eng., 45, 1980, 61-70.

B. A. Ash and C. H. Hamilton, "Strain and Strain-rate Hardening Characteristics of a Superplastic Al-Li-Cu-Zr-Alloy," Scripta Metall., 22, 1988, 277-282.

J. E. Bird, A. K. Mukherjee, and J. E. Dorn, "Correlations Between High-Temperature Creep Behavior and Structure," in Quantitative Relation Between Properties and Structure, Israel Univ. Press, Jerusalem, 1969.

E. L. Bradley, III, R. A. Emigh, and J. W. Morris, Jr., "Superplastic Properties of an Al-2.4Mg-1.8Li-0.5Sc Alloy," Scripta Metall., 25, 1991, 717-721.

E. L. Bradley, III and J. W. Morris, Jr. Unpublished work, 1992.

J. Cadek, Creep in Metallic Materials, Elsevier, Amsterdam, 1988.

D. Caillard and J. L. Martin, "Microstructure of Aluminium during Creep at Intermediate Temperature-II. *In Situ* Study of Subboundary Properties," Acta Metall., 30, 1982, 791-798.

R. L. Coble, "A Model for Boundary Diffusion Controlled Creep in Polycrystalline Materials," J. Appl. Phys., 34, 1963, 1679-1682.

A. H. Cottrell, The Properties of Materials at High Rates of Strain, Institute of Mechanical Engineering, London, 1957.

A. M. Diskin, V. K. Portnoi, A. M. Drits, and A. A. Alalykin, "Superplasticity of Alloy of the Al-Cu-Mg System with Additions of Transition Metals," Sov. Non-Ferrous Met. Res., 14, 1986, 499-500.

M. E. Drits, Yu G. Bykov, and L. S. Toropova, "Effect of $ScAl_3$ Phase Disperity on Hardening of Al-6.3Mg-0.21Sc Alloy," Met. Sci. Heat Treat. (USSR), 27, 1985, 309-312.

J. W. Edington, Electron Diffraction in the Electron Microscope, MacMillan Press, London, 1975, 42-44.

J. W. Edington, "Physical Metallurgy of Superplasticity," Met. Tech., March, 1976, 138-153.

J. W. Edington, K. N. Melton, and C. P. Cutler, "Superplasticity", Prog. Mat. Sci., 21, 1976, 61-158.

R. A. Emigh, E. L. Bradley, and J. W. Morris, Jr., "The Al-Sc-Li-Mg System as a Potential Source of Superplastically Formable Alloys," to be published in Light-Weight Alloys for Aerospace Applications, TMS, 1992.

R. A. Emigh, Ph.D. Thesis, University of California, Berkeley, 1990.

S. F. Exell and D. H. Warrington, "Sub-grain Boundary Migration in Aluminium," Phil. Mag., 26, 1972, 1121-1136.

H. M. Flower and P. J. Gregson, "Solid State Transformations in Aluminium Alloys Containing Lithium," Mater. Sci. Tech., 3, 1987, 81-90.

H. J. Frost, "Transient Deformation Mechanism Maps," in Flow and Fracture at Elevated Temperatures, ed. R. Raj, American Society for Metals, Metals Park, OH, 1985, 65-82.

H. Frost and M. F. Ashby, Deformation-Mechanism Maps: The Plasticity and Creep of Metals, Pergamon Press, New York, 1982.

P. C. J. Gallagher, "The Influence of Alloying, Temperature, and Related Effects on the Stacking Fault Energy," Metall. Trans., 1, 1970, 2429-2461.

C. Gandhi, "Fracture Mechanism Maps for Metals and Alloys," in Flow and Fracture at Elevated Temperatures, ed. R. Raj, American Society for Metals, Metals Park, OH, 1985, 83-119.

K. J. Gardner and R. Grimes, "Recrystallization during Hot Deformation of Aluminium Alloys," Metal Sci., 13, 1979, 216-222.

A. K. Ghosh and R. A. Ayers, "On Reported Anomalies in Relating Strain-rate Sensitivity (m) to Ductility," Metall. Trans., 7A, 1976, 1589-1591.

R. C. Gifkins, "Grain-Boundary Sliding and its Accommodation During Creep and Superplasticity," Metall. Trans., 7A, 1976, 1225-1232.

H. Gleiter and B. Chalmers, "High-Angle Grain Boundaries," Prog. Mater. Sci., 16, 1972.

D. J. Goodman, H. J. Frost, and M. F. Ashby, "The Plasticity of Polycrystalline Ice," Phil. Mag., A43, 1981, 655-695.

P. Gordon, Trans. A.I.M.E., 203, 1955, 1043.

R. Grimes, M. J. Stowell, and B. M. Watts, "Superplastic Aluminium-Based Alloys," Metal Tech., 3, 1976, 154-160.

K. A. Gschneider, Jr. and F. W. Calderwood, "The Al-Sc (Aluminum-Scandium) System," Bulletin of Alloy Phase Diagrams, 10, 1989, 34-36.

H. Gudmundsson, D. Brooks, and J. A. Wert, "Mechanisms of Continuous Recrystallization in an Al-Zr-Si Alloy," Acta Metall., 39, 1991, 19-35.

M. Guillope and J. P. Poirier, "Dynamic Recrystallization during Creep of Single-Crystalline Halite: An Experimental Study," J. Geophys. Res., 84, 1979, 5557-5567.

M. Hahn, Northrop Corp., Private Communication, 1991.

S. J. Hales and T. R. McNelley, "Microstructural Evolution by Continuous Recrystallization in a Superplastic Al-Mg Alloy," Acta Metall., 36, 1988, 1229-1239.

S. J. Hales, T. R. McNelley, and H. J. McQueen, "Recrystallization and Superplasticity at 300°C in an Aluminum-Magnesium Alloy," Metall. Trans., 22A, 1991, 1037-1047.

M. Hansen, Constitution of Binary Alloys, McGraw-Hill, New York, 1958.

H. K. Hardy and J. M. Silcock, "The Phase Sections at 500°C and 350°C of Aluminium-Rich Aluminium-Copper-Lithium Alloys," J. Inst. Metals, 84, 1955-56, 423-428.

John E. Hatch, ed., Aluminum: Properties and Physical Metallurgy, American Society for Metals, Metals Park, OH, 1984.

J. Hedworth and M. J. Stowell, "The Measurement of Strain-Rate Sensitivity in Superplastic Alloys," J. Mater. Sci., 6, 1971, 1061-1069.

C. Herring, "Diffusional Viscosity of a Polycrystalline Solid," J. Appl. Phys., 21, 1950, 437-445.

J. P. Hirth and J. Lothe, Theory of Dislocations, John Wiley and Sons, New York, 1982.

R. W. K. Honeycombe, Plastic Deformation of Metals, Edward Arnold, London, 1984.

A. Khachaturyan, T. F. Lindsey, and J. W. Morris, Jr., "Theoretical Investigation of the Precipitation of δ' in Al-Li," Metall. Trans., 19A, 1988, 249-258.

D.-H. Lee, K. T. Hong, D. H. Shin, and S. W. Nam, "Effects of Grain Boundary Deformation on the Creep Transition under the Power Law Regime in an Al-Mg Soild Solution Alloy," Mater. Sci. Eng., A156, 1992, 43-52.

K. Linga Murty, F. A. Mohamed, and J. E. Dorn, "Viscous Glide, Dislocation Climb, and Newtonian Viscous Deformation Mechanisms of High Temperature Creep in Al-3Mg," Acta Metall., 20, 1972, 1009-1018.

H. Luthy, A. K. Miller, and O. D. Sherby, "The Stress and Temperature Dependence of Steady-State Flow at Intermediate Temperatures for Pure Polycrystalline Aluminum," Acta Metall., 28, 1980, 169-178.

Y. Maehara and T. Langdon, "Review: Superplasticity in Ceramics," J. Mater. Sci., 25, 1990, 2275-2286.

T. B. Massalski, ed., Binary Alloy Phase Diagrams, Vol. 1, American Society for Metals, Metals Park, OH, 1986.

D. McLean, "Creep Processes in Coarse-Grained Aluminium," J. Inst. Metals., 80, 1951-52, 507-519.

T. R. McNelley, P. N. Kalu, and R. R. Crooks, "Thermomechanical Processing and Grain Refinement for Superplasticity in Aluminum Alloys," presented at the 1993 TMS Annual Meeting, February 23, 1993.

H. J. McQueen and J. J. Jonas, "Recovery and Recrystallization during High Temperature Deformation," in Treatise on Materials Science and Technology, Vol 6, ed. R. J. Arsenault, Academic Press, New York, 1975, 1393-493.

F. A. Mohamed, K. L. Murty, and J. W. Morris, Jr., "Harper-Dorn Creep in Al, Pb, and Sn," Metall. Trans., 4, 1973, 935-940.

F. A. Mohamed, "Incorporation of the Suzuki and the Fisher Interactions in the Analysis of Creep Behavior of Solid Solution Alloys," Mater. Sci. Eng., 61, 1983, 149-165.

P. R. Mould and P. Cotterill, "The Effect of Particle Content and Matrix Grain Size on the Recrystallisation of Two-Phase Aluminium-Iron Alloys," J. Mater. Sci., 2, 1967, 241-255.

A. K. Mukherjee, "High-Temperature Creep," in Treatise on Materials Science and Technology, Vol 6, ed. R. J. Arsenault, Academic Press, New York, 1975, 163-224.
A. K. Mukherjee, "Deformation Mechanisms in Superplasticity," Ann. Rev. Mater. Sci., 9, 1979, 191-217.

G. S. Murty and M. J. Koczak, "Investigation of Region I of a Superplastic Al-Zn-Mg-Cu-Mn Alloy," Mater. Sci. Eng., 96, 1987, 117-124.

F. R. N. Nabarro, Theory of Crystal Dislocations, Dover, New York, 1987.

E. Nes, "Continuous Recrystallization and Grain Growth during Superplastic Flow," in Superplasticity, eds. B. Baudelet and M. Suery, 1985, 7.1-7.13.

W. D. Nix and J. C. Gibeling, "Mechanisms of Time-Dependent Flow and Fracture of Metals," in Flow and Fracture at Elevated Temperatures, ed. R. Raj, ASM, Metals Park, OH, 1985, 1-63.

A. Orlova, Z. Tobolova, and J. Cadek, "Internal Stress and Dislocation Structure of Aluminium in High-temperature Creep," Phil. Mag., 26, 1972, 1263-1274.

Kyung-Tae Park, E. J. Lavernia, and Farghalli A. Mohamed, "Creep Behavior and Substructure in an Al-Li Alloy", Acta Metall. Mater., 38, 1990, 1837-1848.

J. Pilling and N. Ridley, "Effect of Hydrostatic Pressure on Cavitation in Superplastic Aluminium Alloys," Acta Metall., 34, 1986, 669-679.

J. P. Poirier, Creep of Crystals, Cambridge Univ. Press, Cambridge, U.K., 1985.

Liu Qing, "An Equation to Determine the Practical Tilt Angle of a Double-Tilt Specimen Holder and its Application to Transmission Electron Microscopy," Micron and Micros. Acta., 3/4, 1989, 255-259.

L. Qing, Y. Jinfeng, and Y. Mei, "Effect of Two-Stage Strain-rate Test on the Superplastic Behavior of an Al-Li-Cu-Mg-Zr Alloy--Mechanical Behavior," Scripta Metall. et Mater., 25, 1991, 109-114.

L. Qing, Y. Jinfeng, and Y. Mei, "Effect of Two-Stage Strain-rate Test on the Superplastic Behavior of an Al-Li-Cu-Mg-Zr Alloy--Microstructural Characterization," Scripta Metall. Mater., 25, 1991, 115-120.

Liu Qing, Huang Xiaoxu, Yao Mei, and Yang Jinfeng, "On Deformation-Induced Continuous Recrystallization in a Superplastic Alloy," Acta Metall. Mater., 40, 1992, 1753-1762.

R. E. Reed-Hill, Physical Metallurgy Principles, PWS Publishing, Boston, 1982.

F. N. Rhines, W. E. Bond, and M. A. Kissel, "Grain Boundary Creep in Aluminum Bicrystals," Trans. ASM, 48, 1956, 919-949.

J. Rösler, R. Joos and E. Artz, "Microstructure and Creep Properties of Dispersion-Strengthened Aluminum Alloys," Metall. Trans., 23A, 1992, 1521-1539.

A. W. Ruff, Jr., "Measurement of Stacking Fault Energy from Dislocation Interactions," Metall. Trans., 1, 1970, 2391-2413.

N. Ryum, O. Hunderi, and E. Nes, "On Grain Boundary Drag from Second Phase Particles," Scripta Metall., 17, 1983, 1281-1283.

R. R. Sawtell and C. L. Jensen, "Mechanical Properties and Microstructure of Al-Mg-Sc Alloys," Metall. Trans., 21A, 1990, 421-430.

J. A. Schey, Introduction to Manufacturing Processes, McGraw-Hill, New York, 1977.

A. Seeger, in Dislocations and Mechanical Properties of Crystals, ed. Fisher, John Wiley, New York, 1957.

I. S. Servi and N. J. Grant, "Creep and Stress Rupture Behavior of Aluminum as a Function of Purity," Trans. A.I.M.E., 209, 1951, 909-916.

T. Sheppard, M. A. Zaidi, M. G. Tutcher, and N. C. Parson, "Dynamic Recrystallization in Aluminium Alloys," in Microstructural Control in Aluminum Alloys: Deformation, Recovery, and Recrystallization, eds. E. Henry Chia and H. J. McQueen, The Metallurgical Society, Warrendale, PA, 1986, 155-178.

Oleg. D. Sherby and Jeffery Wadsworth, "Superplasticity-Recent Advances and Future Directions", Prog. Mater. Sci., 33, 1989, 169-221.

Oleg. D. Sherby and Jeffery Wadsworth, "Development and Characterization of Fine-Grain Superplastic Materials", in Deformation, Processing and Structure, ed. G. Krauss, American Society for Metals, Metals Park, OH, 1984, 355-389.

Dong H. Shin, Young H. Shin, Young W. Chang, and Sun C. Maeng, "Development of Superplasticity in 8090 Al-Li Alloy by Static Recrystallization," Scripta Metall. Mater., 26, 1992, 117-121.

C. J. Smithells, Smithells Metal Reference Book, 6th edition, ed. E. A. Brandes, Butterworths, London, 1983.

S. Takeuchi and A. S. Argon, "Review: Steady-state Creep of Single-phase Crystalline Matter at High Temperature," J. Mater. Sci., 11, 1976, 1542-1566.

G. Thomas and J. Nutting, "The Aging Characteristics of Aluminium Alloys," J. Inst. Metals, 88, 1959-60, 81-90.

D. Tribula, "A Microstructural Study of Creep and Thermal Fatigue Deformation in 60Sn-40Pb Solder Joints," Ph.D. Thesis, University of California, Berkeley, 1990.

Trouton and A. O. Rankine, "On the Stretching and Torsion of Lead Wire Beyond the Elastic Limit," Philos. Mag., 8, 1904, 538-556.

P. D. Tungatt and F. J. Humphreys, :"An In-situ Optical Investigation of the Deformation Behaviour of Sodium Nitrate - An Analogue for Calcite," Tectonophysics, 78, 1981, 661-675.

G. F. VanderVoort, Metallography: Principles and Practice, McGraw-Hill, New York, 1984.

J. Wadsworth, I. G. Palmer, and D. D. Crooks, "Superplasticity in Al-Li Based Alloys," Scripta Metall., 17, 1983, 347-352.

B. M. Watts, M. J. Stowell, B. L. Baikie, and D. G. E. Owen, "Superplasticity in Al-Cu-Zr alloys, Part I: Materials Preparation and Properties," Metal Sci., 1976, 189-197.

B. M. Watts, M. J. Stowell, B. L. Baikie, and D. G. E. Owen, "Superplasticity in Al-Cu-Zr alloys, Part II: Microstructural Study," Metal Sci., 1976, 198-206.

F. Weinberg, Trans. AIME, 212, 1958, 808.

H. S. Yang, M. G. Zelin, R. Z. Valiev, and A. K. Mukherjee, "High Temperature Deformation of a Magnesium Alloy with Controlled Grain Structures," Mater. Sci. Eng., A158, 1992, 167-175.

P. Yavari and T. G. Langdon, "An Examination of the Breakdown in Creep by Viscous Glide in Solid Solution Alloys at High Stress Levels," Acta Metall., 30, 1982, 2181-2196.

H. Yoshida, H. Tanaka, S. Tsuchida, T. Tsuzuku, and A. Takahashi, "Superplasticity of Al-Li Alloys," in Proc. 5th Al-Li Conf., eds. T. H. Sanders and E. A. Starke, Jr., Materials and Component Engineering Publications, Birmingham, England, 1989, 179-188.

C. Zener, cited in C. S. Smith, Trans AIME, 175, 1948, 15.

General Creep References

J. E. Bird, A. K. Mukherjee, and J. E. Dorn, "Correlations Between High-Temperature Creep Behavior and Structure," in Quantitative Relation Between Properties and Structure, Israel Univ. Press, Jerusalem, 1969.

J. Cadek, Creep in Metallic Materials, Elsevier, Amsterdam, 1988.

A. K. Mukherjee, "High-Temperature Creep," in Treatise on Materials Science and Technology, Vol 6, ed. R. J. Arsenault, Academic Press, New York, 1975, 163-224.

J. P. Poirier, Creep of Crystals, Cambridge Univ. Press, Cambridge, U.K., 1985.

General Superplasticity References

Thomas H. Alden, "Review Topics in Superplasticity," in Treatise on Materials Science and Technology, Vol 6, ed. R. J. Arsenault, Academic Press, New York, 1975, 225-266.
J. W. Edington, K. N. Melton, and C. P. Cutler, "Superplasticity", Prog. Mat. Sci., 21, 1976, 61-158.

C. C. Bampton, J. Wadsworth, and A. K. Ghosh, "Superplastic Aluminum Alloys," Treatise on Materials Science and Technology, 31, 1989, 189-216.
Y. Maehara and T. Langdon, "Review: Superplasticity in Ceramics," J. Mater. Sci., 25, 1990, 2275-2286.

A. K. Mukherjee, "Deformation Mechanisms in Superplasticity," Ann. Rev. Mater. Sci., 9, 1979, 191-217.

K. A. Padmanabhan and G. J. Davies, Superplasticity, Springer-Verlag, 1980
Oleg. D. Sherby and Jeffery Wadsworth, "Superplasticity-Recent Advances and Future Directions", Prog. Mater. Sci., 33, 1989, 169-221.

D. M. R. Taplin, G. L. Dunlop, and T. G. Langdon, "Flow and Fracture of Superplastic Materials," Ann. Rev. Mater. Sci., 9, 1979, 151-189.

Aluminum-Lithium Conference Proceedings

Proceedings of the First International Aluminum-Lithium Conference, T. H. Sanders, Jr. and E. A. Starke, Jr., eds, The Metallurgical Society, Warrendale, PA, 1981.

Proceedings of the Second International Aluminum-Lithium Conference, T. H. Sanders, Jr. and E. A. Starke, Jr., eds, The Metallurgical Society, Warrendale, PA, 1984.

Proceedings of the Third International Aluminum-Lithium Conference, C. Baker, P. J. Gregson, S. J. Harris and C. J. Peel, eds, The Insitute of Metals, London, 1986.

Proceedings of the Fourth International Aluminum-Lithium Conference, Journal de Physique, Colloque C3, supplement au no 9, Tome 48, 1987.

Proceedings of the Fifth International Aluminum-Lithium Conference, T. H. Sanders, Jr. and E. A. Starke, Jr., eds, Materials and Component Engineering Publications, Ltd., Birmingham, U.K., 1989.

Appendix A: Activation Energy

Activation energies (Q) have been used to help discern the mechanisms of high temperature deformation and are calculated from the Dorn equation at constant flow stress [Mohamed and Langdon, 1975]. The true activation energy is that of the diffusional process and is

$$Q = \left[\frac{\partial \ln D}{\partial (1/T)}\right]_{d,\sigma}, \tag{A1}$$

where D = diffusivity, T = absolute temperature, d = grain size, and σ = flow stress. The apparent activation energy is

$$Q_{app} = \left[\frac{\partial \ln \dot{\varepsilon}}{\partial (1/T)}\right]_{d,\sigma}, \tag{A2}$$

where $\dot{\varepsilon}$ = strain rate. This works out to be

$$Q_{app} = \frac{kT_1T_2 \ln\left(\dot{\varepsilon}_2/\dot{\varepsilon}_1\right)}{(T_2 - T_1)}. \tag{A3}$$

The true activation energy can be calculated if the value of the shear modulus at the various temperatures is known and the temperature term in the denominator of the Dorn equation is incorporated

$$Q = \frac{k \ln\left(\dot{\varepsilon}_2 T_2 G_2^{n-1} / \dot{\varepsilon}_1 T_1 G_1^{n-1}\right)}{(T_2 - T_1)/T_1T_2}. \tag{A4}$$

It has been shown that power-law creep typically has activation energies associated with lattice diffusion (Q_l). This is not surprising since the rate-controlling process is the climb of edge dislocation segments in the grain interiors and requires the diffusion of vacancies to the dislocation for deformation to occur. Superplasticity has been shown to often have a Q about one-half that of bulk diffusion, or close to that of the value of grain boundary diffusion. However there are also many cases where Q for superplasticity is close to Q_l. This is common at high temperatures where bulk diffusion overwhelms grain boundary diffusion and is expected at the homologous temperatures used in this study.

Bird *et al.* showed that the G correction is typically about 5% of the total Q and ignoring it does not contribute greatly to the error of Q. It has been shown that

$$Q_{(\sigma)} = \frac{1}{m} Q_{(\dot{\varepsilon})} \tag{A5}$$

so that tests run at constant strain rate can be utilized for calculating Q.

REFERENCES

J. E. Bird, A. K. Mukherjee, and J. E. Dorn, "Correlations Between High-Temperature Creep Behavior and Structure," in Quantitative Relation Between Properties and Structure, Israel Univ. Press, Jerusalem, 1969.

F. A. Mohamed and T. G. Langdon, "The Determination of the Activation Energy for Superplastic Flow," phys. stat. sol. (a), 33, 1976, 375-381.

Appendix B: The Theory of Stable Deformation and its Relationship to the Tensile Creep Test

The general criterion for the onset of unstable deformation (necking) during a tensile test is the local deviation of the strain rate in change of the cross-sectional area at some point in the gage relative to the rest of the gage. A number of different criteria have been derived to determine the onset of tensile instability during deformation. However, the derivation by Hart [1967] was the first to incorporate the strain-rate sensitivity (m) in the analysis. He showed that the onset occurs when

$$\gamma + m \geq 1$$

where $\gamma = \frac{1}{\sigma}\frac{d\sigma}{d\varepsilon}$ and $\frac{d\sigma}{d\varepsilon}$ is the instantaneous work hardening rate and σ is the true stress. The famous Considére criterion, $\frac{d\sigma}{d\varepsilon} = \sigma$ follows from this definition when m is ignored.

Based on the Hart criterion, a tensile test must be in unstable deformation during steady state creep since steady state is defined as a constant strain rate at a constant stress, *i.e.* $\gamma = 0$. However, this does not mean tensile tests cannot be used to generate creep data. What saves us is when the deviation from stability is small enough with respect to the stable case. Hart also showed that the rate of neck development during tension is highly related to m. High m yield high elongations and slow development of the neck after it has formed. Thus, the slower the development of the neck the greater the similarity of the results to stable flow after instability. Burke and Nix [1975] have calculated that for a constant stress test (analogous to constant strain rate) for a material with$m$ = 0.2, the deviation in strain rate (stress) only becomes noticable at true strains around 0.4. The discrepancy is even less important when considering the strain-rate change tests used to calculate m since in this case m is measured from a single specimen over a small strain increment. If the rate of necking is slow , the measured difference in m between a stable and unstable specimen should be negligible. In the tests done in this thesis, all m values were measured using the strain-rate change method on specimens with relativley high m-values, meaning the accuracy of the data is sufficient for comparative purposes.

REFERENCES

M. A. Burke and W. D. Nix, "Plastic Instabilities in Tension Creep," Acta Metall., 23, 1975, 793-798.

E. W. Hart, "Theory of the Tensile Test," Acta Metall., 15, 1967, 351-355.

LAWRENCE BERKELEY LABORATORY
UNIVERSITY OF CALIFORNIA
TECHNICAL INFORMATION DEPARTMENT
BERKELEY, CALIFORNIA 94720